universität wien

MASTERARBEIT / MASTER'S THESIS

Titel der Masterarbeit / Title of the Master's Thesis

„Increasing the negative ionization efficiency for the detection of ^{236}U and ^{233}U by AMS“

verfasst von / submitted by

Michael Kern, BSc

angestrebter akademischer Grad / in partial fulfilment of the requirements for the degree of

Master of Science (MSc)

Wien, 2020 / Vienna, 2020

Studienkennzahl lt. Studienblatt / degree programme code as it appears on the student record sheet:	UA 066 876
Studienrichtung lt. Studienblatt / degree programme as it appears on the student record sheet:	Masterstudium Physik
Betreut von / Supervisor:	Univ.-Prof. Dipl.-Ing. Dr. Robin Golser
Mitbetreut von / Co-Supervisor:	Dr. Karin Hain

Abstract

The highly sensitive technique of accelerator mass spectrometry (AMS) enables measuring extremely low concentrations of trace isotopes in the environment. A new method uses the $^{233}U/^{236}U$ ratio for uranium source assessment. The detection of ^{233}U is most critical because of abundance ratios below 10^{-12}. The Vienna Environmental Research Accelerator (VERA) is the first AMS facility world-wide to deliver sufficient detection efficiency for measurements of ^{233}U from environmental samples. The main limiting factor for AMS is the ionization efficiency for negative ions by Cs sputtering ($\approx 10^{-3}$). The formation of negative ions depends on the electron affinity of an atom or molecule. A group of flourine-rich molecules with exceptionally high electron affinity called "superhalogens" were found to produce strong ion currents by caesium sputtering. So far, the production of UF_5^- was examined for purely metallic uranium powder and by directly preparing U in the form of UF_4. U is normally extracted from the ion source in the form of UO^- for AMS.

The main objectives of this Master's thesis were to improve UO^- and UF_5^- ionization efficiency and the investigation of environmental samples by AMS using UF_5^-. The in-house uranium standard Vienna-KkU was prepared by three different methods as a proxy for environmental samples. One method was newly developed to handle sub-milligram amounts of Fe_2O_3. Vienna-KkU was diluted 1:30 in Fe_2O_3 powder (Vienna-KkU-D30) and mixed with metallic Nb powder 1:1, which yielded the best ionization efficiency results for UO^- of $(0.80 \pm 0.14)\%$.
Vienna-KkU-D30 powder mixed roughly 1:9 with PbF_2 was found optimal for UF_5^- extraction and showed an ionization efficiency of up to $(2.49 \pm 0.12)\%$. Apart from UF_5^- other $UO_xF_y^-$ ions were formed with powder mixtures, most prominently UO_3F^- and $UO_2F_2^-$ each to about 70% of the UF_5^- results. Cu_5F^- interference

on UF_5^- was estimated to 10% of overall ionization efficiency. Investigation of the UF_5^- ionization efficiency for different total mass sizes with the same relative U concentration showed an optimal region of 1.5 mg to 2 mg. Over 90% of total UF_5^- ionization efficiency was achieved in under 2 hours. Forming a cone-shaped crater at the surface of the sample could not significantly increase ionization efficiency. The standard precipitation method for environmental actinide samples in combination with the optimal PbF_2 admixture ratio of 1:9 was found to yield impractically high total sample masses (about 10 mg to 30 mg). Therefore, a new sample preparation method for sub-milligram matrices of Fe_2O_3 containing U and mixed with 1:9 PbF_2 was designed. This method achieved an ionization efficiency of $(1.30 \pm 0.45)\%$. An alternative method of directly co-precipitated UF_4 on either NdF_3 or PrF_3 mixed with 1:9 PbF_2 showed ionization efficiency of $(3.40 \pm 0.28)\%$ and $(4.67 \pm 0.28)\%$ respectively.

An AMS measurement to determine the isotope ratios $^{236}U/^{238}U$, $^{233}U/^{238}U$ and $^{233}U/^{236}U$ was successfully conducted using UF_5^- that was extracted from three proxy materials and one environmental air filter sample. Vienna-KkU-D30 mixed 1:9 with PbF_2 agreed within 1σ of its $^{236}U/^{238}U$ ratio of $(6.83 \pm 0.38) \times 10^{-11}$ to the Vienna-KkU consensus value. Both mixtures of co-precipitated UF_4 on either NdF_3 or PrF_3 mixed with 1:9 PbF_2 showed higher $^{236}U/^{238}U$ ratios. $^{236}U/^{238}U$ results of a known environmental sample, extracted via UO^-, were confirmed within 1σ. Considering $^{233}U/^{238}U$ all three mixtures are suitable as machine blanks with ratios below $(1.27 \pm 0.14) \times 10^{-12}$. Furthermore, the combined $^{233}U/^{236}U$ ratio exposed, that most probable the incorporated PbF_2 contributed minimal uranium traces of global fallout signature, while the co-precipitated mixtures showed lower $^{233}U/^{236}U$ ratios that likely correspond to civil nuclear industry influence. The interference of $^{235}UH^{3+}$ on ^{236}U counts was estimated by the ratio "mass 239"/$^{238}U^{3+}$. Higher upper limits than previously measured at VERA were obtained. Cross-contamination due to real ^{239}Pu in the environmental sample could not be ruled out. The results found in this work confirm the suitability of UF_5^- extraction as a low-energy U molecule for AMS applications.

Zusammenfassung

Die hochempfindliche Technik der Beschleuniger-Massenspektrometrie (AMS) ermöglicht die Messung von extrem niedrigen Spurenisotop-Konzentrationen in der Umwelt. Eine neue Methode verwendet das Verhältnis $^{233}U/^{236}U$ zur Analyse von Spurenisotop-Quellen. Der Nachweis von ^{233}U ist besonders kritisch, durch seine relative Häufigkeit bis unter 10^{-12}. Der Vienna Environmental Research Accelerator (VERA) ist die weltweit erste AMS Einrichtung, die eine ausreichende Detektionseffizienz zur Messung von ^{233}U aus Umweltproben besitzt. Der am stärksten limitierende Faktor für AMS ist die niedrige Ionisationseffizienz negativer Ionen durch Cs-Sputtern ($\approx 10^{-3}$). Die Bildung negativer Ionen ist abhängig von der Elektronenaffinität eines Atoms oder Moleküls. Eine Gruppe von fluorhaltigen Molekülen mit außergewöhnlich hoher Elektronenaffinität, "Superhalogene" genannt, zeigte besonders starke Ionenströme in Cs-Sputterquellen. Bislang wurde für Uran insbesondere die Extraktion von UF_5^-, vorwiegend für rein metallisches Uranpulver und die direkte Fällung von U als UF_4 untersucht. Normalerweise wird U für AMS in Ionenquellen als UO^- extrahiert.

Die Hauptziele dieser Masterarbeit waren die Verbesserung der Ionisationseffizienz von UO^- und UF_5^- und die Untersuchung von Umweltproben durch AMS mittels UF_5^-. Der hauseigene Uranstandard Vienna-KkU wurde mit drei verschiedenen Methoden stellvertretend für Umweltproben aufbereitet. Eine Methode wurde zur Verwendung von Sub-Milligramm Mengen von Fe_2O_3 neu entwickelt. Ausgehend von Vienna-KkU, 1:30 in Fe_2O_3-Pulver verdünnt (Vienna-KkU-D30), ergab die Beimischung von metallischem Nb-Pulver 1:1 die besten Ergebnisse der Ionisationseffizienz für UO^- von $(0.80 \pm 0.14)\%$.
Vienna-KkU-D30-Pulver, 1:9 mit PbF_2 gemischt, zeigte für die Extraktion von UF_5^- eine optimale Ionisationseffizienz von bis zu $(2.49 \pm 0.12)\%$. Neben UF_5^- wur-

den noch andere $UO_xF_y^-$-Ionen mittels Pulvermischungen gebildet, wobei UO_3F^- und $UO_2F_2^-$ jeweils etwa 70% der UF_5^--Resultate erzielten. Die Cu_5F^--Interferenz auf UF_5^- wurde auf 10% der gesamten Ionisationseffizienz abgeschätzt. Die Untersuchung der Ionisationseffizienz von UF_5^- für verschiedene Gesamtprobenmassen bei gleicher relativer U-Konzentration ergab einen optimalen Bereich von 1.5 mg bis 2 mg. Über 90% der gesamten UF_5^--Ionisationseffizienz wurde in weniger als 2 Stunden erreicht. Die Formung eines kegelförmigen Kraters an der Oberfläche der Probe konnte die Ionisationseffizienz nicht signifikant erhöhen. Die Standard-Ausfällungsmethode für Umweltaktinidenproben in Kombination mit dem optimalen PbF_2-Mischungsverhältnis von 1:9, ergab unbrauchbar hohe Gesamtprobenmassen (ca. 10 mg bis 30 mg). Daher wurde eine neue Probenpräparationsmethode für U in Sub-Milligramm Mengen von Fe_2O_3, gemischt mit 1:9 PbF_2, entwickelt. Diese Methode erreichte eine Ionisationseffizienz von $(1.30 \pm 0.45)\%$. Eine alternative Methode der direkten Kopräzipitation von UF_4, entweder mit NdF_3 oder PrF_3 gemischt mit 1:9 PbF_2, zeigte eine Ionisationseffizienz von $(3.40 \pm 0.28)\%$ bzw. $(4.67 \pm 0.28)\%$.

Eine AMS-Messung zur Bestimmung der Isotopenverhältnisse $^{236}U/^{238}U$, $^{233}U/^{238}U$ und $^{233}U/^{236}U$ wurde mittels UF_5^- durchgeführt, welches aus drei Stellvertreter-Materialien und einer Luftfilter-Umweltprobe extrahiert wurde. Vienna-KkU-D30, 1:9 gemischt mit PbF_2, stimmte innerhalb von 1σ seines $^{236}U/^{238}U$-Verhältnisses von $(6.83 \pm 0.38) \times 10^{-11}$ zum Vienna-KkU Konsensuswert mittels UO^--Extraktion überein. Beide Mischungen von ausgefälltem UF_4 in NdF_3 oder PrF_3 mit PbF_2 im Verhältnis 1:9, zeigten höhere $^{236}U/^{238}U$ Verhältnisse. Das $^{236}U/^{238}U$ Verhältnis einer bekannten Luftfilter-Umweltprobe, bestimmt mittels UO^--Extraktion, wurden innerhalb von 1σ bestätigt. Anhand der $^{233}U/^{238}U$ Ergebnisse sind alle drei Mischungen mit Obergrenzen von unter $(1.27 \pm 0.14) \times 10^{-12}$, als Maschinen-Blanks geeignet. Darüber hinaus ergab das kombinierte Verhältnis $^{233}U/^{236}U$, dass das verwendete PbF_2 minimale Uranspuren der globalen Fallout-Signatur enthielt. Andererseits wiesen die gemeinsam ausgefällten Mischungen niedrigere Verhältnisse von $^{233}U/^{236}U$ auf, was auf den wahrscheinlichen Eintrag von Spuren ziviler Kernbrennstoffe entstand. Die Interferenz von $^{235}UH^{3+}$ auf ^{236}U-Zählungen wurde anhand des Verhältnisses "Masse 239"$/^{238}U^{3+}$ abgeschätzt. Es ergaben sich höhere Obergrenzen als zuvor bei VERA gemessen. Eine Kreuzkontamination

durch reales ^{239}Pu in der Umweltprobe konnte nicht ausgeschlossen werden. Die in dieser Arbeit gefundenen Resultate bestätigen die Eignung von UF_5^- als U-Molekül für AMS-Anwendungen.

Contents

1. Motivation

For the determination of long-lived radioactive trace nuclides in the environment, an ultra-sensitive detection method is needed. One that is especially suited for this aim is accelerator mass spectrometry (AMS). Its most prominent application is radiocarbon dating and measures the $^{14}C/^{12}C$ isotope ratio for age determination of organic samples [3]. Until now many different methods have been developed for the determination of other rare long-lived radio-isotopes [62; 67]. The term "long-lived" refers to half-lifes in the range of few thousand years up to several million years. With respect to the field of application most prominent ones are the cosmogenic nuclides (e.g. ^{10}Be, ^{26}Al, ^{36}Cl, ^{41}Ca, ^{60}Fe) [16; 35; 32], long-lived fission products (e.g. ^{99}Tc, $^{127,129}I$, ^{137}Cs etc.) [29; 52; 21] and elements of the group of actinides like $^{233,236}U$, $^{239-241}Pu$ as well as other actinide group isotopes of Np, Am and Cm [64; 57; 22; 24]. Furthermore, methods to determine additional radionuclides facing strong isobaric background are in development. The chemical properties of the above radioisotopes combined with their individual half-life, enables their application for dating techniques and migration studies in the scientific fields of archeology, astronomy, earth sciences, hydrology and life sciences.

The method of AMS facilitates the search for trace isotopes as it is only dependent on counting individual ions and their corresponding statistics. For AMS it is critical to achieve a high efficiency in sputtering negatively charged particles from a sample, high atomic mass resolution and proton number discrimination to detect the isotope in question. Ions get accelerated to a high electrostatic potential where electrons are stripped off inside a gas volume. This efficiently removes molecular interference. Isotopes are then further separated through magnetic fields. AMS does not rely on the half-life of the investigated isotope [67; 47]. Conventional radiometric techniques would need a much larger sample size compared to AMS

or long counting durations for radioactive isotopes with $T_{1/2} \geq 1000a$. Especially, investigations of long-lived anthropogenic and natural isotopes radionuclides are routinely conducted with AMS. Other mass spectrometry techniques like TIMS, ICP-MS and RIMS sometimes do not provide sufficiently high molecular suppression and low detection limits [64]. AMS reaches levels of mass resolution between neighboring isotopes reached below 10^{-15} [55].

Uranium, being an element of the actinides group with primordial isotopes ^{238}U and ^{235}U, is well-known for its use during the Second World War as well as for subsequent atmospheric nuclear weapons testing and the nuclear power industry. The atmospheric tests represent the biggest share of released ^{236}U and ^{233}U trace isotope emission to the environment [8; 63]. Fortunately, the isotopes ^{236}U and ^{233}U can be used as tracers for the investigation of water transport processes. They provide means for the identification of possible releases from the nuclear industry, as they behave conservatively in Sea and fresh water like their primordial counterparts ^{235}U and ^{238}U [50; 40; 49]. Most recent developments in this area make the discrimination between different contributing reservoirs with varying ^{233}U/^{236}U ratios possible [24].

Facing the importance of the detection of ^{233}U and ^{236}U for the future application in environmental studies and nuclear industry monitoring and forensics, the single most crucial goal is to increase the ionization efficiency, of $\approx 10^{-4}$, which comprises a common drawback for the method of AMS. To put this into perspective, the relative abundance of ^{236}U/^{238}U is of the magnitude of 10^{-9} in the Pacific Ocean and for ^{233}U/^{238}U even two orders lower. The ^{233}U/^{236}U ratio to distinguish atmospheric weapons fallout from Irish Sea water influenced from civil nuclear industry releases only vary between $(1.40 \pm 0.15) \times 10^{-2}$ and $(0.12 \pm 0.01) \times 10^{-2}$. For this recently established method by Hain et al. 2020 [24], especially the low ^{233}U count rates of $< 10^{-2}\mathrm{s}^{-1}$ needs several hours per sample to achieve the required uncertainty for ultra-trace isotope measurements [64]. AMS facilities like the Vienna Environmental Research Accelerator (VERA) already have to prioritize measurements due to the available instrument utilization time. Every gain in ionization efficiency offers a substantial lever for further improvement of the method of AMS

in terms of even smaller sample sizes, faster measurements or even better precision.

Zhao et al. 2010 [77] and Cornett et al. 2015 [10] indicated, that the use of U embedded in PbF_2 powder enables the formation of a strong UF_5^- current by caesium sputtering. However, they presented rather artificial setups which can not be directly implemented to the standard actinide sample preparation. Zhao et al. 2010, used pure U powder and Cornett et al. 2015 showed results for co-precipitated Pu or Am with NdF_3. In addition, earlier research showed that that UF_5^- currents are reduced in the presence of metals e.g. Al. They seem to bind with F instead, as indicated by a former diploma thesis at VERA [75].

The main objectives of this thesis were the investigation of matrix compositions to efficiently produce UO^- and UF_5^- currents by using Fe or Nb and PbF_2 powders. The majority of experiments were conducted using a caesium sputter ion source at an injection beamline of VERA. Shorter measurement duration and higher ionization efficiency would enable higher sample throughput. Easier and faster alternatives of chemical sample preparation were investigated. Therefore, drying procedures to reduce the sample size, inspired by Eigl et al. 2020 [13], were assessed. Subsequently, the UF_5^- results should be adopted to find a suitable AMS setup for the subsequent detection of ^{233}U and ^{236}U by UF_5^- extraction. Finally, the obtained method was compared to the present UO^- extraction used for routine measurements at VERA.

2. Introduction

2.1. Isotopes of uranium

The element uranium has a proton number of 92 and its most abundant isotopes is the primordial ^{238}U with 99.2742(10)% and a half-life $t_{1/2} = 4.468(6) \times 10^9$ yrs. The next most abundant isotopes are the primordial ^{235}U accounting for 0.7204(6)% with $t_{1/2} = 7.04(1) \times 10^8$ yrs and ^{234}U for (54 ± 5) ppm characterized by $t_{1/2} = 2.342(4) \times 10^9$ yrs which forms as part of the uranium-radium series beginning with ^{238}U [36; 39]. In addition, there are two long-lived trace isotopes of uranium, namely ^{236}U and ^{233}U which are mainly of anthropogenic origin. They are released to the environment in the course of human nuclear activities as nuclear power plants and atmospheric weapons testing [8; 24]. To a minor extent they are naturally produced in uranium rich minerals [63]. The fact, that U is soluble in water and especially in Sea water, makes it favorable to comprehend natural transport processes [11; 33].

2.1.1. Abundance of ^{236}U in the environment

The trace isotope ^{236}U has a half-life of $t_{1/2} = 2.342(4) \times 10^7$ yrs [39]. The two most relevant nuclear reactions that lead to ^{236}U are outlined. First, it is formed by the ^{235}U(n,γ)^{236}U reaction which has a thermal neutron capture cross-section of 98.7 b [58], about 1/6 of $\sigma[^{235}\mathrm{U(n,f)}] = 585$ b, where the nucleus undergoes fission instead. For fast neutrons the production of ^{236}U through this reaction is reduced due to a low cross-section of only (0.4 - 0.1) b, which is substantially suppressed. A second path for ^{236}U to form is via ^{238}U(n_f,3n)^{236}U with a cross section of approximately $(0.1 - 0.9)$ b in the region of 12 MeV to 25 MeV neutrons[74], which is predominantly reached by thermonuclear weapons and fast breeder or fast spectrum nuclear reactors types.

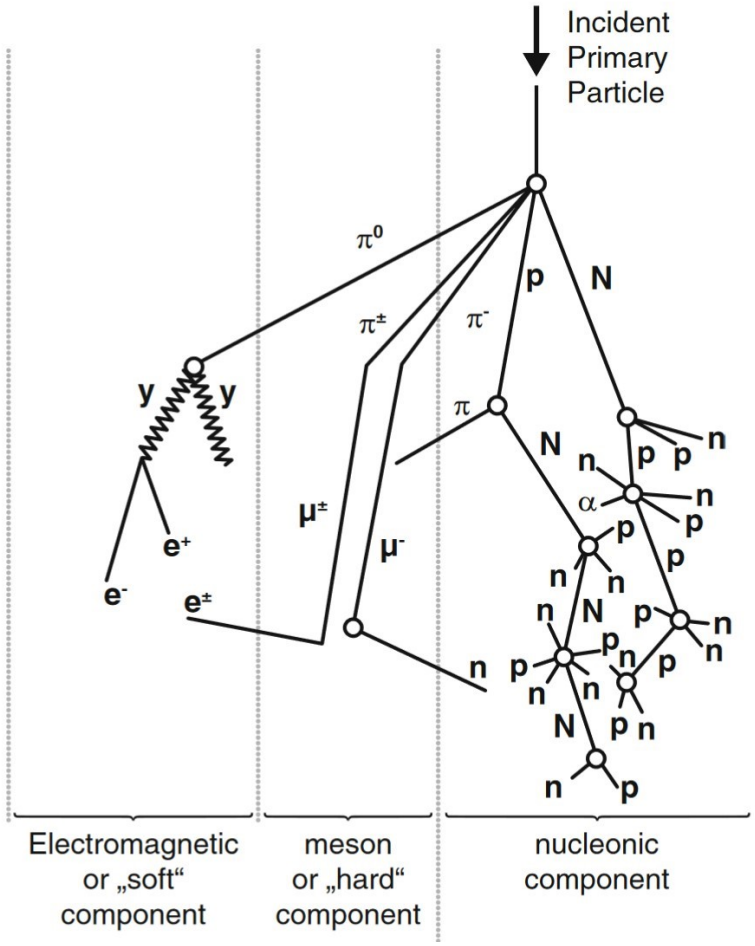

Figure 2.1.: Cascade of secondary particles produced by incident primary cosmic ray (taken from [59]). Circles represent nuclear disintegration of nuclides in atmospheric molecules and capital letters N, P are used for high energy nucleons.

The neutrons for the (n,γ)-reaction may have various sources, e.g. moderated neutrons from (α,n) reactions on light nuclei, where α-particles stem from thorium and uranium in rocks and ores or neutrons moderated on the Earth's surface from cosmic rays. The leading anthropogenic source for overall ^{236}U inventory, that is still stored in reactor cores, are moderated neutrons inside thermal nuclear reactors [63]. Nevertheless, substantial amounts of anthropogenic ^{236}U has been released to the environment by nuclear fuel reprocessing plants as Sellafield (UK) and La

Hague (FR) [8]. While fast breeders are a possible source of considerable ^{236}U releases via (n_f,3n) for the future, atmospheric nuclear weapons testing between 1952 and 1962, already led to the most substantial increase in global ^{236}U inventory. For the North Atlantic, the amount of ^{236}U from global fallout and direct releases of reprocessing plants was calculated to range from 1000-1400 kg and 115-250 kg for the respective sources [8]. Moreover, the total amount of anthropogenic ^{236}U ever produced in the world, assumed by total uranium mined, is in the order 10^6 kg stored in facilities for nuclear waste [63]. Hence, measuring the ratio ^{236}U/^{238}U is a useful tool for monitoring activated uranium content in the environment.

Natural production of ^{236}U is also due to neutrons emanating from secondary cosmic particles colliding with atoms in the atmosphere. In Fig. 2.1 the three main components of secondary cosmic particles are depicted. From both the mesonic or "hard" component and the nucleonic component, generated neutrons are able to reach ground and lead to ^{236}U formation. In these collisions not only fast neutrons are produced from incident primary cosmic rays but also a fraction of neutrons with thermal energies. In addition, ^{236}U is derived by the formerly stated production via alpha-induced neutron emission (α,n) for light nuclei like ^{6,7}Li, ^{9}Be, ^{10,11}B, ^{12,13}C, ^{6,7}Li, ^{14,15}N and ^{17,18}O. The incident α particles emanate from ^{232}Th and ^{238}U. Natural ^{236}U of about 22 kg originate from rock formations, further 10 kg from surface neutron exposure and only 1.5 kg within natural uranium ore by neutron capture [63]. To sum up, the estimated amount of $\simeq$ 35 kg of natural ^{236}U in the top-most 1000 m of land surface is clearly outweighed by anthropogenic contribution by nuclear weapons fallout and the worldwide nuclear industry. ^{236}U is accordingly a predominantly anthropogenic radionuclide.

The amount of ^{236}U in a solid or aqueous sample and also the ratio ^{236}U/^{238}U varies in orders of magnitude with composition of the underlying rock composition and possible for anthropogenic influence. In Irish Sea surface water levels of ^{236}U/^{238}U of $\approx 2 \times 10^{-6}$ can be found, whereas pre-anthropogenic levels of $\approx 6 \times 10^{-12}$ were found for subsurface well water in Gastein (Austria). These typical abundances of ^{236}U from natural and anthropogenic sources have been investigated by AMS. Facilities especially suited for the determination of actinides

Table 2.1.: Overview on ^{236}U concentration and ^{236}U/^{238}U ratios for natural and anthropogenically influenced samples.

Sample	conc. ^{236}U(atoms/g)	^{236}U/^{238}U	Sample description
Gastein 1	-	$(6.5 \pm 2.1) \times 10^{-12}$	2.5 l subsurface well water, Bad Gastein (Austria) [63]
Vienna-KkU	$(9.0 \pm 0.4) \times 10^{10}$	$(6.98 \pm 0.32) \times 10^{-11}$	In-house standard, K.k Uranfabrik Joachimsthal [63]
BD17_60m	$(9.26 \pm 0.42) \times 10^{3}$	$(12.30 \pm 0.54) \times 10^{-10}$	1 l North Pacific Ocean water 60 m depth, KH-12-04 GEOTRACES [13]
IAEA-381(443)	-	$(2.04 \pm 0.02) \times 10^{-6}$	5 l IAEA reference material from Irish Sea surface water, sampled 1993 [14]

down to the levels of $\approx 10^{-13}$ and below, enable the use of ^{236}U as environmental tracer in aqueous environments [8; 13]. Furthermore local input from river discharge of nuclear power plants as well as global fallout determination and inspection of resulting particle migration routes are prime examples [49; 50]. In case of the North Pacific isotopic ratios in the order of $^{236}\mathrm{U}/^{238}\mathrm{U} \simeq 10^{-11} - 10^{-9}$ were found [1; 13]. Additional investigations of depth-distributions in the water column indicated mainly surface deposition anthropogenic input to explain the higher concentration in surface waters compared to greater depths. An overview of ^{236}U concentration in different compartments of the environment, is given in table 2.1 for comparison.

2.1.2. ^{233}U and its relevance to source identification

The second long-lived trace isotope of uranium is ^{233}U. It has a half-life of $t_{1/2} = 1.592(2) \times 10^5$ years [39]. In case of trace isotope analysis, ^{233}U is often used for the absolute determination of the ^{236}U concentration via isotopic dilution [8; 6]. On the other hand it was produced as the proposed thorium cycle fuel for the nuclear industry [34]. Furthermore, ^{233}U was directly used as fissile material for nuclear weapons testing, as well as generated as a byproduct during operations that used blankets of highly enriched ^{235}U in thermonuclear devices [24].

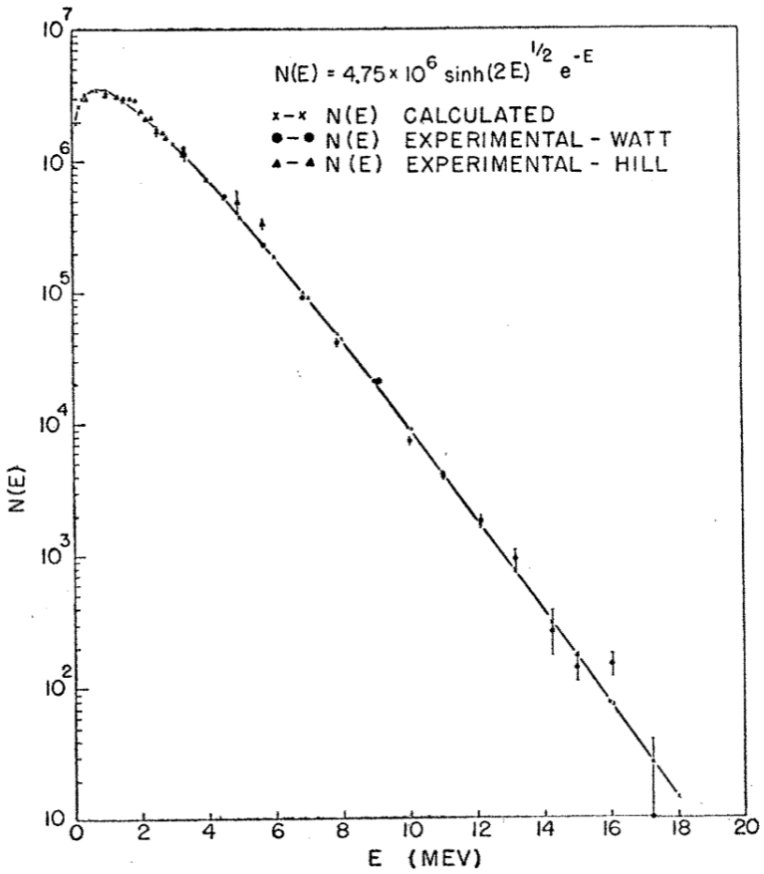

Figure 2.2.: Neutron flux spectrum of the ^{235}U(n,f) reaction, taken from [72]

The first of two prominent paths of production is via ^{232}Th(n,γ), thus creating ^{233}Th ($t_{1/2}$ = 21.83(4) minutes [39]) followed by two successive β^--decays creating the nuclide ^{233}Pa ($t_{1/2}$ = 26.975(13) days [39]) and leading to ^{233}U. The second path is directly by ^{235}U(n$_f$,3n)^{233}U. For the reaction path via ^{233}Th, detailed cross-section data for $\sigma[^{232}\mathrm{Th}(n,\gamma)]$ shows a maximum of around 10 b for thermal neutrons and decreases from thereon down to to 0.1 b at 2 MeV, which represents fast neutrons [74].
The reaction ^{235}U(n$_f$,3n)^{233}U occurs according to cross-sectional data only above a threshold value of about 13 MeV [74]. Neutrons with energies above this threshold, are provided by thermonuclear devices. For instance, the fusion reaction of deuterium and tritium in equation 2.1 generates neutrons with 14.1 MeV sufficiently energetic for ^{235}U(n$_f$,3n)^{233}U reaction. In contrast to thermonuclear weapons only a very limited amount of 0.01% of neutrons from nuclear fission reach energies above 13 MeV. The Watt spectrum for neutron flux distribution versus emitted neutron energy from ^{235}U(n,f) is depicted in Fig. 2.2. Cross-sectional data for both major ^{233}U generation paths is shown in the appendix in Fig. A.4a and Fig. A.4b.

$$\mathrm{d} + \mathrm{t} \rightarrow \alpha(3.5\,\mathrm{MeV}) + n(14.1\,\mathrm{MeV}) \tag{2.1}$$

Two sequences of events are thought to dominate anthropogenic ^{233}U emissions to the environment. The first is direct release of ^{233}U used as fissile material in atmospheric nuclear weapons testing. Incidents like the "MET" explosion of the operation named Teapot, at the Nevada Test Site in early 1955, represent a probable emission scenario [66]. Secondly, the path via ^{235}U(n$_f$,3n)^{233}U is strongly indicated where thermonuclear weapons using highly enriched blankets of ^{235}U were tested. One of the supposed operations was Hardtack I in 1958 at Enewetak Atoll, a part of the Pacific Proving Grounds (PPG) [65]. The generation of natural ^{233}U via thermal neutrons in Th-rich minerals as pitchblende and Brazillian monazite has been identified to exhibit ^{233}U/^{238}U concentrations [42] below reservoirs with antropogenic influence from global fallout. It has to be assumed that natural ^{233}U is mainly stored in such mineral formations [24].

The Relative abundance of $^{233}U/^{236}U$ in the environment is about 1% [24] and therefore even harder to detect than ^{236}U. Recently the VERA facility in Vienna reached high enough instrumental sensitivity to detect uranium isotopes on the level of $^{236}U/^{238}U \approx 10^{-13}$ [64]. The promising method of simultaneous detection of ^{233}U and ^{236}U was already used for source assessment of anthropogenic radionuclides and the corresponding reservoir as well as their mixing ratios. Hain et al. 2020 [24] obtained the first isotopic ratios of $^{233}U/^{236}U$ to distinguish between samples influenced by nuclear weapons fallout and civil nuclear industry emissions. Values stretch about one order of magnitude, from $(1.40 \pm 0.15) \times 10^{-2}$ for Black Forest peat core representative for global fallout and $(0.12 \pm 0.01) \times 10^{-2}$ for Irish Sea sediment mainly influenced by nuclear industry remains as contamination source [24].

To sum up, the method of combined detection of $^{233}U/^{236}U$ [24] enables the identification of possible contamination reservoirs like $^{239-241}Pu$ [23] while benefiting from conservative behaviour of U in aquatic environments. Increasing the ionization efficiency of U containing molecules is most critical where the relative abundance of ^{236}U or ^{233}U in comparison to ^{238}U is in the region of the detection limit. This limit for $^{236}U/^{238}U$ and $^{233}U/^{238}U$ is presently on the level of several 10^{-13} using UO^- extraction [64]. Samples with isotope ratios near this limit are of low natural ^{236}U production [63] or low anthropogenic ^{233}U influence [24].

2.2. Analysis of Actinides by AMS

Typical uranium extraction from caesium sputtering for AMS applications is performed by using uranium oxides in the form of $^{238}U^{16}O^-$ [73]. U^- doesn't readily form stable atomic anions due to its low electron affinity of $\leq 0.52\,eV$ [19]. For the investigation of an environmental sample U hast to be present in a manageable macroscopic matrix material. Using the standard actinide preparation method, the uranium fraction is co-precipitated with iron solution. To achieve $>90\%$ U extraction from the solution at least 2-3 mg Fe have to be used [48]. Otherwise U remains in solution. By an annealing step of several hours above 800° the remaining moisture is removed. The sample gets oxidized to Fe_2O_3 and UO_3. Thereafter, the sample is pressed into cathodes and measured.
Trace isotope analysis at VERA, involving ^{236}U, ^{233}U and actinide isotopes of Np, Pu and Am, are carried out using a 3-MV Pelletron AMS instrument. The detailed setup is described in section 3.1 and the most recent measurement procedure for actinides is given in [24]. A molecular beam of UO^- is introduced to the accelerator and extracted in the optimal charge state for ion optical transmission and suppression of molecular isobars. This is ^{3+}U [31]. Trace isotope events and the stable ^{238}U current are used to calculate the isotopic ratios. Subsequently they are corrected with a standard and weighted by their individual uncertainty (section A.7). In case of ^{236}U measurements, the in-house standard Vienna-KkU ($^{236}U/^{238}U = (6.98 \pm 0.32) \times 10^{-11}$) [63] is mixed with Fe_2O_3 (1:30 by weight) when used for correction. For measurements of ^{233}U it serves as machine blank. With the outlined VERA setup, an overall detection efficiency of up to 5×10^{-4} was achieved [73]. The major limiting factor for U isotope detection is the efficiency for forming negative UO^- ions of up to 3×10^{-3} inside the caesium sputter source [17]. Even though earlier research at VERA to reduce the matrix mass showed an increase in ionization efficiency [13], this did not prove to be easily adoptable. Electrostatic charge makes handling of dry sub-milligram samples unmanagable for routine sample preparation.

2.3. Production of negatively charged ions

The formation of a negative ion is based on the physical mechanism that a molecule or an atom captures a surplus electron [54]. This is characterized by the electron affinity. The processes to describe the production of negatively charged particles are named after the origin of electrons taken up. In ion sources for negative ions, they are categorized as "surface effect", "volume production" and "charge transfer" whether electrons are taken up from a conduction band of a metal, a plasma or a free particle [5]. The main focus of this work will be on the surface and volume production. Until now, not one of them could be ruled out. Both seem to be relevant for Middleton-type, caesium sputtering ion sources, which are used for AMS.

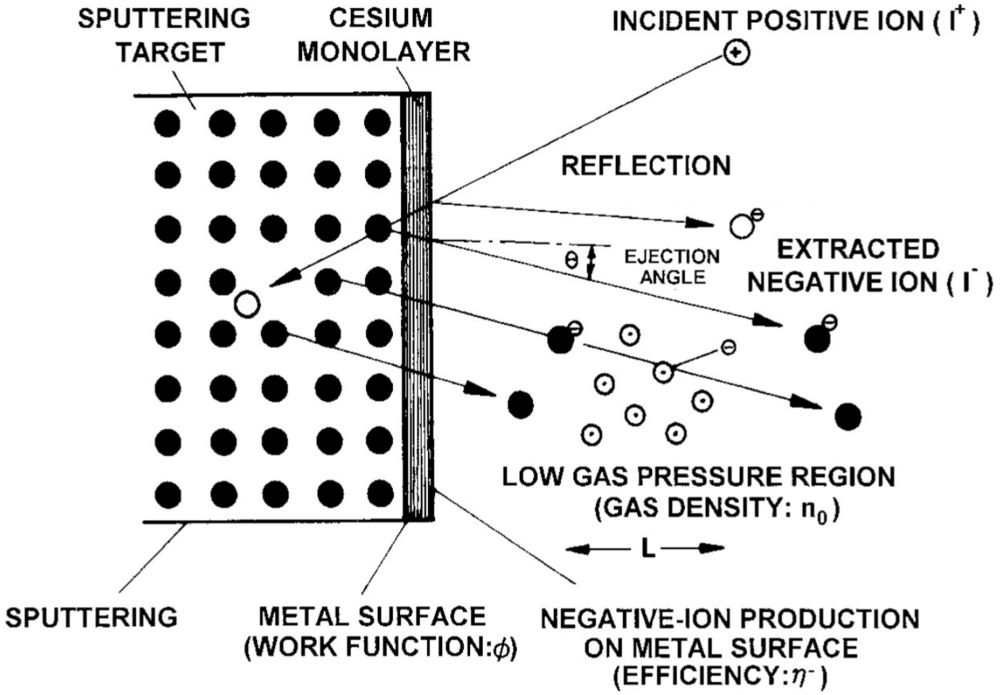

Figure 2.3.: This figure was taken from [5] and edited. It gives a schematic overview how positive incident ions sputter neutral atoms from a bulk metal through an adsorbed caesium monolayer. In light of the surface effect, the negative ion formation takes place in the region of the ceasium monolayer surface [26].

2.3.1. Negative ion production by surface effect

The surface effect describes the tunneling of an electron from the Fermi level in the conduction band of a metal to the electron affinity level of an atom or molecule that approaches the metal surface. The probability of this effect to take place is strongly facilitated by lowering the effective work function of the metal surface. Two processes are connected to the ion ejection from a metal surface. The heavy particle reflection and sputtering of heavy particle by positive ions. In Fig. 2.3 the processes participating in the surface effect are shown as well as the most critical quantities. These are the positive sputter ion current, I^+ and the negative ion production yield, η^-. Counteractions for the negative ion production are electron detachment collisions of neutral particles (i.e. neutral Cs, sputtered particles) in front of the sputter target. n_0 denotes the density of neutral particles, L the mean free path and σ_d is the electron detachment cross section for a produced particle [26; 5]. Equation 2.2 shows the extracted negative ion current I^-. The negative ion production efficiency is dependent on the velocity distribution $f(v)$ of the incident or reflected particles, combined with the production probability $P^-(v)$. Velocity v is the normal velocity relative to the sputter target in equation 2.3.

$$I^- = I^+ A \eta^- e^{-n_0 L \sigma_d} \tag{2.2}$$

$$\eta^- = \int P^-(v) f(v) dv \tag{2.3}$$

The theoretical analysis of the negative ion production probability was done by Rasser et al. 1982 [53] and led to equation 2.4. It describes the dependency of negatively charged ions from the metal surface work function ϕ, the electron affinity of the incident molecule or atom E_a, the ejection angle of the emitted particle θ and the decay factor a. The decay factor a can be understood as constant of a decaying probability of charge transitions between charge states of outward scattered particles from an ionizing/heated surface [41].

$$P^-(v) = \frac{2}{\pi} \exp\left[\frac{-\pi(\phi - E_a)}{2av\cos\theta}\right] \tag{2.4}$$

The above equation holds as long as the velocity of emitted particles normal to the metal surface, the term $v\cos\theta$, is higher than $10^4\,\mathrm{m}\,s^{-1}$. This corresponds to light particles as in hydrogen ion sources where also the decay factor has been examined [70]. For heavy ions like negatively charged uranium molecules with oxygen or fluorine components the extraction velocity normal to the metal surface is far lower than hydrogen, than equation 2.4 was primarily intended for. A modified semi-empirical equation for the production probability of massive negative ions was found by Ishikawa et al. 1994 [28], given in equation 2.5. To facilitate the formation of negative ions, a decrease in the work function yields a substantial increase in production probability (equation 2.5). Decreasing the work function of the metal surface is therefore fundamental for a highly efficient production of negatively charged ions. This is especially the fact for ion sources where the surface effect is predominantly seen as the production mechanism for secondary negative ion emission [5].

$$P^{-}(v) = \frac{2}{\pi}\exp\left[\frac{-(\phi - E_a)}{(2av\cos\theta)/\pi + k_B T_{\mathrm{eff}}}\right] \tag{2.5}$$

Depending on the literature [60; 5], Cs has the lowest work function of all the elements with ϕ between 1.81 eV and 2.0 eV, dependent on the crystal direction. The work function describes the energy needed to remove an electron from a material surface that from the Fermi level to an outside vacuum in the band model. Application of Cs deposited onto another metal surface consistently decreases the work function of the layered metal compound, even lower than the work function of a caesium bulk material and is calculated by the given empirical equation 2.6. V_i is the first ionization potential, E_a the electron affinity of the deposited material (e.g. Cs) on the metal surface and ϕ_0 the work function of the metal substrate surface [2].

$$\phi_{\mathrm{min}} = 0.62 \cdot (V_i + E_a) - 0.24 \cdot \phi_0 \ [\mathrm{eV}] \tag{2.6}$$

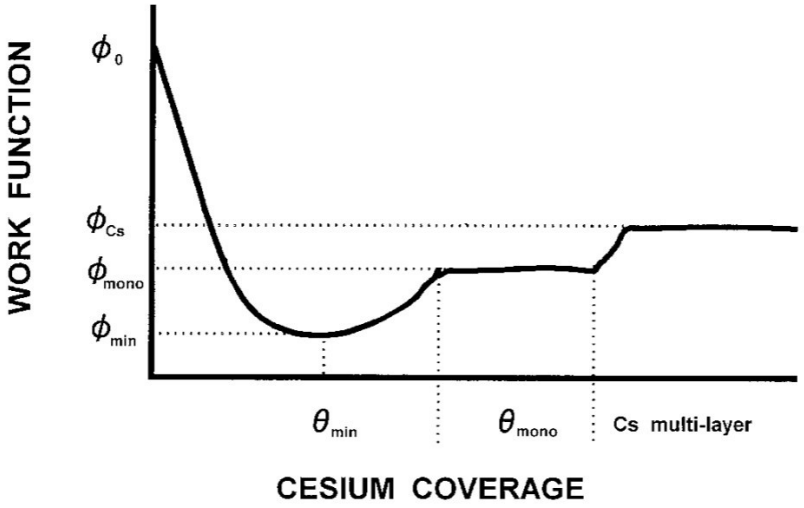

Figure 2.4.: The characteristics of the work function of a metal-Cs surface with increasing caesium coverage, taken from [18]. Sub monolayer depositions of Cs e.g on a clean W surface generate the lowest (ϕ_{min}) known work function ϕ of metal-metal surfaces. Further increased Cs layer thickness generate higher compound work functions [5].

The work function of a clean tungsten surface without oxidation declines with a build up in caesium layer thickness by a characteristic curve, given in Fig. 2.4. Without any caesium the work function remains at $\phi_0 = 4.5\text{-}6\,\text{eV}$, with increasing Cs deposition, but nonetheless thinner than a monolayer, ϕ drops to the minimum $\phi_{\text{min}} = 1.37\text{-}1.45\,\text{eV}$ [5; 70] that equals about 0.6 atomic Cs layers. ϕ_{min} can be calculated with equation 2.6. With further caesium supply, its thickness arrives at one monolayer and a plateau at ϕ_{mono} corresponding to 1.56-2.15 eV is reached [18].

The metal-Cs bonding remains stable from room temperature to several hundred °C and no further build up in Cs occurs. This temperature range allows for highly efficient negative ion production by incident positive ion sputtering. Only if the caesium is cooled too much, e.g. with liquid nitrogen, Cs-Cs bonding is strong enough to sustain a multilayered structure upon the metal surface [5].

Negatively charged ions that exit the region of their origin at the metal-Cs surface are subject to the process of single (σ_{-10}) and double electron detachment (σ_{-11}) with the respective cross sections adding up to $\sigma_{-10} + \sigma_{-11} \approx \sigma_d$ in equation

2.2. The most contributing factor in the case of ion sources is the single electron detachment and its effect can be lowered by reducing the gas pressure in the ion source to get an ion survival rate of over 93% at a pressure of 0.13 Pa [27; 68].

2.3.2. Negative ion production by resonant electron transfer (RET)

The theory of surface ionization explains the relation between negative ion production and sputtered material properties together with caesium layer thickness and relative incident particle velocity in a precise manner. However, it lacks in explaining why sputter target geometry and surrounding target material also seem to change the production characteristics for negative ions [25]. A competing theory by Vogel et al. 2015 [71] states that surface ionization extracts merely a small fraction of atoms as anions. Most of the anion formation, according to Vogel, takes place in a recessed caesium plasma within a sputtered cone right in front of the sample material. This plasma interacts with neutral atoms from sputtering. Ionization happens when an electron is provided by a donor atom like Cs to the sputtered neutral particle (acceptor) and the ionization potential (IP) of the donor (Cs) matches the IP of an unoccupied acceptor electron state. Moreover, for the acceptor atom or molecule to become a stable anion, the empty electron IP has to be "nearly equal" to its electron affinity. The process taking place is called resonant electron transfer (RET). The basic mechanism was explained in Dutta et al. 1979 [12].

2.4. Fluoride as light secondary ion

The formation of stable single negatively charged ions is very much dependent on the electron affinity of an atom or molecule as it describes how well a certain element or molecule holds onto the surplus electron. [54]. To increase the electron affinity of a certain elemental compound, it is possible to utilize the formation of negative molecular ions through a second atom with substantially higher electron affinity. Since the resulting molecular weight is higher than the atomic mass of the pure element, this means a decline in the examined element's share of kinetic energy if accelerated. Moreover, this increases beam scattering, due to coulomb explosion in the stripper gas used for AMS [38].
These shortcomings can be mitigated, if high electron affinity compounds with light secondary ions exist. Notable combinations to form molecules alike include hydrides, oxides and fluorides, which can provide stable compounds with higher electron affinity than the atomic anion. On the other hand, the multiplicity of hydrides leads to the possible injection of different isotopes of the same element. In addition, oxygen likewise provides three possible stable isotopes to be coupled with the isotope of interest, namely ^{16}O, ^{17}O and ^{18}O with a natural abundance of about 99.762%, 0.038% and 0.200% [36]. In comparison with hydrogen and oxygen as secondary ion to form negatively charged particles, fluorine proved to be advantageous [76]. Possessing the highest electron affinity of the halogenes and in general of all the chemical elements, it elevates the electron affinity of the formed molecular ion containing it. Secondly, fluorine has only a single stable isotope which inhibits the effect that isotopes of the same element pose risk for isobaric interference effectively. The formation of molecules with multiple fluorine atoms bound to one element M are called "superhalogen" ions of the form MF_n^- [20]. Another possible notification is MF_{k+1}^- taking into account the valency k of the element M. Examination of superhalogen anions for negative ion formation inside caesium sputter sources showed a considerable increase in total ion current for actinides and other elements [77]. Various molecular systems in combination with fluoride and especially metal fluoride compounds prove to possess higher electron affinity than that of Cl^- (3.61 eV) [4]. The above characteristics are underlined by the findings of Zhao et al. 2010 [77] for superhalogen molecules. In the case of

the most prominent actinides, the molecules UF_5^- and PuF_4^- / PuF_5^- indicated higher ion currents in comparison to their routinely used oxide counterparts. A possible downturn of fluorine-rich molecules for AMS would be the increased beam scattering. In example for UF_5^- the F fraction accounts for about 6 times higher share of total mass compared to the UO^-, which is normally used for AMS of U.

2.4.1. PbF_2 facilitating fluoride formation

Superhalogens indicate beneficial molecule formation for their use in AMS. High ionization efficiency and isobaric suppression are fundamental to increase the analysis speed and overall detection efficiency of the AMS method. To aid the formation of MF_n^- molecules, mainly PbF_2 was used as fluorinating agent [77]. Already in 1838 Michael Faraday reported that the electrical conductivity of PbF_2 increases with temperature [15], specifically above $\approx 250\,°C$. This effect was later attributed to a phase transition where upon the fluorine crystal's atomic mobility rises to levels where it seems more like a liquid electrolyte with F^- ions released from their lattice positions [7]. Zhao et al. 2010 reported an instant surge in the electric conductivity upon sputtering with Cs^+. These observations indicate that even electrically non-conducting compounds produce superhalogen anions as long as PbF_2 was present and heated up above its phase transition temperature. No additional conductivity enhancers were needed. Elements throughout the periodic table were tried out for their ability to form superhalogen compounds, which laid the most important track for thorough research on uranium fluorides as UF_5^- [77]. Another advantage of superhalogen molecules is that neighboring elements tend to attach one more or less fluorine atoms leading to significant isobaric discrimination between them [77]. Previously, the extraction of other actinides i.e. Pu and Am as superhalogen molecules was investigated. The optimal mixing ratio of PbF_2 to a NdF_3 matrix material for Pu and Am ranged from 6 to 9 [10]. In addition, PbF_2 facilitates the formation of UF_5^- from samples of co-precipitated UF_4 with NdF_3 [43]. However, a recent diploma thesis at VERA found, that different sample holder materials (i.e. Al, Cu, Au,..) result in significant variations in ionization efficiency. Al sample liners reduced UF_5^- formation, whereas Au increased its ionization efficiency [75]. With the underlying mechanism still remaining unknown,

this work wants to identify reliable conditions for UF_5^- extraction in caesium sputter sources.

3. Methods

3.1. Vienna Environmental Research Accelerator (VERA)

The Vienna Environmental Research Accelerator (VERA) is a facility dedicated to accelerator mass spectrometry (AMS). The whole instrument is located at the University of Vienna, Austria and was financed in the year 1993 by the Austrian Federal Ministry of Science and Research [30]. It performed the first radiocarbon precision measurements in 1996 and was expanded to measure cosmogenic ^{182}Hf, actinides (e.g. ^{236}U, ^{244}Pu) and other lighter isotopes (e.g. ^{10}Be, ^{26}Al, ^{36}Cl) [44; 62; 35]. A scheme with the essential componets labeled is given in Fig. 3.1.

The AMS setup at the VERA facility provides two multi-cathode sources for negative ions by caesium sputtering (MC-SNICS) situated at two different injection beamlines prior to the accelerator. Both feature 40-cathode wheels, adapted for automated cathode change [45; 46] and produce negatively charged ions through interaction of caesium vapour depositions (section 2.3) and preaccelerate them to energies ranging from 20 keV to 70 keV. Thereafter the ions are separated and filtered in subsequent steps by electrostatic analyzers (ESA) as well as analyzer or bending magnets (BM) with a 90° deflection angle in the horizontal plane. A Multi Beam Switcher (MBS) at the first bending magnet allows for fast sequential injection of ions of different masses by changing the particle energy. Afterwards, the molecules are injected into the accelerator which provides a high positively charged electrostatic potential in combination with a so-called "stripper gas" or foil that constitutes an interaction target for the negative ions to break up molecular bonds. The stripper gas selection depends on the introduced particle species

with the aim of efficiently removing electrons, while sustaining high particle transmission in one specific charge state. Ions with different positive charge states are once more accelerated by the now repulsive potential of the positive high-voltage terminal. This type of accelerator is called "tandem accelerator, which in the case of VERA is a 3-MV Pelletron, constructed by the National Electrostatics Corporation (NEC). Following the accelerator, the separation of ions with a defined momentum-over-charge ratio, is repeatedly performed with BM and ESA components to reach an ever higher discrimination of particles with adjacent atomic masses. Other beam optical elements (e.g. steerers and lenses) and diagnostical components like Faraday Cups (FC) and beam profile monitors (BPM) enable the dynamic tuning of the facility for the various isotopes and to obtain maximum ion-optical transmission. Faraday Cups are devices to measure the charge of ions deposited inside a cylindrical volume. For the detection of single ions there are several options available at VERA, like gas ionization chambers (GIC) with two anodes to discriminate elemental species by Z-dependent energy loss in gases or one Bragg-type GIC that is commonly used for the detection of trace actinides at the very end of the instrument [64].

Figure 3.1 illustrates the whole AMS setup at VERA, where only the most important details for this thesis are highlighted. FCs are indicated by the beamline section where they are situated and an ongoing number. The presented setup allows for independent measurements using ion source S2 and the corresponding low energy beamline up to the position of FC I2-2 (see Fig. 3.1, if the accelerator is occupied with measurements run from ion source S1.

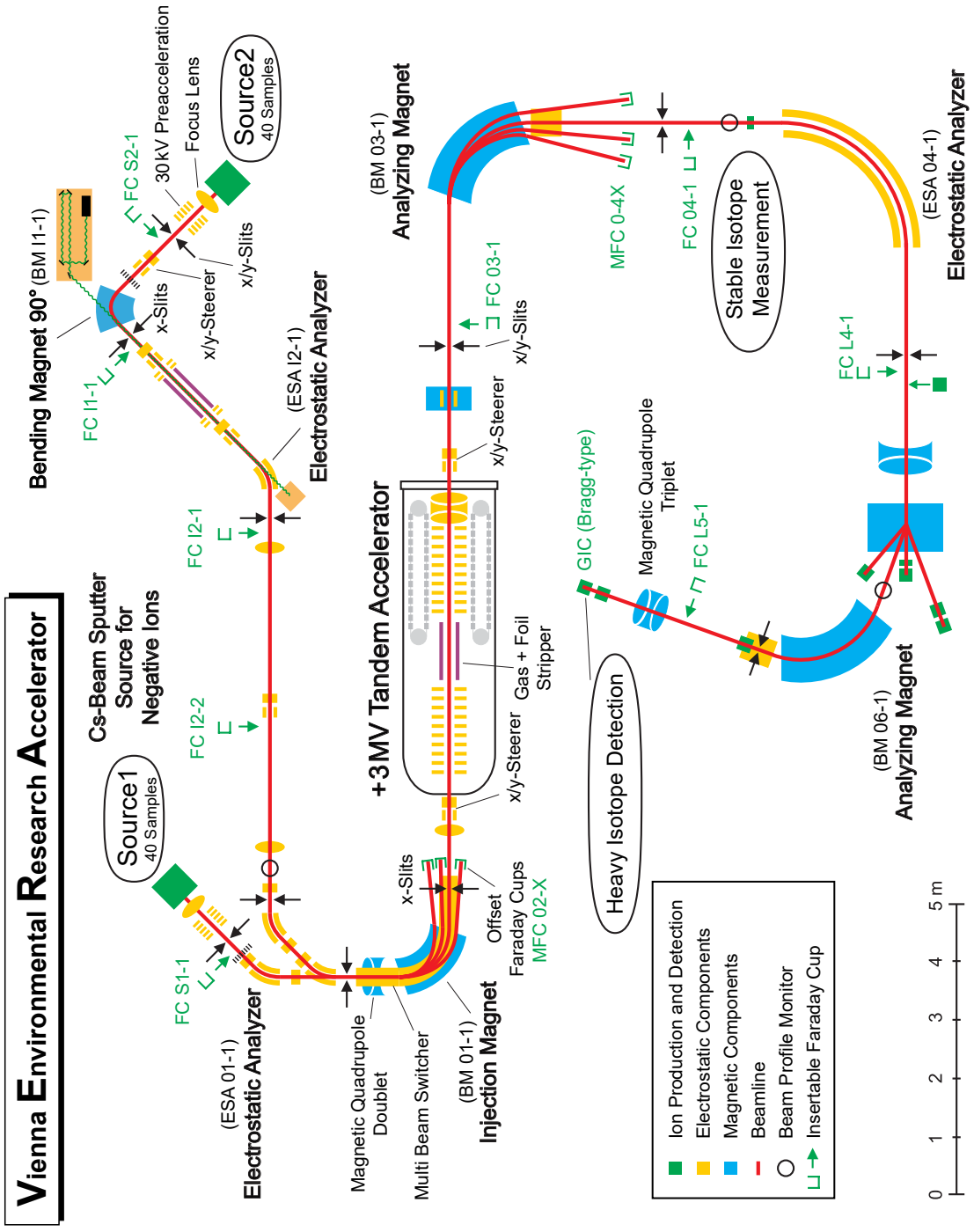

Figure 3.1.: A scheme of the whole VERA instrument where the most significant parts for this Master's thesis are shown. The fully labeled VERA scheme taken from a VERA intern repository is given in the appendix A.1

3.2. Multi cathode source for negative ions by caesium sputtering (MC-SNICS)

SNICS, or otherwise called "Versatile negative ion source" (VNIS) by R. Middleton [37], are ion sources with a broad range of applications for the production of negatively charged particle beams. VERA utilizes two 40-cathode MC-SNICS from NEC with an automated cathode changing mechanism. Cathodes are provided by NEC (Middleton, USA). As most of the experiments relevant for this thesis have been conducted at ion source S2, the corresponding low-energy beamline will be explained in more detail. The innermost ion source chamber is equipped with the cathode or sample wheel, the tantalum ionizer assembly and the caesium capillary which is connected to the caesium oven reservoir as its main components in Fig. 3.2.

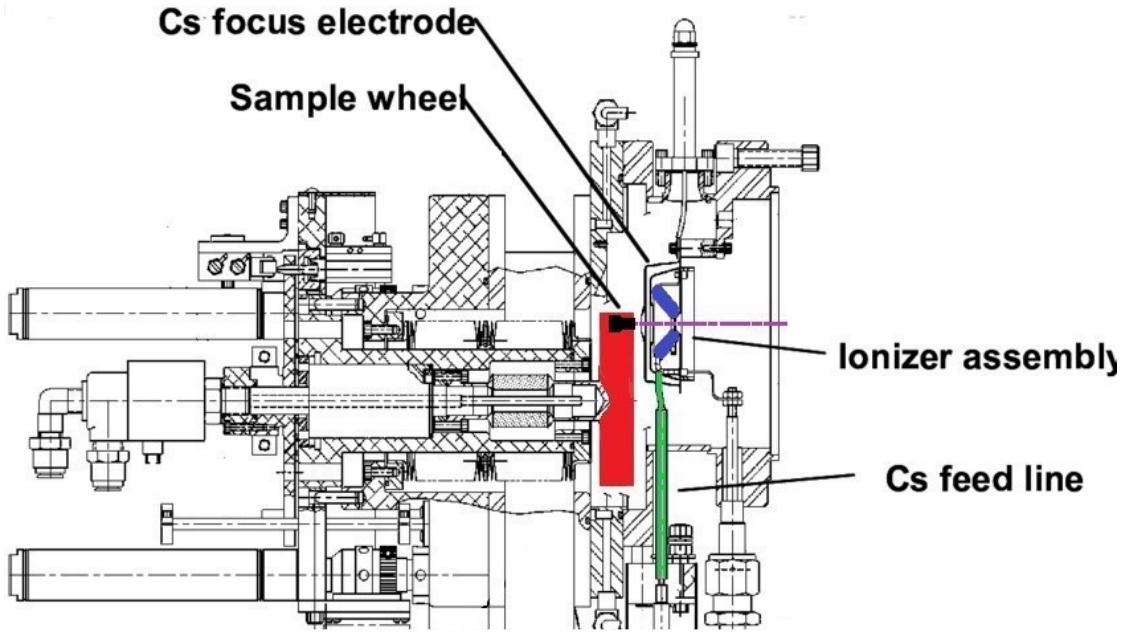

Figure 3.2.: NEC 40-cathode MC-SNICS as sectional view cut in z-direction showing the ion source chamber equipped with sample wheel, tantalum ionizer assembly and the caesium capillary connected to the caesium oven reservoir. Ions leaving the ion source are indicated by the dashed purple line. Figure taken and modified from [61].

The purple dashed line indicates the path of negatively charged particles extracted from the ion source. The cooled sample wheel is kept at a constant $-5\,\mathrm{kV}$ potential (Fig. 3.3) for most of the measurements for which beam optics is optimized. Cs vapour released from the capillary condenses on the walls enclosing the source chamber including the cathode wheel as well as the sample material.

Neutral caesium gets ionized on the hemispherical heated tantalum surface [45] denoted as ionizer (ION, compare fig.3.3). The resulting Cs^+ ions are accelerated towards the negative cathode potential (CAT), where a target shield defines the electric field geometry [45]. The incident Cs beam on the target cathode is optimized via the "caesium focus" (CSF). The positive caesium ion bombardment acts as incident particles for sputtering and ionization (see section 2.3). Electrons get deflected in a magnetic field after the extraction. The extracted ions are much less affected due to their higher momentum to charge ratio. A focus einzel lens (FOC) corrects possible distortions of the beam shape [46]. Ions are then accelerated by the extraction (EXT) and preacceleration stage (HVS). The extraction potential is maintained at about $+15\,\mathrm{kV}$ that attracts negative ions right after the ionizer. The last stage inside the ion source structure is a preacceleration section to boost the energy of extracted negative ions to up to $70\,\mathrm{keV}$.

Raising the temperature of the ionizer as well as caesium supply can be used to control the ion output. Both quantities are controlled by a regulation system to achieve stable ion currents. The needed ionizer temperature and Cs supply to extract sufficient ion current varies over time. Oxide molecule extraction from SNICS usually needs a certain sputter duration to reach maximum output current. This phenomenon is called cathode "burn-in" [45].

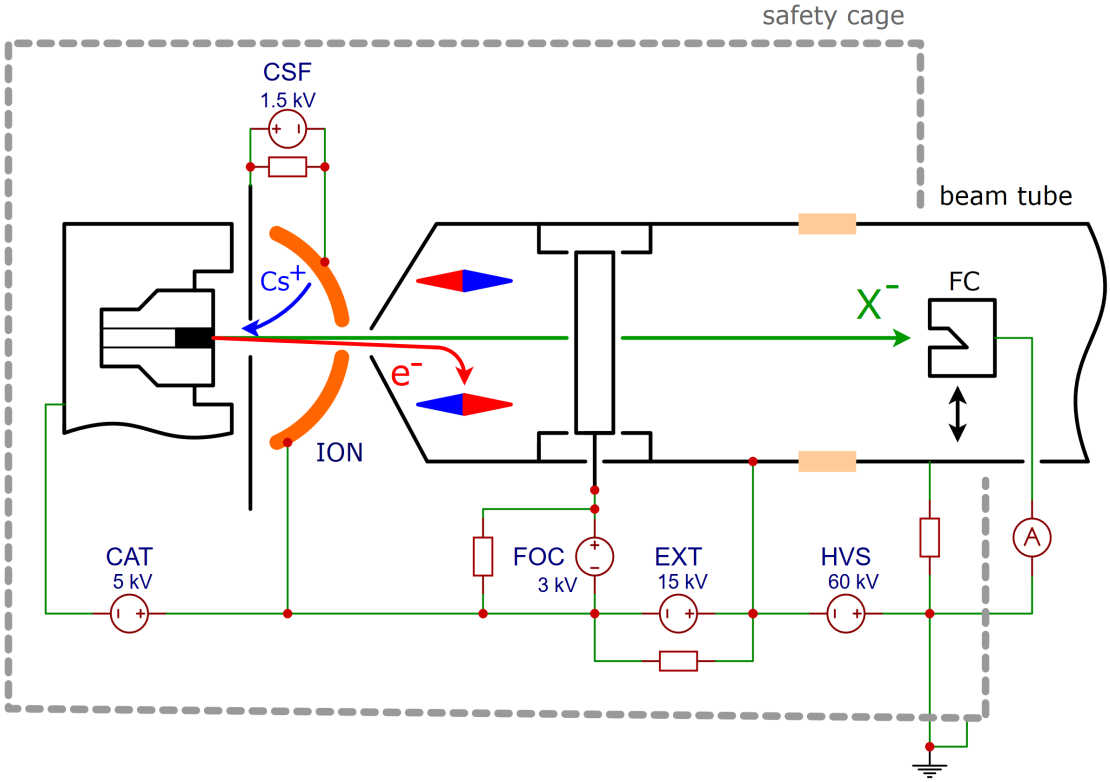

Figure 3.3.: Sketch made by the author, showing a scheme of the electric circuits of one of the caesium sputter ion sources at VERA. The sample is indicated on the left, which is hit by a Cs^+ beam (blue arrow). Sputtered particles are illustrated by the green arrow and electrons deflected in a magnetic field (blue and red dipoles) are shown in red. Important source parameters are the negative cathode voltage (CAT), the ionizer (ION) and the einzel lens (FOC), which is the first beam optical focus element. Subsequent ion acceleration steps are indicated by the voltages of the extraction (EXT) and high-voltage supply (HVS). The sum of the voltages of CAT, EXT and HVS determined the kinetic energy of extracted ions X^-. FC indicates the first, movable Faraday cup.

3.3. Methods and materials for ionization efficiency experiments

3.3.1. Materials for ionization efficiency measurements

To investigate the ionization efficiency of uranium molecule extraction proxy materials were prepared from the in-house $^{236}U/^{238}U$ standard Vienna-KkU [63]. The chemical composition of proxy materials should be similar to the final matrix that the environmental sample is embedded in. Therefore, Vienna-KkU was diluted 1:30 in pre-nuclear iron and fully oxidized above 800°C in a muffle furnace. This dilution was called Vienna-KkU-D30 which is used throughout this thesis as well. Vienna-KkU-D30 was mixed with Fe and Nb in different weight ratios for the investigation of UO^- ionization efficiencies. To examine the ionization efficiency of UF_5^- extraction Vienna-KkU-D30 was mixed with PbF_2 in various weight ratios.

3.3.2. Measurement setup

The negative ions produced in the MC-SNICS ion source were introduced to a beam line setup shown in Fig. 3.4 The first segment outside of the source assembly with focus and preacceleration was a set of remote controlled adjustable slits in x and y direction (SLT S2-1). Every negatively ionized particle from the source was measured in FC S2-1. Right after the FC the beam could be deviated by electrostatic x/y-direction steerers.
Preaccelerated anions influenced by the magnetic field B of the bending magnet BM I1-1, are deflected according to the Lorentz force ($\vec{F}_{\text{Lorentz}}$) and follow a different gyroradius according to their specific $m_{ion}v_{\perp}/|q|$ ratio. In equation 3.1 the centripetal force is denoted by $\vec{F}_{\text{c}}$, the particle charge as q, the particle velocity as $\vec{v}$, as well as the electrical and magentic field as $\vec{E}$ and $\vec{B}$. m_{ion} is the ion mass, $\vec{\omega}$ the angular velocity. The most probable velocity of the ion species of interest $v_{\perp}$ (normal to radial vector $\vec{r}$) at the kinetic energy T determined the pilot beam path following the gyroradius r_g.

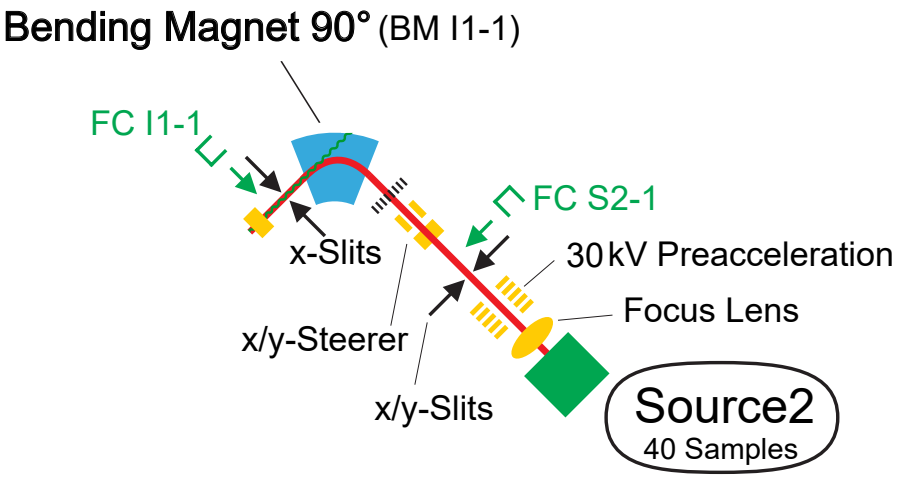

Figure 3.4.: Scheme of the second beamline at VERA, labeled up to FC I1-1. Cut and modified from Fig. A.1

$$\begin{aligned} \vec{F}_{\text{Lorentz}} &= \vec{F}_{\text{c}} \\ q(\vec{E} + \vec{v} \times \vec{B}) &= m(\vec{\omega} \times (\vec{\omega} \times \vec{r})) \\ \Rightarrow r_g &= \frac{m v_\perp}{|q||\vec{B}|} = \frac{\sqrt{2mT}}{|q||\vec{B}|} \end{aligned} \tag{3.1}$$

The bending magnet BM I1-1 was a double focussing 90° magnet with a center line radius of ca. 350 mm, that set the gyroradius for the ion of interest. For better mass resolution the focal point after the magnet is situated near the faraday cup FC I1-1. It was possible to define the beam position with a slit aperture in x-direction right in front of the FC I1-1.
By changing either $\vec{B}$ or T, ion beams with different molecular masses reached the Faraday cup. T and therefore the velocity $v_\perp$ was set by the sum of cathode voltage (U_{CAT}), the extraction voltage (U_{EXT}) and the preacceleration voltage (U_{HVS}, compare Fig. 3.3). The recorded ion currents versus a range of $\vec{B}$ or U_{HVS} were called "mass scans". Equation 3.2 was used to check the molecular mass of ion current peaks in the mass scans.

$$m_{ion} = \frac{|q|^2 r_g^2 |\vec{B}|^2}{2T} = \frac{|q| r_g^2 |\vec{B}|^2}{2 \sum U_{CAT} + U_{EXT} + U_{HVS}} \tag{3.2}$$

3.3.3. Ionization efficiency measurement procedure

Firstly, a pilot beam of the negatively charged molecule or atom in question was needed. For this task Vienna-KkU-D30 mixed with Fe or Nb powder was sputtered for the extraction of UO^- ($m = 254.03\,u$) and UF_5^- ($m = 333.04\,u$) currents. The pilot beam was used for the first manual alignment of all beam optical components. This included the manual adjustment of sample wheel tilt and rotational position in the ion source chamber (see Fig. 3.2). For the following measurements the slit aperture was set to 2 mm for the first manual alignment of the beam and 1 mm during the automatic tuning procedure. Then the bending magnet was set to the constant magnetic field $\vec{B}$, for which the UO^- pilot beam reaches the FC I1-1. Several mass scans were taken for peak identification and mass calibration. Therefore, the preacceleration voltage U_{HVS} was scanned to voltages corresponding to mass 250 u to 305 u in the case of UO^-. Measurements of the UF_5^- ionization efficiency used an atomic mass region of about 285 u to 360 u. Possible differences to this procedure due to different mass regions of the specific investigations, will be stated in every corresponding section of chapter 5 and 6. Subsequently the voltage was set back to the UO^- / UF_5^- pilot beam settings.
Then, an automatic tuning procedure was started and the combined instrument of ion source, preacceleration voltage and bending magnet was optimized for the pilot beam to be detected at FC I1-1. To obtain a mass spectrum of a specified region around the formerly optimized mass, we chose to change the preacceleration voltage U_{HVS} and therefore the kinetic ion energy T instead of the magnetic field $\vec{B}$. This enabled increased reproducibility of the procedure and fast scanning of the individual adjacent atomic masses.
By ramping down the preacceleration voltage U_{HVS}, the observed ions in the Faraday cup increase in mass (see equation 3.1 for fixed $\vec{B}$-field). The detected ion current for every incremental voltage step was then saved in log files. A modified Bash program was used to handle cathode changes, the scanning of U_{HVS} and logging of measured ion currents. Moreover, it controlled the start and end voltage of each mass scan as well as the number of scans taken for each cathode. Usually three scans were taken for every turn of the sample wheel. The source code is given in the appendix A.4. Every mass scan was named after the corresponding

sample wheel turn number `TURN`, the cathode number `CAT` and the scan number per turn `SCAN`. This information is shown in the format (`TURN`,`CAT`,`SCAN`) for every mass scan in the following chapters 5 and 6.

3.3.4. Evaluation automation

The recorded mass spectra were calibrated with known peaks i.e. Cu ions sputtered from cathode materials, or with peaks clearly corresponding to U molecules. A mass region-of-interest was set for every measurement to evaluate the ionization efficiency of either UO^- or UF_5^-. The region was defined by 3 to 10 fixed sampling steps of the preacceleration voltage. Subsequent mass scans logged the delivered ion currents in these selected bins.
The search for the peak of interest was automated by a modified Bash program named extract_peak_massXXX (XXX = ion mass), developed in earlier experiments [75]. The source code of the final version is shown in the appendix A.5. It searches the data within the preset region of interest (voltage bins) for the highest ion current value in every scan and writes it into a text file with the corresponding time stamp. The resulting output file was copied to a spreadsheet for further evaluation of the data. Samples were defined as empty, if an ion current was measured below a threshold value of 0.1 nA at the current amplifier of FC I1-1 (specifications in the appendix (h)). The corresponding extracted current was set to 0 nA in the spreadsheet.

3.4. Calculation of the ionization efficiency

Table 3.1.: Single negative ion currents from SNICS/VNIS at typical Cs currents of 5-15 mA.[5]

Extracted ion	Ion current (μA)	Extracted ion	Ion current (μA)
Be^-	0.1	P^-	25
B^-	35	Fe^-	4
C^-	300	Cu^-	150
F^-	250	Ni^-	150
Al^-	6	Pt^-	150
Si^-	250	Au^-	200

The ionization mechanism creates an ion current leaving the source that is the basis for all the following beam manipulating components and beam diagnostic elements. The typical ion currents for various ion species extracted from a caeium sputter source are displayed in table 3.1. The given ion currents are not stable over time and vary widely from one investigated ion to the next. Furthermore the ion current deteriorates with sputter duration of the target material (e.g. crystal structure, availability of secondary ions, etc.). Not only atomic but also molecular ions, mostly in combination with H, O and C are simultaneously extracted [38]. Most actinides do not readily form negatively charged ions. Instead they are routinely analyzed as oxides like e.g. UO^-, PuO^- [64; 23]. In case of Uranium the typical ion currents for $^{238}U^{16}O^-$ extraction from the in-house standard Vienna-KkU-D30 are in the region of several nA. Molecules incorporating minor uranium isotopes as ^{235}U constitute few pA and ^{236}U or ^{233}U show up as rare events and are not detectable with a Faraday cup.

Whereas the ion current is the single most important quantity for applications as beam deposition and implantation, the ionization efficiency is critical for analytical methods like AMS due to limited sample size and measurement time. It is defined as the fraction of an isotope extracted as negative ion divided by the total amount of the same isotope present inside the given sample. In the following chapters of this work, the cumulative ionization efficiency η_{ion} is calculated as given in equation

3.3.

$$\eta_{ion} = \sum_i \frac{\tau_i \cdot I_i^q}{m_{\text{sample}} \cdot n_{iso} \cdot q \cdot e} \tag{3.3}$$

The quantities to determine this ionization efficiency of an extracted ion from a material in a single cathode are the sample mass and number of atoms of the investigated isotope inside the sample material ($m_{\text{sample}} \cdot n_{iso}$), the duration of the i-th mass scan (τ_i) and the measured ion current per i-th mass scan of the charge state q (I_i^q) at FC I1-1. The quantity e is the elementary charge. Square brackets are used for better visibility and do not refer to any unit considerations. An example for the UO^- ionization efficiency is given in equation 3.4.

$$\eta_{[^{238}\text{UO}^-]} = \sum_i \frac{\tau_i \cdot I_{\text{i}}^-}{m_{\text{sample}} \cdot n_{[^{238}\text{U}]} \cdot q \cdot e} \tag{3.4}$$

$$n_{[^{238}\text{U}]} = \frac{\text{f}_{\text{[Vienna-KkU-D30]}} \cdot c_{\text{U}} \cdot \text{N}_{\text{A}}}{M_{[^{238}\text{U}]}} \tag{3.5}$$

The specific number of ^{238}U atoms per sample mass $n_{[^{238}\text{U}]}$ was calculated according to 3.5. The term $\text{f}_{\text{[Vienna-KkU-D30]}}$ denotes the matrix (U containing material) fraction of Vienna-KkU-D30 material relative to the total mixture mass per sample including i.e. Fe, Nb and PbF_2. $M_{^{238}\text{U}}$ is the molar mass of ^{238}U. N_{A} denotes Avogadro's constant and c_{U} the concentration of ^{238}U in Vienna-KkU-D30. To calculate the ionization efficiency, ion currents are summed over all single scan durations. The implication was that every molecule only contained one U atom.
The uncertainty of the total sample mass per cathode m_c were calculated from the accuracy of the used scale (A.1 (i)) and the uncertainty of the uranium mass share per cathode $m_{\text{U}_{\text{cat}}}$ were assessed by estimating a worst case variation in the uranium mass fraction of every mixture that equalled 2.5%. The typical ionization efficiency for uranium extracted in the form of UO^- range up to $\approx 10^{-3}$ from a caesium sputter source [17]. Measurements with improved sample preparation concluding with a single iron carrier pellet set a benchmark value of up to 0.3% for the ionization efficiency for UO^- [13].

4. Dried sample preparation for actinide analysis

Previous research by Cornett et al. 2015 [10] indicated that the sample matrix needs to be diluted 6-8 fold in Pbf_2 to achieve an actinide fluoride ionization efficiency of $\approx 10^{-2}$ in caesium sputter sources. Furthermore, Eigl et al. 2016 [13] indicated that sub-milligram total sample masses increase the ionization efficiency for UO^- extraction. In addition to the investigation of the UF_5^- extraction from Vienna-KkU-D30 mixed with PbF_2 powder, UF_5^- extraction should be applied to environmental samples. Two sample preparation procedures were designed to bind the U content of Seawater samples within a sub-milligram amount of Fe carrier by drying of a solution instead of $Fe(OH)_3$ precipitation. This should allow dilution ratios above 1:6 of the Fe carrier to PbF_2. At the same time the total mixture mass should remain below 10 mg that it could be loaded to standard NEC cathodes. Both procedures started with a drying step. Then, for the first method the sample matrix was mixed with PbF_2 without calcination. The second method used calcination of the Fe matrix for 2 h at 600 °C. Results on the ionization efficiency of UF_5^- for mixtures prepared with both of the preparation procedures are given in section 6.5.

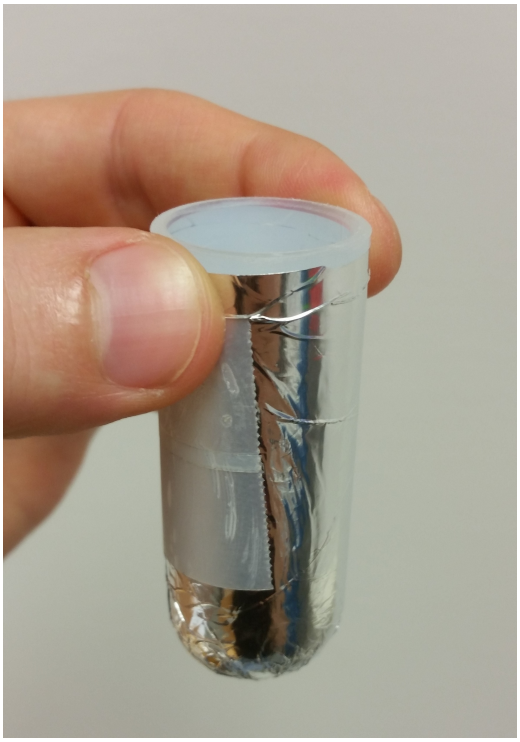

(a) Custom vial cut from 30 ml FEP centrifuge tubes (g) with attached aluminium foil.

(b) Aluminium block with four vials for homogeneous temperature distribution. Vial positions marked A, B, C and D.

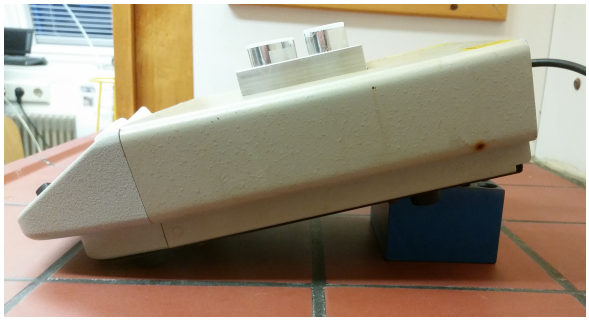

(c) The aluminium block (Fig. 4.1b) in a tilted heating plate, to ensure optimal matrix formation at 60-80 °C.

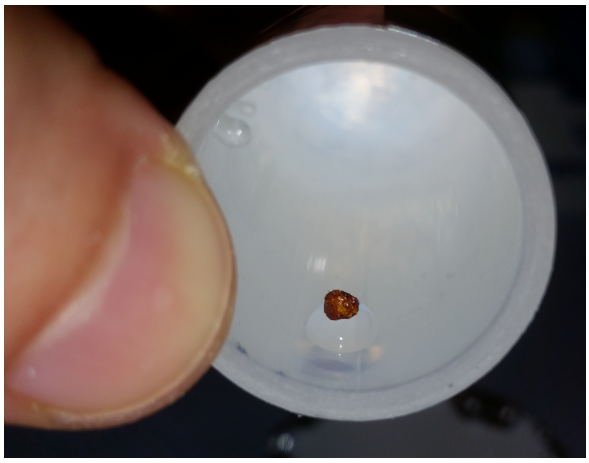

(d) Showcase of a dried pellet that was easily transferrable with 50 μl to 100 μl droplet for further preparation.

Figure 4.1.: Overview for the first drying step of both preparation procedures. The sample matrix was introduced to the vials(a) as aqueous U-Fe solution and then arranged inside an Al heating block(b). A properly tilted heating plate(c) supported the formation of compact matrix pellets or flakes(d).

The well established and currently used preparation procedure for actinide samples analyzed with AMS uses about 2-3 mg of Fe in the last step [48]. Fe co-precipitates as $Fe(OH)_3$ with U, which ultimately determines the resulting macroscopic sample size for AMS measurements. The total amount of U from 10 l Seawater samples is usually in the μg range. The admixture of nearly 3 mg Fe is needed to yield high efficiency during the $Fe(OH)_3$ precipitation. Subsequently, the precipitate is centrifuged, dried at 70°C and annealed for 4 h at 800°C to form Fe_2O_3 and fully oxidized uranium as UO_3 or U_3O_8 [56]. The resulting material is then pressed into aluminium sample holders and investigated by AMS. From suchlike samples it is possible to extract UO^- inside a caesium sputter source.
The dilution of the Fe_2O_3 matrix 6-8 fold in PbF_2 would yield a total mass sample of $\geq$ 18 mg using the standard precipitation method. This mixture mass is unsuitable for NEC cathodes used at VERA, that contain 10 mg to 12 mg at most. Additionally, the needed sputter duration to fully consume a sample of this size would inflate the total measurement duration. Facing these facts, a new preparation to replace the $Fe(OH)_3$ precipitation had to be developed to allow UF_5^- extraction for the investigation by AMS.

Two different methods were designed and tested, using the procedure published by Eigl et al. 2016 [13] as starting point for sub-milligram dried material preparation. Both started from an aqueous solution of Fe and U to simulate the last step of the standard Seawater preparation procedure for actinide analysis ([48; 51].
To dry the sample solution, four 30 ml centrifuge tubes (compare appendix 4.1a for details), made from FEP Teflon were cut below their screw closure. The cleaned vials were filled with about 10 ml of Milli-Q H_2O. Then 150-200 μg of Fe in 0.5 M HNO_3 (compare material (d)) and about 5 μg of U in 4 M HNO3 prepared from Vienna-KkU uranyl nitrate [63] (material information in appendix (e)).
Each sample batch consisted of four vials filled with the sample solution and placed in an aluminium block that was suitable for the used heating plate in Fig. 4.1b. To avoid that the dried material would stick to a seam right at the bottom of the vials, the heating plate was tilted (Fig. 4.1c) and set to a temperature of 60-80 °C. The low temperature was chosen, to avoid boiling of the aqueous solution. The result were nicely formed pellets, or flakes as depicted in Fig. 4.1d after 6-8 h.

The produced compact aggregate could be transferred via 50 μl to 100 μl water or alcohol droplets for PbF_2 admixture or calcination. In case of flake-like material the wet transfer was even possible inside a 1 ml pipette. Dry transfer was not possible at all, due to the apparent electrostatic charge with any kind of used spatula or the FEP vial surface. After this initial drying step, two different preparation steps were tested. The first included the admixture of PbF_2 and transfer to a cathode without further calcination. The second method uses dried material that was calcined inside quartz crucibles and mixed with PbF_2 afterwards.

4.1. Procedure without calcination

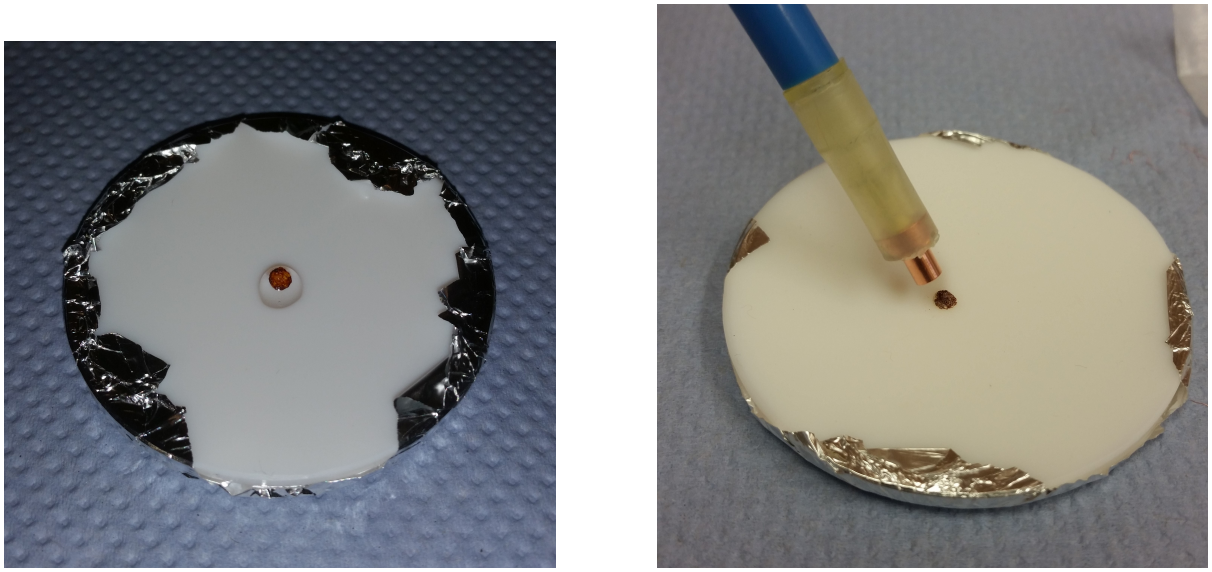

(a) Wet transfer of the dried sample transfer directly as the resulting pellet from Fig. 4.1d to a PTFE watchglass. The admixture of PbF_2 was carried out with the transfer droplet.

(b) Vacuum sample transfer from a PTFE polymer watch glass where samples were dried to its NEC copper cathode with the self-built "sample vacuum cleaner". The blue tube was connected to a water jet pump to provide the necessary vacuum.

Figure 4.2.: Preparation steps of the directly dried sample material without annealing. The transfer to PTFE watchglass and subsequent vacuum transfer after PbF_2 admixture to a Cu cathode is shown.

Following the initial drying step a wet transfer of the resulting Fe-U carrier pellet was needed. Using a 50-100 μl MilliQ H_2O or alcohol droplet, the pellet detached

easily from the FEP vial and could be carefully poured out of the vial onto a PTFE watchglass (fig. 4.2a). Relative to the Fe mass of the carrier pellet PbF_2 was added by the optimal ratio of 1:9. Typically, this amounted for 150 to 200 μg Fe and 1.4 to 1.8 mg PbF_2. The matrix and PbF_2 powder were then mixed in the remaining droplet of water or alcohol and dried at 80 °C. Each individual mixture was then transferred to a copper cathode using the vaccum from a water jet pump. Therefore, a cathode was loaded with a filter surrogate from fine copper wires and copper powder. Then, the mixture could be placed on the filter with the drawn-in air and it was pressed into the cathode with a Cu pin. This transfer assembly was called "sample vacuum cleaner" (compare Fig. 4.2b). In addition, a batch of mixtures was transferred from the PTFE watchglass with powder weighing paper for comparison of transfer losses.

4.2. Procedure with additional annealing step

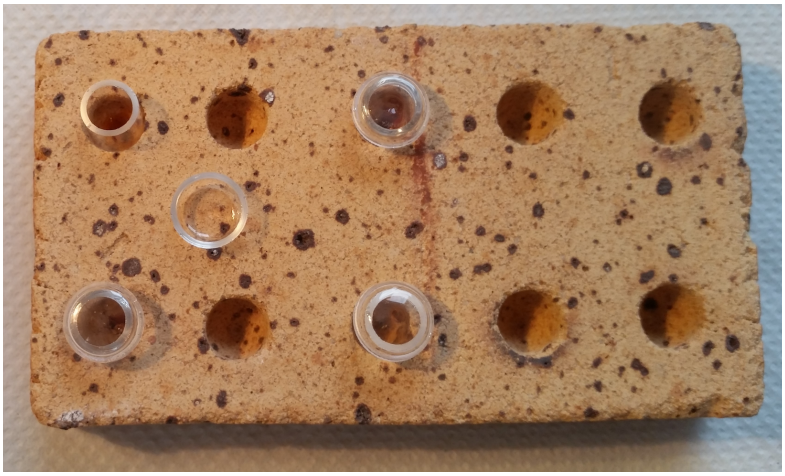

Figure 4.3.: Four quartz crucibles with a volume of ≈ 3 ml with dried samples inside and covered by quartz caps. The samples were calcined for 2 h at 600 °C.

After the initial step of matrix confinement by drying, the second investigated procedure involved additional calcination before PbF_2 admixture. This step was needed to investigate whether mixtures with residual humidity would show decreased ionization efficiency of UF_5^- extraction compared to calcined matrix materials prior to PbF_2 admixture.

The samples were transferred from the FEP vials into ≈ 3 ml quartz crucibles

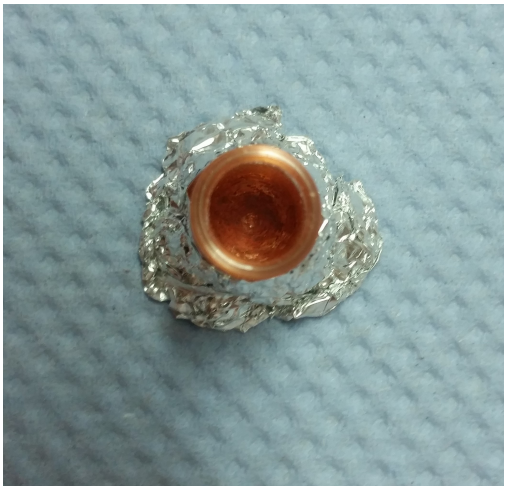

(a) Top view of one quartz crucible with annealed matrix material before PbF_2 admixture. An Al foil stand was used for easier handling.

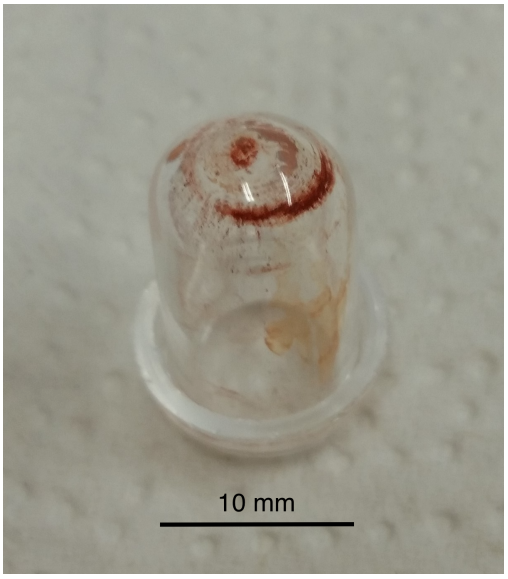

(b) Flipped view of a quartz crucible bottom with sample material that remained attached inside using quartz rods for homogenization.

Figure 4.4.: Crucibles used for sample preparation with additional annealing, before adding PbF_2 and after homogenization with a quartz rod.

(compare fig. 4.3) with a 50-100 μl alcohol droplet. Then, the samples inside the quartz crucibles underwent pre-heating at 400 °C for only 15 minutes to speed up the annealing process. Afterwards a shortened annealing run of 2 h at 600 °C inside a muffle furnace was performed. This means a significant reduction of the annealing duration compared with 4 h at 800 ° for the standard procedure [51]. After the crucibles reached room temperature (Fig. 4.4a), PbF_2 was added to every crucible. Then each sample was homogenized with a quartz rod inside the crucibles. Using quartz rods, the mixtures attached firmly to the quartz crucibles (compare 4.4b). This resulted in only about 50-60% of transfer efficiency from the crucible to Cu cathodes. To avoid these losses, subsequent sample batches were mixed with non electrostatic spatulas. This increased the transfer efficiency from the quartz crucibles to Cu cathodes to above 80%. The main reason for the still occurring losses was electrostatic charging of the crucibles that attracted the mixture material.

5. Improving the $^{238}U^{16}O^-$ ionization efficiency

Prior studies indicated an increase in ionization efficiency achieved by admixture of conductive material to the uranium oxide (U_3O_8, UO_3) containing iron matrix (FeOH and Fe_2O_3 powder from precipitate). This yielded an ionization efficiency of about 0.3% [17; 13]. In addition, mixing conductive material (i.e. Fe, Nb) to a uranium containing matrix material showed promising results to elevate the actinide ionization efficiency [9]. The aim of the following series of experiments was to establish an optimal sample mixing scheme, in terms of ionization efficiency for the primarily extracted uranium oxide anion UO^-. The influence of conductive material admixture like Fe and Nb, as well as the influence of smaller overall sample sizes were examined.

5.1. $^{238}U^{16}O^-$ extracted from Vienna-KkU-D30 with Fe or Nb admixture

The objective was to find a material that had the same properties and chemical constituents like the result of environmental sample preparation. The Vienna-KkU-D30 matrix contains mostly Fe_2O_3. Additives as Fe and Nb (compare specifications in the appendix (a) and (b)) are good conductors in contrast to the insulator Fe_2O_3. Previous research by Child et al. 2010 [9] indicated increased ionization efficiency by Fe or Nb admixture. UO^- investigations in this work conducted at VERA tried to investigate the optimal mixing ratios for Fe or Nb relative to Vienna-KkU-D30. The $^{238}U^{16}O^-$ ion current was measured by a series of mass scans.

Sample preparation was carried out by first crushing the Vienna-KkU-D30 in a mortar. Three mass proportions (roughly 1:1, 1:3 and 1:9) of Vienna-KkU-D30 to metal powder were processed as in table A.1. Two batches included four samples per mixture ratio. The sample preparation tried to resemble environmental material for routine measurements of 2-3 mg in total mass each.
Each material was pressed into aluminium sample holders to avoid isobaric interference from molecular copper clusters i.e. $^{63}Cu_3\,^{65}Cu$ with a mass of 253.72 u at the $^{238}U^{16}O^-$ at 254.03 u. In addition samples were separated into two batches (see wheel pos. in appendix A.1) on opposite positions on the sample wheel. Mass scans were executed from about 250 u to 305 u to include higher order uranium oxide compounds like UO_2^- and UO_3^- as well. Every mass scan took about 240 seconds for three consecutive times per turn and 25 turns per cathode. During one scan the ion current output was assumed to be constant. Typical mass scans for investigated samples are presented in fig 5.1 together with ionization efficiency data in fig 5.2b. The current detected in FC I1-1 is plotted against a mass scale calculated from the preacceleration voltage U_{HVS} (3.2) that determined the ion energy and therefore the mass at constant magnetic field and the peak positions of UO^-, UO_2^- and UO_3^-.

5.1.1. Results for Fe mixtures

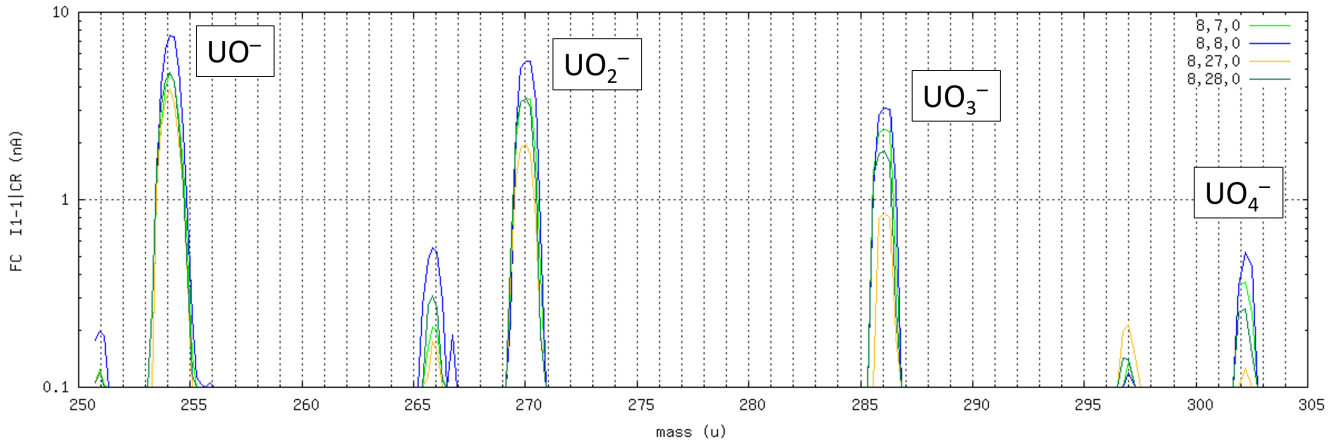

Figure 5.1.: Logarithmic ion current vs. mass for four selected samples of Vienna-KkU-D30 mixed with Fe by 1:3 wt. ratio (in table A.1). Mass scans are labeled "turn#, cathode# , scan#" in the top right corner.

Mass scans provided the necessary information for the calculation of the ionization efficiency as well to track the current characteristics in Fig. 5.2b and Fig. 5.2a. The shown mass scans were taken at peak UO^- current. Vienna-KkU-D30 mixed with Fe showed a uranium oxide extraction pattern. In Fig. 5.1 The peak of UO^- (254.03 u) showed the highest ion current, followed by UO_2^- (270.03 u), UO_3^- (286.03 u) and even UO_4^- (302.02 u) in descending intensity of UO^-:$UO_2^- \approx 1.5$. There were also signals of negative ion currents most probably from UCO^- at roughly 266 u and Al_{11}^- at 296.8 u. This indicates impurities of carbon within the sample and sputtered aluminium from the sample holder.

The ion currents of UO^- started at low levels, around 1 nA consistently for all mixtures and increased after about 30 minutes and reached their maximum around 1.5 h sputter duration. For the mixtures Vienna-KkU-D30 1:1 with Fe and Vienna-KkU-D30 with 1:3 Fe admixture, it increased up to 9-fold and decreased continuously from that level. Comparison between 1:1 and 1:3 Fe admixture shows slightly higher ion currents for 1:1 in fig 5.2a, but their respective ionization efficiency results overlap within 1σ uncertainty while Vienna-KkU-D30 mixed 1:3 with Fe performed slightly higher (compare table 5.1). Fig. 5.2b presents the

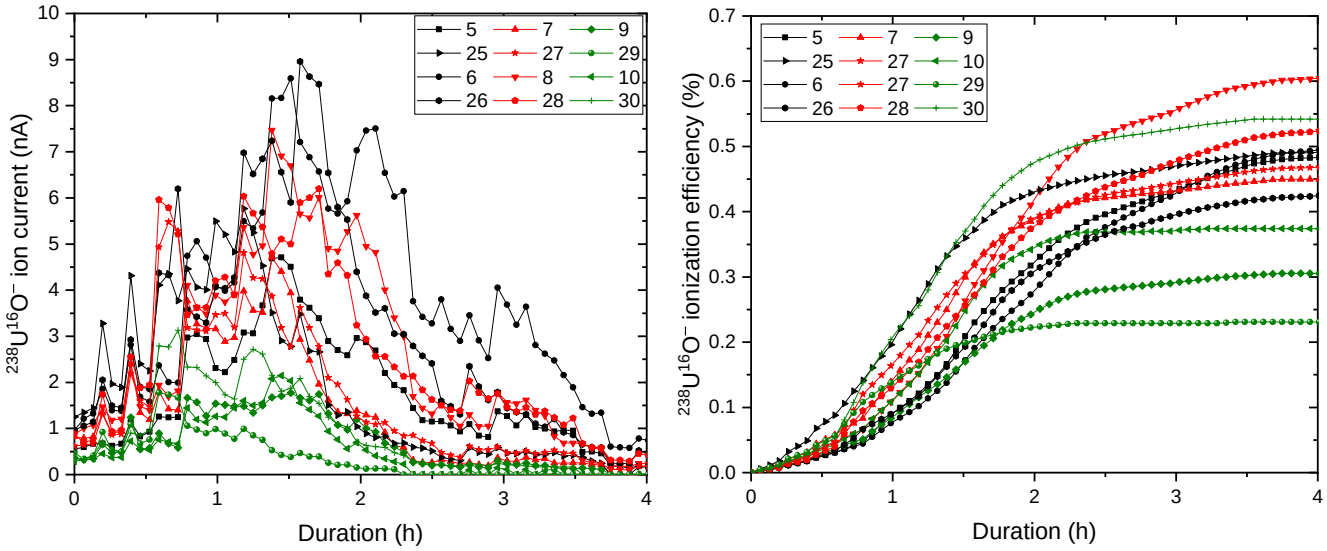

(a) UO^- ion current per scan for the Fe-mixed samples (see table A.1 for details).

(b) Cumulative UO^- ionization efficiency for the Fe-mixed samples in table A.1

Figure 5.2.: Results for 1:1 (black), 1:3 (red) and 1:8 (green) Fe admixtures

cumulative ionization efficiency over time. It clearly shows that variations in the obtained ionization efficiency between targets containing the same mixture can be large. The data in table 5.1 was obtained after 4 h total sputter duration, with about 90% of material extracted after 3 h. The optimal mixture of Vienna-KkU-D30 to Fe of 1:3 weight ratio resulted in an ionization efficiency of $(0.519 \pm 0.073)\%$ compared to about 0.3% for UO^- extracted from Vienna-KkU-D30.

Table 5.1.: UO^- ionization efficiency results with 1σ uncertainty for Fe mixed samples 1:1, 1:3 and 1:8 by weight ratio.

mixture	ionization efficiency η (%)
Vienna-KkU-D30+Fe_1-1	(0.482 ± 0.034)
Vienna-KkU-D30+Fe_1-3	(0.519 ± 0.073)
Vienna-KkU-D30+Fe_1-8	(0.36 ± 0.14)

5.1.2. Results for Nb mixtures

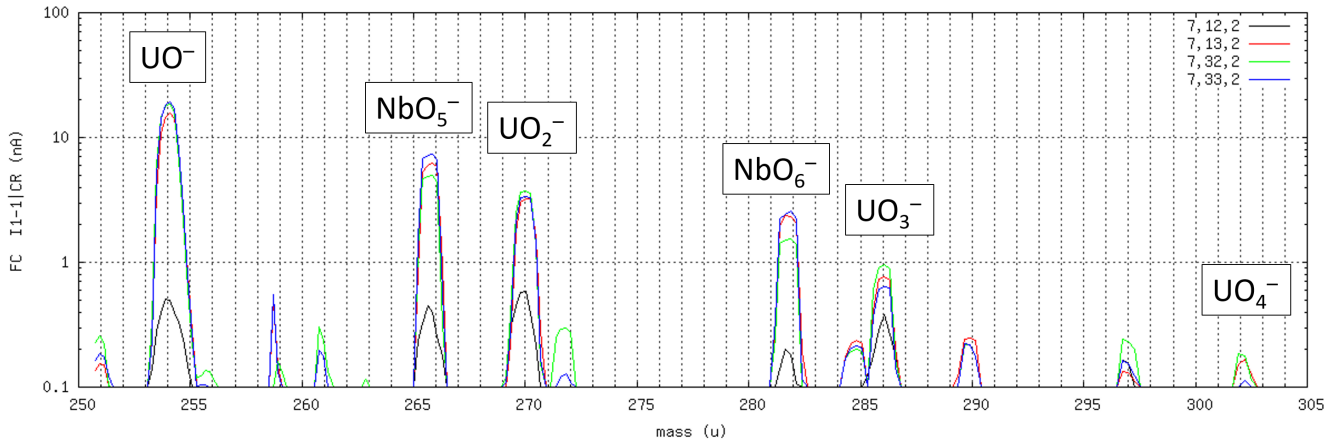

Figure 5.3.: Logarithmic ion current vs. mass for the samples of Vienna-KkU-D30 mixed with Nb by 1:1 wt. ratio (in table A.1) for the scan number 2. Mass scans are labeled "turn#, cathode# , scan#" in the top right corner and were taken at the time of maximum extracted UO^- ion current.

The mass scans of Nb mixture samples showed the same uranium peaks as in the Fe-powder material, but in slightly different proportions of UO^-:UO_2^- $\approx$ 4.5 (see Fig. 5.3). Furthermore the mass scans revealed the formation of NbO_5^- at 265.8 u most probably, with an even higher ion current than UO_2^-. Samples with added Nb matrix mixed 1:1 with Vienna-KkU-D30 yielded higher UO^- ion currents than Fe mixed, by a factor of up to 2 with the ratio 1:1 of Vienna-KkU-D30 : Nb in line with the highest uranium content. Nevertheless the ion current also started around 1 nA and needed about a half hour of Cs^+ sputtering. Depicted in Fig. 5.4a, the current of three 1:3 mixed samples could reach almost similar levels as the 1:1 mixtures while the last one stayed far below below. Given ionization efficiency per material is reached after 4 hours of total sputtering time. After 2 h the increase in ionization efficiency in Fig. 5.4b slows as the ion current goes down in Fig. 5.4a. The moderate gains in efficiency could be attributed to how cathodes are sputtered, as the Cs^+ beam needs to be focused on the sample material [45].

The introduction of metallic Nb powder to the matrix material Vienna-KkU-

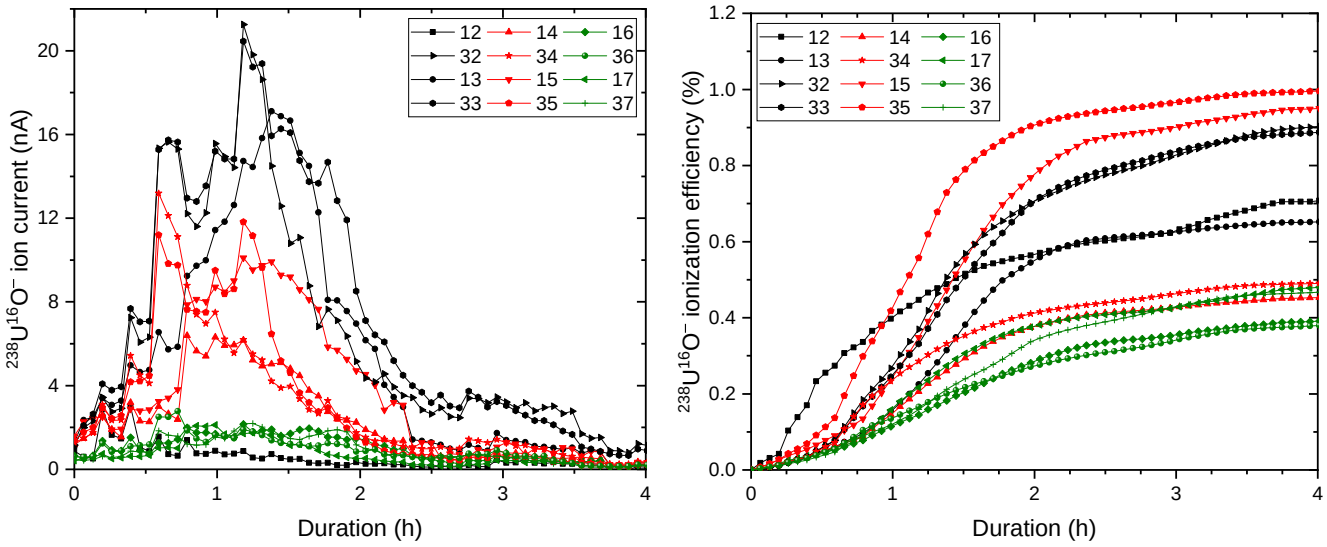

(a) UO^- ion current per scan for the Nb-mixed samples with details in table A.1

(b) Cumulative UO^- ionization efficiency for the Nb-mixed samples with details in table A.1

Figure 5.4.: Results for 1:1 (black), 1:3 (red) and 1:8 (green) Nb admixtures

Table 5.2.: Ionization efficiency results with 1σ uncertainty for Nb mixed samples 1:1, 1:3 and 1:8 by weight ratio.

mixture	ionization efficiency η (%)
Vienna-KkU-D30+Nb_1-1	(0.80 ± 0.14)
Vienna-KkU-D30+Nb_1-3	(0.73 ± 0.30)
Vienna-KkU-D30+Nb_1-8	(0.443 ± 0.055)

D30 from which U was extracted in the form of UO^- yielded a substantial increase in ionization efficiency relative to Fe admixture or the pure matrix material Vienna-KkU-D30. This is in good agreement with Child et al. 2010 [9]. The optimal mixing ratio for Nb to Vienna-KkU-D30 was 1:1 weight ratio. It showed an ionization efficiency of $(0.80 \pm 0.14)\%$. Compared to the optimal Fe admixture of $(0.519 \pm 0.073)\%$ it extracted 50% more UO^-. Furthermore, the Nb mixtures showed about 2.5 times the ionization efficiency of UO^- extraction from Vienna-KkU-D30 (about 0.3% [17]). Nevertheless, the Nb mixed Vienna-KkU-D30 samples showed increased variability per sample resulting in a higher relative uncertainty as compared to Fe mixed material. Within the $1\,\sigma$ uncertainties of

these measurements the 1:1 and 1:3 Nb mixtures perform equally well, whereas a large surplus of Nb (1:8 mixture) significantly reduces the ionization efficiency. The admixed Nb provides a possibility to easily increase UO^- ionization efficiency. However, additional material introduced to environmental samples can also create significant cross-contamination of trace isotopes.

5.2. $^{238}U^{16}O^-$ ionization for different sample sizes

Subsequent to material mixtures it was investigated whether a correlation between sample size and ionization efficiency exists. For this experiment Vienna-KkU-D30 mixed 1:3 with Fe was used, which was the optimal Fe mixture in the previous experiment. The proportionate lower UO_2^- peak obtained from the Nb matrix lead to the wrong conclusion of a better ionization efficiency of Fe compared to Nb. There fore the optimization of total sample masses for the UO^- ionization efficiency only focused on the Fe mixtures. Another aim was to observe if possible variations in ion current production and ionization efficiency can be explained by conditioning of the sample surface by additional Cs vapour deposition. Two batches of identical sample material were prepared for this experiment. Cathodes were loaded with three different total sample masses, i.e. about 0.5 mg (small), 1.5 mg (medium) and 4.5 mg (large). Four cathodes were prepared for each sample mass size. Detailed information is given in table A.2. The first sample batch was immediately measured. The second batch was delayed by 2.7 h compared to the first. During this time Cs vapour could reach the sample material surface. To prevent pre-sputtering of these samples the negative cathode potential was generally turned off during cathode changes. Apart from delaying the second batch the measurement procedure was the same as previously. The investigated negative ion was again $^{238}U^{16}O^-$.

5.2.1. Results on the influence of total sample mass on UO^- extraction

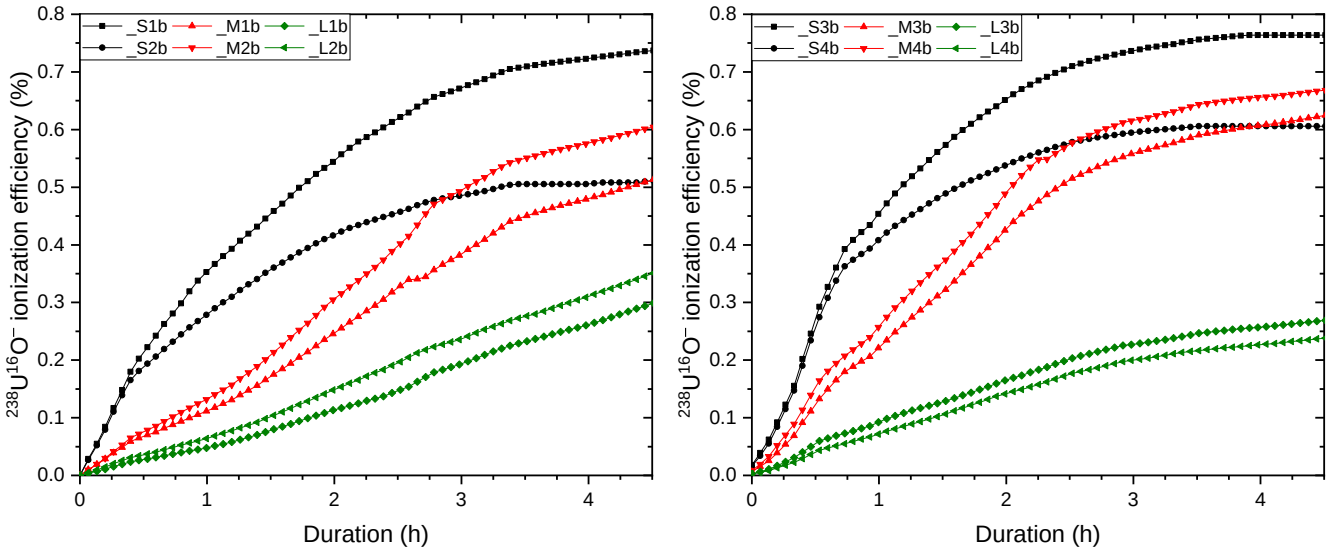

(a) Cumulative ionization efficiency of UO^- for the Fe mixed (1:3) samples of increasing total sample mass per cathode (table A.2).

(b) Cumulative ionization efficiency of UO^- for the Fe mixed (1:3) samples of prolonged Cs deposition (2.7 h longer) and increasing total sample mass per cathode (table A.2).

Figure 5.5.: Results for small (black), medium (red) and large (green) sized samples for short (a) or prolonged (b) Cs-vapour deposition.

The mass scans of samples examined in the course of this experiment showed analogous peaks and therefore contained the same molecular species as previously (compare fig 5.1). The ionization efficiency data for the first sample batch with short Cs vapour exposition and immediate sputtering is shown in Fig. 5.5a. Results for the first batch after 2 h of sputter duration show that the ionization efficiency is about 1.7 times higher for small compared to medium and more than 3.5 times for small relative to large samples. The values for individual sample sizes after 2.05 h are shown in table 5.3. The cumulative ionization efficiency of the second sample batch with additional Cs vapour exposition is displayed in Fig. 5.5b. The cumulative ionization efficiency was slightly higher than compared to the samples without additional Cs exposition for all sample sizes (table 5.3). It was significantly increased for medium samples, which resemble the minimal achiev-

able sample size after standard sample preparation. They reached levels otherwise only attained by small samples. Ionization efficiency of large samples with a total mass around 4.5 mg each, did not reach levels of small to medium-sized samples.

Table 5.3.: UO^- ionization efficiency results with 1σ uncertainty for two sample batches wich were immediately measured or with additional Cs exposition for 2.7 h. Small (S), medium (M) and large (L) total sample sizes correspond to about 0.5 mg, 1.5 mg and 4.5 mg. Presented values were taken 2 h after individual sputter duration. The investigated material was Vienna-KkU-D30 mixed 1:3 with Fe (compare material specs (a)).

sample batch	mixture	ionization efficiency η (%)
immediate sputtering	Vienna-KkU-D30+Fe_1-3 S	(0.490 ± 0.095)
	Vienna-KkU-D30+Fe_1-3 M	(0.286 ± 0.043)
	Vienna-KkU-D30+Fe_1-3 L	(0.135 ± 0.027)
additional Cs exposition	Vienna-KkU-D30+Fe_1-3 S	(0.602 ± 0.084)
	Vienna-KkU-D30+Fe_1-3 M	(0.472 ± 0.046)
	Vienna-KkU-D30+Fe_1-3 L	(0.157 ± 0.017)

To compare the ionization efficiency results 2 h of sputter duration was chosen, because this would represent a desired measurement duration for environmental samples. Lowering the total sample size by maintaining the same relative U amount showed a significant increase for smaller total sample sizes. These results support the indications by Eigl et al. 2016 [13] and show the possibility to increase UO^- ionization efficiency by preparing more compact samples. Samples of total mass of 4.5 mg or above did not show ionization efficiency results near small or medium-sized samples. The use of samples with total mass of about 4.5 mg or above does not support efficient UO^- extraction. The underlying reason is not completely clear. Only AMS facilities that are able to operate two ion sources independently, like VERA, additional Cs exposition could significantly increase the ionization efficiency of 0.5 mg to 1.5 mg-sized samples. Otherwise, the additional Cs exposition does not yield an increase in ionization efficiency that would justify the measurement delay.

6. Experiments on the $^{238}U^{19}F_5^-$ ionization efficiency

UF_5^- was investigated whether its ion currents and ionization efficiency is high and stable enough for AMS measurements of ^{233}U and ^{236}U in environmental samples. In a series of experiments, several sample preparation methods were examined to find the optimal mixing ratio of uranium containing matrix material to PbF_2. They could be divided in three main categories. The first starting with Vienna-KkU-D30 [63], which represents standard sample matrix preparation for environmental samples with Fe_2O_3 precipitation [48; 13]. The second category consisted of sample matrices prepared by U dried with about 200 μg Fe carrier. The third set of samples was based upon changing the preparation to UF_4 co-precipitated under the use of HF together with NdF_3 or PrF_3 [43]. In addition, the possible influence of sample holder geometry and dried sample calcination on the UF_5^- ionization efficiency was investigated.

6.1. The optimal PbF_2 matrix ratio for $^{238}U^{19}F_5^-$

The first measurement investigated the optimal mixing ratio of the in-house uranium standard Vienna-KkU-D30 and PbF_2 (material description in (c)) for the UF_5^- ionization efficiency. Three different mixtures of Vienna-KkU-D30 with PbF_2 by 1:1, 1:3 and 1:9 weight ratio were tested. In short they were denoted as the three mixtures Vienna-KkU-D30+PbF_2_1-1, Vienna-KkU-D30+PbF_2_1-3 and Vienna-KkU-D30+PbF_2_1-9 in the following tables. Details on the individual samples are shown in table A.3. The material was pressed into copper sample holders. It was shown in a former diploma thesis [75] at VERA, that by using Al sample holders it was not possible to extract high and stable enough UF_5^- ion currents needed for

AMS measurements.

Table 6.1.: List of all known electron affinity values for $UO_xF_y^-$ molecules ordered by mass. Taken from [4].

Mass (u)	Ion	E_a (eV)
286.04	UO_3^-	2.125
308.04	$UO_2F_2^-$	3.356
314.04	UF_4^-	1.244
327.04	$UO_2F_3^-$	6.250
330.04	UOF_4^-	3.803
333.04	UF_5^-	3.820
352.04	UF_6^-	5.056

As U is present as oxide molecule in the Vienna-KkU-D30, we expected the formation of all the oxides discussed in the previous chapter and oxide-fluoride mixed compounds apart from the different UF_y^-. The known electron affinity for $UO_xF_y^-$ molecules are given in table 6.1. The ionization efficiency of other occurring $UO_xF_y^-$ molecules as well as possible isobaric interference for UF_5^- should be identified. Data collection was carried out similar to the previous ionization experiments in this thesis (see chapter 3.3.3). Mass scans were taken for each were investigated for the most prominent peaks. The only difference was, that this time the overall mass range was set from 240 u to 340 u to inspect the whole range of negatively charged molecules being produced in the ionization process, when PbF_2 was added.

6.1.1. Results for UF_5^- extraction from PbF_2 material mixtures

To inspect the formation of all $UO_xF_y^-$ molecules the mass range was initially set from 240 u to 340 u. The scanned region from 240 u to about 300 u showed peaks of Cu_4^- clusters and PbF_x^- molecules. No $UO_xF_y^-$ molecules were found below 300 u for all material mixtures. Therefore, the mass range in Fig. 6.1 was changed to about 300 u to 340 u. The raw data mass scan in Fig. 6.1 shows peaks that

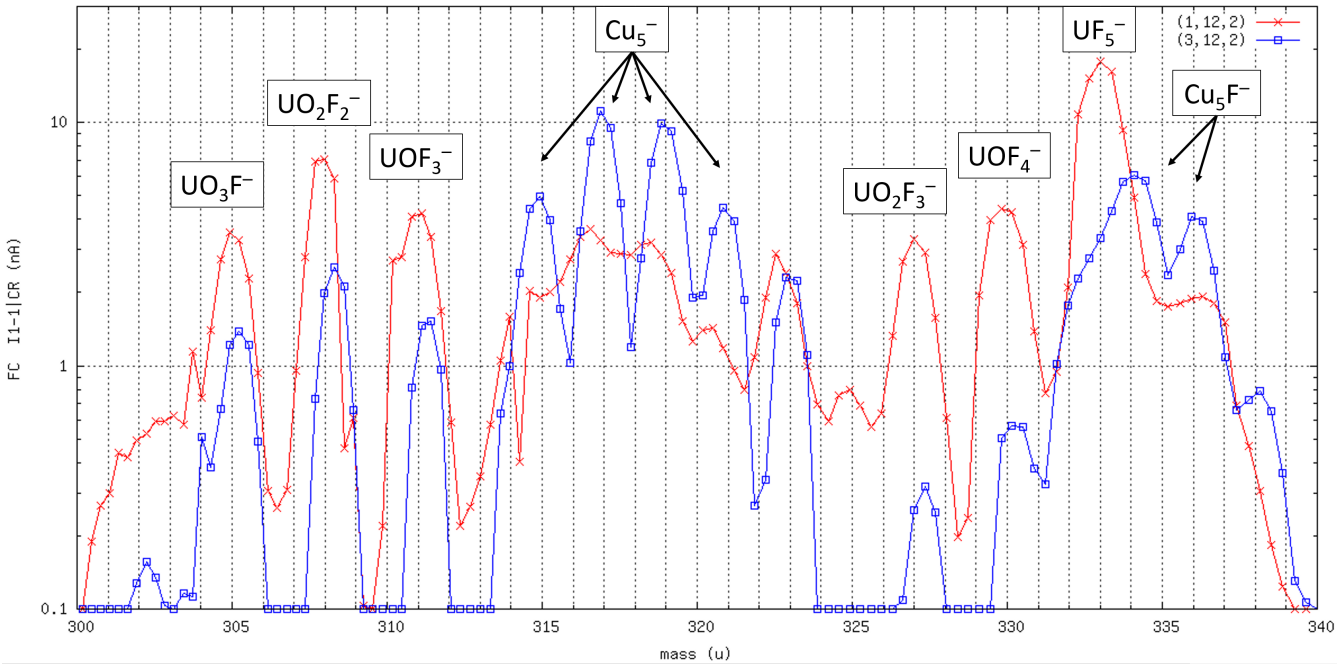

Figure 6.1.: Logarithmic ion current measured at FC I1-1 vs. mass for two scans of sample 12, consisting of the Vienna-KkU-D30 mixed about 1:9 with PbF_2. The red line corresponds to the first turn and the blue line to the third turn of the sample wheel after 20 min of sputter duration. Detailed information about samples is presented in table A.3.

are attributed to possible $UO_xF_y^-$ molecules in this mass range, including those in table 6.2. The red line in the first turn shows a mass scan at the start of Cs sputtering on the sample material Vienna-KkU-D30 mixed 1:9 with PbF_2. The blue line shows the third turn and therefore a mass scan 20 min later. The red mass scan clearly shows a high UF_5^- peak and a signal of other molecules that contain U (i.e. $UO_2F_2^-$ and UOF_3^-) as well as ion current of Cu_5^- clusters. The mass scan signal changed significantly after 20 min (turn three). Ion currents of Cu_5^- and most probably Cu_5F^- from the sample holder increased. All U containing peaks seem to uniformly decline in ion current.

Table 6.2.: Identified peaks from mass scan `(1,12,2)` (compare section 3.3.3) in Fig. 6.1 and their corresponding masses in the range 300 u to 340 u. The intensities of selected ions are given relative to UF_5^-.

molecule	UO_3F^-	$UO_2F_2^-$	UOF_3^-	$^{63}Cu_5^-$	$^{63}Cu_4^{65}Cu^-$	$^{63}Cu_3^{65}Cu_2^-$	$^{63}Cu_2^{65}Cu_3^-$
mass (u)	305.03	308.04	311.04	314.65	316.65	318.64	320.64
intensity	0.188	0.396	0.239				
molecule	$^{63}Cu^{65}Cu_4^-$	$UO_2F_3^-$	UOF_4^-	UF_5^-	$^{63}Cu_5F^-$	$^{63}Cu_4^{65}CuF^-$	$^{63}Cu_3^{65}Cu_2F^-$
mass (u)	322.64	327.04	330.04	333.04	333.65	335.64	337.64
intensity		0.187	0.249	1			

$$\text{normal}(x, \mu, \sigma) = \frac{1}{(\sigma\sqrt{2\pi})} \cdot \exp \frac{-(x-\mu)^2}{(2\sigma^2)} \tag{6.1}$$

$$f(x) = a_0 \cdot \text{normal}(x, x_0, \sigma_0) + a_r \cdot \text{normal}(x, x_l, \sigma_l) + 0.158 \cdot a_{cu}\text{normal}(x, x_{r1}, \sigma_r) \\ +0.353 \cdot a_{cu}\text{normal}(x, x_{r2}, \sigma_r) + 0.315 \cdot a_{cu}\text{normal}(x, x_{r3}, \sigma_r) \tag{6.2}$$

The mass scale was based on the averaged peak center of UF_5^- and $UO_2F_2^-$ during first 5 recorded mass scans. In order to investigate isobaric interference and to estimate the respective contributions to the UF_5^- peak, the neighboring peaks, most probably $^{63}Cu_5F^-$, $^{63}Cu_4^{65}CuF^-$ and $^{63}Cu_3^{65}Cu_2F^-$ were fitted with Gaussians (compare equations 6.1 and 6.2). A simple binomial mixing model was used to calculate the Gaussian coefficients and their amplitudes factors. Cu_5^- molecules consisting of ^{63}Cu and ^{65}Cu isotopes are chemically identical. Different Cu_5^- molecules should therefore bind equally well to F.
The exact Gnuplot code can be found in the appendix A.6. Figure 6.2 presents the obtained fit for the detected ion current in FC I1-1 vs. atomic mass with Gnuplot. The used fit is given in equation 6.2. The mass positions were fixed and the independent factors characterized the following features. The quantities indexed with 0 change the UF_5^- peak, `1` quantities belong to the "left" peak UOF_4^- and

quantities indexed `cu` apply to the copper peaks. The amplitude factors (compare a_{cu} in eq. 6.2) for the copper peaks were taken from the binomial mixing of ^{63}Cu and ^{65}Cu to the respective Cu_5 compound with their abundances of 30.83% and 69.17%. For the copper cluster, the measured curve could not be reproduced, starting from 337 u.

The peak fits justify to estimate the Cu_5F^- (light blue line in fig. 6.2) contribution of about 3% compared to the UF_5^- peak at 333.04 u. It was not possible to distinguish both due to the narrow peak positions. The contribution from Cu_5F^- over the whole measurement, however increases for subsequent mass scans and was estimated to 10% to 15%. The $UO_2F_2^-$ peak was used as indication that U was still present in the sample. For $UO_2F_2^-$ no isobaric interference from the sample holder or matrix components was visible. Data for which the $UO_2F_2^-$ dropped below 0.1 nA for the first time, data for UF_5^- ionization efficiency were not taken into account. All UF_5^- ionization efficiency results were corrected for increasing Cu_5F^- amount by subtracting 10% of the total ionization efficiency per sample.

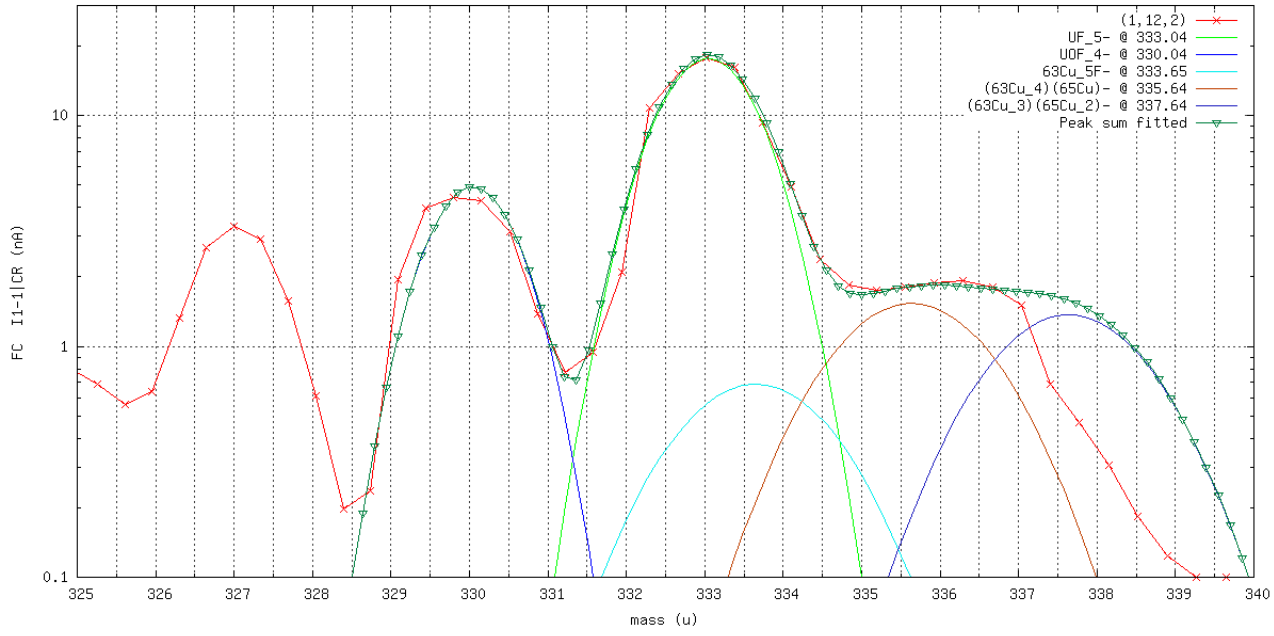

Figure 6.2.: Logarithmic ion current vs. mass for the first turn sample 12 from Fig. 6.1. Peaks correspond to the indicated molecules including copper fluoride background in the top right corner. The fitted UF_5^- current is drawn in green.

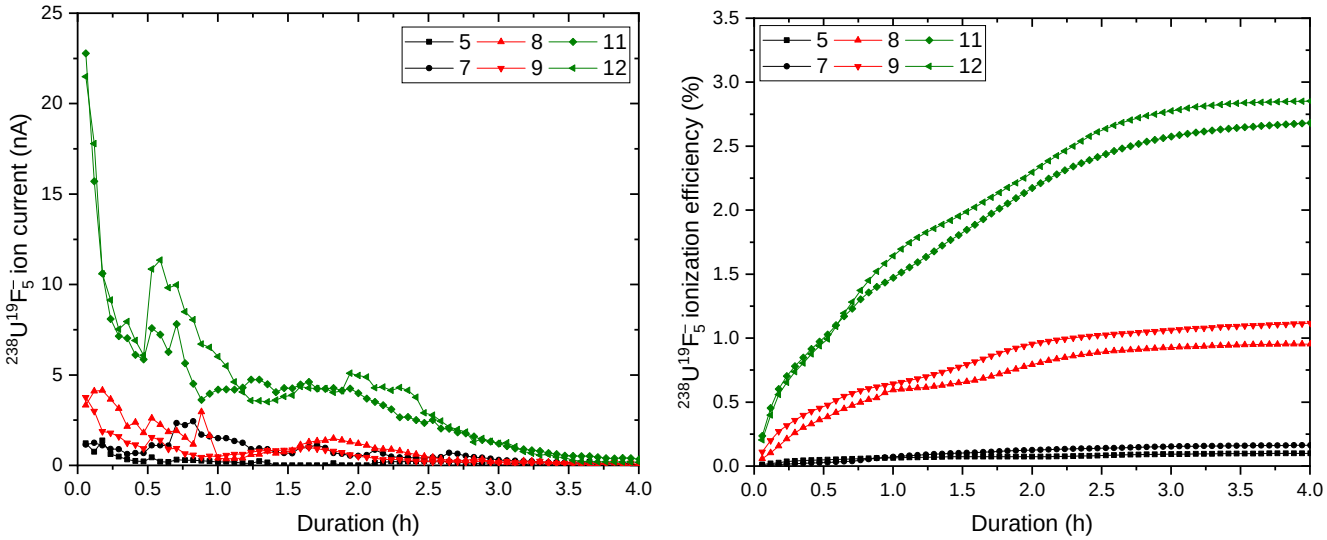

(a) UF_5^- ion current per mass scan for the samples in table A.3

(b) Cumulative ionization efficiency of UF_5^- for the PbF_2-mixed samples in table A.3

Figure 6.3.: Results of Vienna-KkU-D30 containing samples mixed by 1:1 (black), 1:3 (red) and 1:9 (green) weight ratio with PbF_2.

Table 6.3.: UF_5^- ionization efficiency results with 1σ uncertainty, for three mixtures of Vienna-KkU-D30 with with PbF_2 by ratios 1:1, 1:3 and 1:9 after 4 h of sputter duration.

mixture	ionization efficiency η (%)
Vienna-KkU-D30+PbF_2_1-1	(0.12 ± 0.05)
Vienna-KkU-D30+PbF_2_1-3	(0.94 ± 0.11)
Vienna-KkU-D30+PbF_2_1-9	(2.49 ± 0.12)

The ion current of evaluated UF_5^- (≈ 20 nA) moreover showed even higher ion currents than Nb matrix samples (Vienna-KkU-D30 with 1:1 Nb admixture in Fig. 5.4a) that gives the highest observed UO^- ion current, while containing only about a quarter of the uranium mass. The obtained ionization efficiency of UF_5^- at 333.04 u was determined for every of the three mixtures. Results after 4 h of sputter duration is given in table 6.3. The measured UF_5^- ionization efficiency in Fig. 6.3b shows, that an increased PbF_2 share of the matrix leads to a significant increase in uranium extraction of about 3-fold compared to UO^- obtained by adding Nb

and 5-fold to UO^- by Fe admixture. Another advantage for AMS measurements is the immediate current production of UF_5^- i.e. the highest currents are obtained directly at the start of sample sputtering. In contrast, it took around 0.5 h to 1 h in average for the oxide targets to arrive at the maximum current output (compare Fig. 5.4a and Fig. 6.3a). The higher ion current is favorable for fast extraction, but demanding for the source output regulation current. The formation of oxygen and fluorine $UO_xF_y^-$ molecules reduce the ionization efficiency for UF_5^- compared to the theoretical achievable efficiency if no oxides were present in the sample. The observed distribution of U containing molecules cannot be only explained by the electron affinities of the molecules like i.e. UF_5^- binds a surplus electron by 3.82 eV, but it gets produced about 2.5 times more efficient than $UO_2F_3^-$ with 6.25 eV (compare Fig. 6.2 and Fig. 6.1). A possible explanation could be the availability of binding ligands during the sputter process.

6.2. Investigating the influence of background and total mass ratio on $^{238}UF_5^-$ extraction

An investigation was started whether an influence of the total sample mass on the ionization efficiency also exists for UF_5^-. Another aim was to investigate the molecules extracted from standard NEC copper cathodes loaded with pure PbF_2, which generated background in the recorded mass scans. Most importantly, this should quantifiy the contribution of Cu_5F^- background that was found by a curve fit approximation (in section 6.1). The third objective was to study the formation of uranium fluorides like UF_6^- in the present source setup. Therefore, the investigated mass range was extended to higher masses up to about 360 u.

6.2.1. Results for background and total sample mass characteristics on UF_5^-

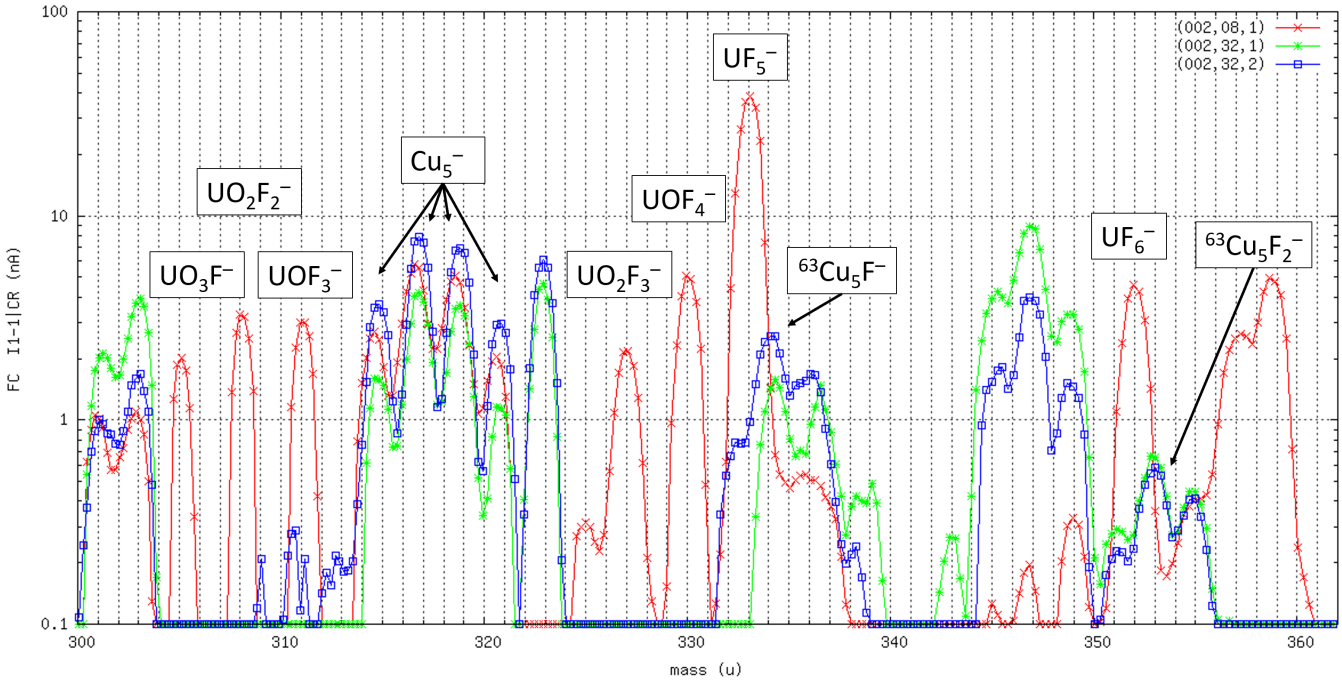

Figure 6.4.: Logarithmic ion current vs. mass for samples containing U (Vienna-KkU-D30 mixed 1:9 with PbF_2) indicated by a red line and pure PbF_2 in copper cathodes in blue and green. See sample details in table A.4.

Table 6.4.: Peak intensities for identified peaks of $UO_xF_y^-$ ions that reached more than 1 nA in mass scan `(002,08,1)` of Fig. 6.4. The mass scan was taken at peak UF_5^- current output.

molecule	UO_3F^-	$UO_2F_2^-$	UOF_3^-	$UO_2F_3^-$	UOF_4^-	UF_5^-	UF_6^-
mass (u)	305.03	308.04	311.04	327.04	330.04	333.04	352.04
rel. intensity	0.052	0.086	0.079	0.057	0.0152	1	0.119

The red line illustrates the U containing Vienna-KkU-D30 mixture with 1:9 PbF_2. blue and green lines represent pure PbF_2 in copper cathodes. The measurement using the enlarged mass range showed that UF_6^- was in fact extracted (fig. 6.4). Moreover, it was found that the ion current of UF_6^- at mass 352.04 u is contributed by overlapping $Cu_5F_2^-$ cluster background. This was especially clear for samples where only pure PbF_2 was loaded to the copper cathode. The intensities of identified peaks relative to UF_5^- are given in table 6.4. For other $UO_xF_y^-$ molecules it was found that they were extracted by a factor of 2 less at peak UF_5^- output than compared to previous mass scans 6.1.

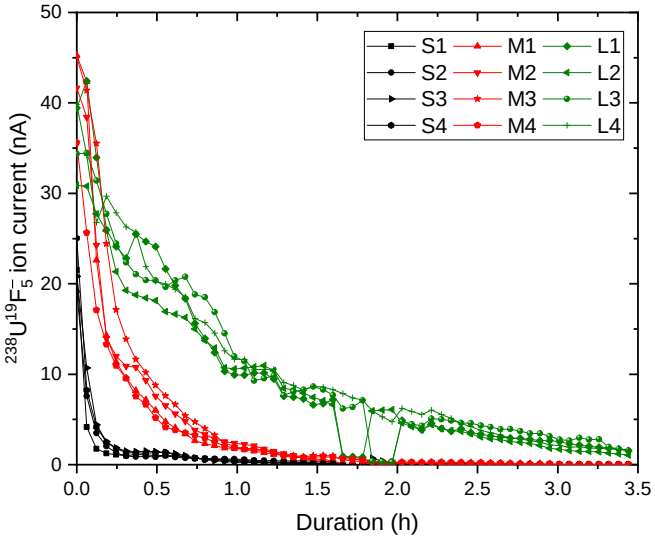

(a) UF_5^- ion current per mass scan for the sample masses given in table A.4.

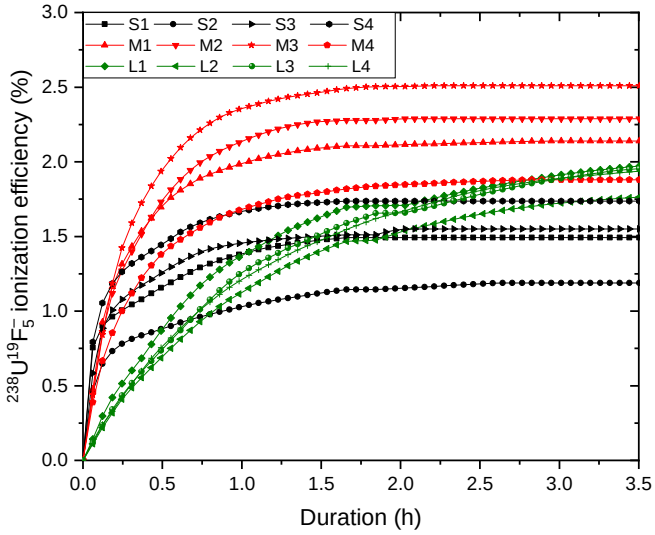

(b) UF_5^- cumulative ionization efficiency for the PbF_2-mixed samples in table A.4 in three different total sample mass sizes.

Figure 6.5.: Results for samples with different sample mass sizes of approximately 0.5 mg (black), 1.5 mg (red) and 4.5 mg (green).

The extracted ion currents of the three total sample sizes of about 0.5 mg (S),

1.5 mg (M) and 4.5 mg (L) are given in Fig. 6.5a. M and L-sized samples showed ion currents that started at about 40-45 nA and decreased thereon. The M-sized samples represent the optimal total mass size for UF_5^- ionization efficiency. About 90% of the total amount of extracted UF_5^- molecules were ionized in less than 1 h (Fig. 6.5b). This changes for L-sized samples to less than 2 h of sputter duration. The investigation of the influence of different total sample mass sizes on the UF_5^- ionization efficiency did show significant results 6.5b. The optimal total sample mass using UF_5^- extraction was found to be in the region of 1.5 mg (M). Results for M and L sized total sample masses overlapped within their respective 1σ uncertainties of ionization efficiency. Smaller sample sizes showed significantly less UF_5^- formation. However, the influence of total sample mass on UF_5^- formation was smaller than in the case of UO^- extraction. The UF_5^- ionization efficiency results found for targets with different total sample mass are shown in table 6.5.

Table 6.5.: UF_5^- ionization efficiency results with 1σ uncertainty. The used material was Vienna-KkU-D30 mixed with PbF_2 by 1:9 weight ratio. Three different total sample mass sizes of about 0.5 mg (S), 1.5 mg (M) and 4.5 mg (L) were measured.

Ion	Ionization efficiency η (%)
Vienna-KkU-D30+PbF_2_1-9 S	(1.34 ± 0.21)
Vienna-KkU-D30+PbF_2_1-9 M	(1.99 ± 0.24)
Vienna-KkU-D30+PbF_2_1-9 L	(1.72 ± 0.09)

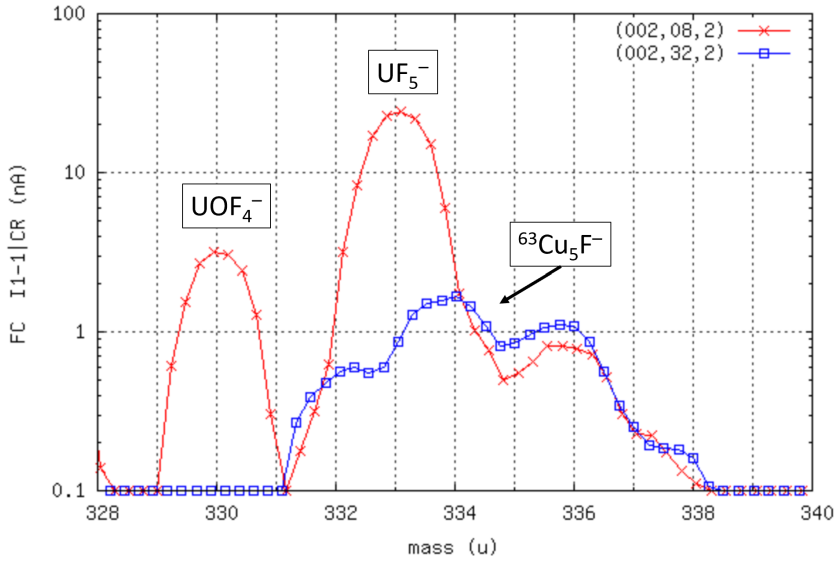

Figure 6.6.: Detailed view of Fig. 6.4 used for the comparison of $^{238}UF_5^-$ and $^{63}Cu_5F^-$ ion currents. The red line indicates a U containing material (Vienna-KkU-D30 mixed 1:9 with PbF_2) and pure PbF_2 in (blue).

An exemplary detail of mass scan 6.4 around UF_5^- is shown in Fig. 6.6. The peak currents of $^{238}UF_5^-$ and $^{63}Cu_5F^-$ were compared between the U containing material (red line) and pure PbF_2 in (blue line). It showed that the evaluation of the topmost three sampling points of the UF_5^- peak consequently minimized the contribution of copper cluster ion currents. In detail, the calculated contribution from $^{63}Cu_5F^-$ at 333.65 u on the current of $^{238}UF_5^-$ at 333.04 u is $(8.55 \pm 0.26)\%$ after the first 5 turns. This is equal to the first hour of Cs sputtering on the sample material. At this time already over 90% of the material of the middle-sized samples had already been extracted. The formation of Cu_5F molecules stopped, when the abundant PbF_2 was sputtered away from the copper cathode holder. The cathodes were checked after the measurement and did not show visible residual PbF_2 material.

6.3. Decreased ion source output current for stable $^{238}UF_5^-$ extraction

The experiments to explore the possibilities of UF_5^- extraction always lead to extraordinary high ionization efficiencies and shortened measurement times due to high ion currents. In case of UO^- multi-isotope AMS measurements using the whole VERA instrument, stable ion current conditions are demanded. to achieve valuable counting statistics. If the delivered beam would drastically change in output between two sets of different species, it would strongly affect the measurement of isotopic ratios.

Previous experiments in this thesis showed, that the extracted UF_5^- ion current reached its peak at the beginning of Cs sputtering and declined sharply thereon. A full run for multi-actinide (i.e. ^{236}U, ^{233}U, ^{239}Pu,) detection takes about 1 h per cathode for UO^- measurements at VERA. Therefore, the extracted UF_5^- ion current needs to be stabilized to enable UF_5^- as low-energy molecule for actinide AMS measurements.

The quantity to regulate the ion current output of Cs sputter sources at VERA is called "control current". By lowering the control current less Cs is introduced to the source and ionized in front of the sputtered target. It was aimed to stabilize the ion current output by lowering the control current I_C of the source regulation. Two batches of samples were prepared from Vienna-KkU-D30 mixed 1:9 with PbF_2 and measured one after the other with two lower control current settings relative to the standard control current I_{init} (compare table A.5 for sample details). The used control current for the respective sample batches was set to 2/3 or 1/3 relative to $I_{\text{init}} = 80\,\mu\text{A}$. This resulted in $I_2 = 52.5\,\mu\text{A}$ and $I_3 = 27,5\,\mu\text{A}$ [1].

[1] All given control current settings are already corrected for a factor of 2.5 lower current reading and offset current ($\approx 7.5\,\mu\text{A}$)

6.3.1. Results for UF_5^- extraction with lowered source output currents

The UF_5^- ion currents extracted from the two sample batches using the respective control currents I_2 and I_3 are shown in Fig. 6.7a. First the batch using I_2 was measured and the batch using I_3 afterwards. Cathodes measured with the use of I_2 showed similar UF_5^- ion currents as in previous measurements in this thesis. However, the lowest control current I_3 (red lines) could indeed stretch the extraction duration of UF_5^-. The three cathodes sputtered under I_3 conditions showed a two different slopes in UF_5^- ionization efficiency (compare red lines in 6.7b) which can be attributed to two different time periods in the UF_5^- extraction current (compare red lines in fig.6.7a).

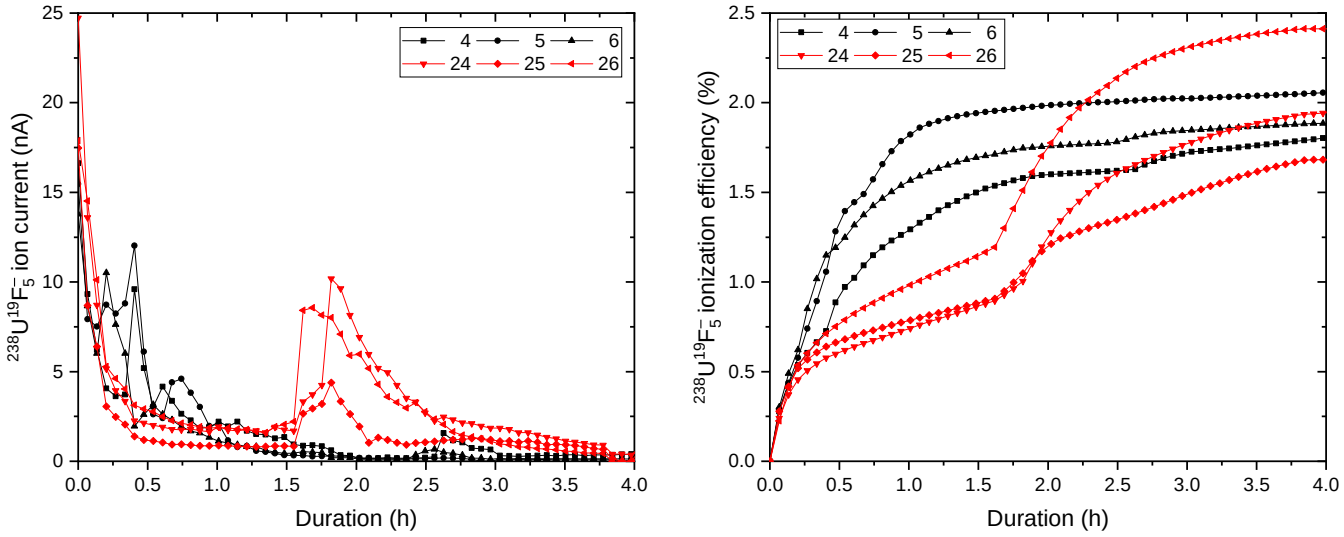

(a) UF_5^- ion current per mass scan for the samples in table A.5.

(b) UF_5^- cumulative ionization efficiency for the PbF_2-mixed samples in table A.5 for two different current output regulation levels.

Figure 6.7.: Results for two batches that were sputtered using two different control currents of I_2 (2/3 I_{init} in black) and I_3 (1/3 I_{init} in red).

The first period starts at the origin and the second after about 1.5 h in Fig. 6.7a. The change between control currents I_2 to I_3 after the first batch lowered the demand in output current. However, the still apparent Cs vapour led to the rapid ion current onset and and more UF_5^- was extracted than demanded by I_3. Between

1-1.5 h of sputter duration for the second batch (red lines fig. 6.7a), the output was below the regulation threshold of I_3 and Cs supply was expanded again. This led to the second period of UF_5^- extraction between 1.5-3.5 h sputer duration. With increased Cs supply, the UF_5^- immediately rose to initial levels of about 10 nA. This indicates that to stabilize the UF_5^- extraction for AMS experiments, the Cs supply has to be minimal, but constant. Therefore, the feed line heater (compare fig. 3.2) needs to be regulated the tipping point, between Cs condensation in the feed line and where Cs vapour still reaches the ionizer[2].
The overall UF_5^- ionization efficiency given in table 6.6 did not show a significant change by using different control current settings compared to previous measurements.

Table 6.6.: UF_5^- ionization efficiency results with 1σ uncertainty for Vienna-KkU-D30 mixed 1:9 with with PbF_2. Two batches of samples were sputtered with two different control currents I_2 or I_3 of the previously used control current.

Current	Ionization efficiency η (%)
I_2	(1.77 ± 0.11)
I_3	(1.89 ± 0.31)

[2]This tipping point was between 14-15 A for the Cs feed line heater at ion source S2

6.4. Sample geometry influence on $^{238}UF_5^-$ ionization yield

Vogel et al. 2015 [71] indicated that the efficient formation of negatively charged ions is connected to a plasma in front of a cathode that is sputtered by Cs^+ ions (compare section 2.3.2). Recession of the sample relative to the front of the cathode would leave a volume for the needed plasma to form. Therefore, a geometry with recessed sample material compared to the Cu cathode should show increased UF_5^- ionization efficiency from Vienna-KkU-D30 mixed 1:9 with PbF_2. An experiment using an adapted NEC sample holder geometry (fig. 6.8) was conducted whether the recession of the sample material would increase the formation of UF_5^-. In addition, the ionization efficiency of the two most extracted $UO_xF_y^-$ molecules, namely UO_3F^- and $UO_2F_2^-$ were measured for comparison.

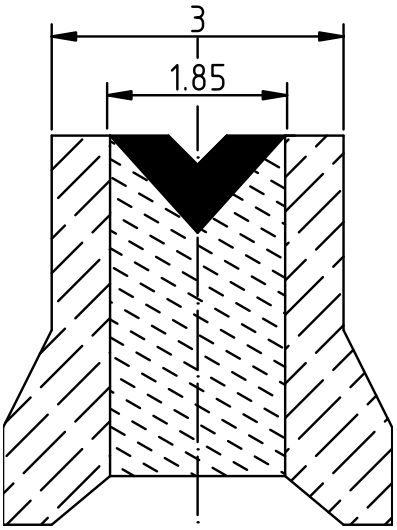

Figure 6.8.: Cut section scheme of the cylindrical NEC copper sample holder with 3 mm outer diameter (reamed to 1.85 mm inner diameter) and new copper wire inlet (2.5 mm^2 cross section) that features a pressed-in conical indentation. The sample material is indicated by the filled black area. Dimensions are given in mm.

The preparation procedure was the following: First, the sample material was prepared from the uranium in-house standard material Vienna-KkU-D30 mixed together with PbF_2 (c) in the ratio 1:9 as presented in table A.6. Then the individual copper wire inlets were indented, filled with the sample material and sub-

sequently pressed with a smaller cone to produce the characteristic double conical shaped sample surface. Thereafter the equipped copper wire inlets were pressed in the reamed NEC sample holder. In the end, six identically prepared samples were mounted to a sample wheel and measured as described in section 6.1.

6.4.1. Results for recessed sample material geometry

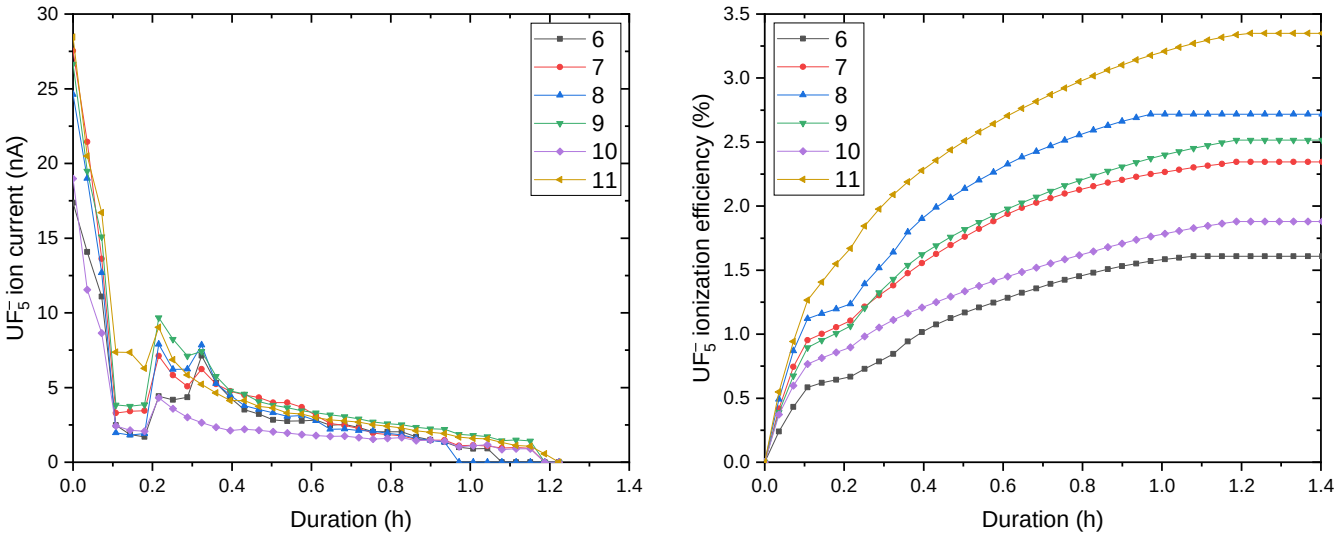

(a) UF_5^- ion current per mass scan.

(b) Cumulative UF_5^- ionization efficiency.

Figure 6.9.: Results on UF_5^- for adapted cathode geometry in Fig. 6.8. Samples were identically prepared and details are given in table A.6 in the appendix.

As shown in Fig. 6.7a the prepared samples of the material Vienna-KkU-D30 mixed 1:9 with PbF_2 were sputtered even faster than in the previous measurements due to their limited size of about 0.5-0.85 mg. After 1 h more than 90% of the total extracted UF_5^- was sputtered from the cathodes. The reason for the decline in UF_5^- ion current after the first three mass scans was not clearly indicated by Cs supply or ionizer power. The investigation of the samples with adapted sample holder geometry could not yield a significantly increased mean cumulative UF_5^- ionization efficiency in comparison with previous target materials and standard geometries. However, the variability of the UF_5^- ionization efficiency results shown in Fig. 6.9b is increased. The increased variability could stem from the small overall sample sizes of 0.5-0.85 mg which were difficult to handle combined

with the experimental preparation procedure for cone-shaped cathode indentation and sample material pressing.

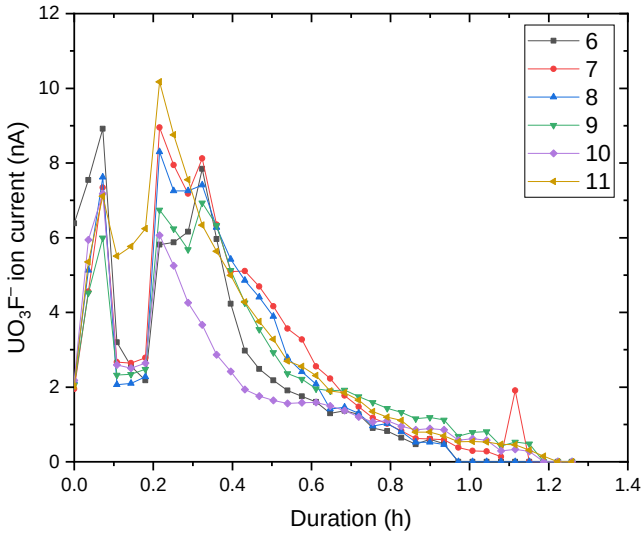

(a) UO_3F^- ion current per mass scan.

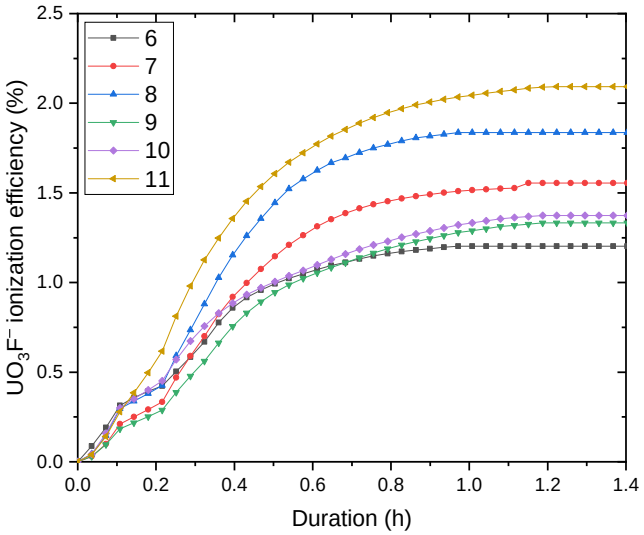

(b) Cumulative UO_3F^- ionization efficiency.

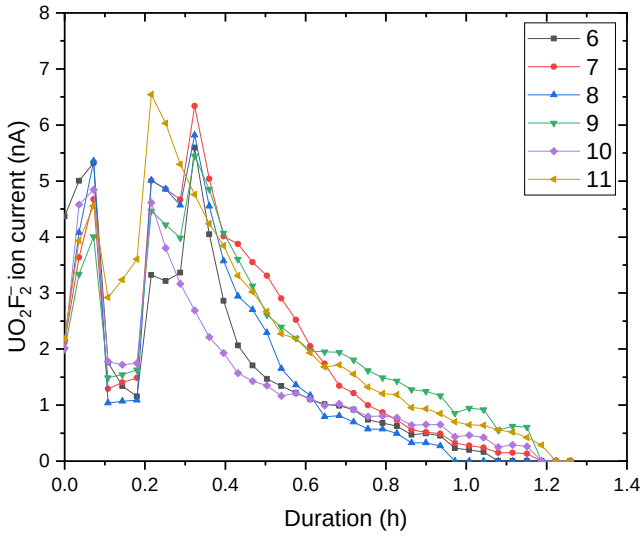

(c) $UO_2F_2^-$ ion current per mass scan.

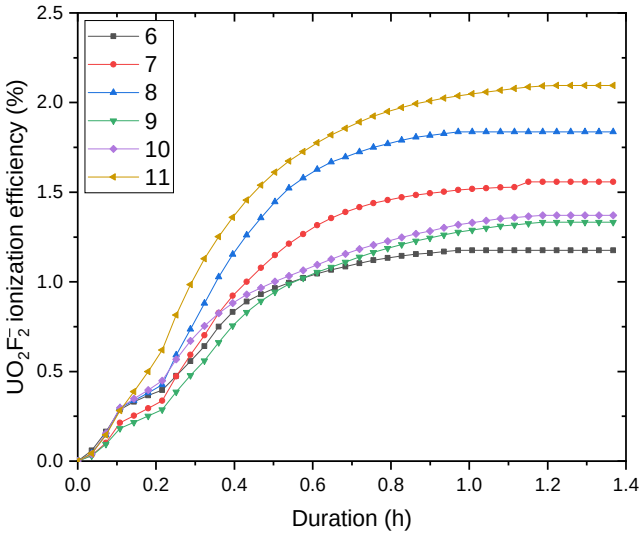

(d) Cumulative $UO_2F_2^-$ ionization efficiency.

Figure 6.10.: Results on UO_3F^- and $UO_2F_2^-$ extraction for adapted cathode geometry in Fig. 6.8. Sample details are given in the appendix A.6.

The ion currents of the molecules UO_3F^- (fig. 6.10a) and $UO_2F_2^-$ (fig. 6.10c) show the same extraction pattern. The prominent drop in ion current that occurred

between 0.1 and 0.2 h in all three ion current graphs (figs. 6.9a, and) was produced by an excessive counter-reaction of the source regulation from too high output currents. It decreased the ionizer for three consecutive mass scans. The comparison of the ion currents from UF_5^- relative to UO_3F^- or $UO_2F_2^-$ show that UF_5^- is only predominantly extracted for the first few scans and then declines to the same levels as UO_3F^- or $UO_2F_2^-$.

Furthermore, the respective ionization efficiencies of the two molecular species UO_3F^- (Fig. 6.10b) and $UO_2F_2^-$ (Fig. 6.10d) have been investigated. They showed, as already indicated in section 6.1, that the production of these molecules also extract a substantial share of the total available U in the sample material.

A summary on the mean ionization efficiency results of all three investigated molecules i.e. UF_5^-, UO_3F^- and $UO_2F_2^-$ is shown in table 6.7. The relative ionization efficiency for the three investigated ions UF_5^-: UO_3F^- : $UO_2F_2^-$ are about 1.0 : 0.7 : 0.7.

Table 6.7.: Ionization efficiency results for the three extracted molecules UF_5^-, UO_3F^- and $UO_2F_2^-$ with 1σ uncertainty. Recessed samples were sputtered from a sample holder with adapted geometry to form a conical shaped sample surface. Compare Fig. 6.8 for details.

Extracted ion	Ionization efficiency η (%)
UF_5^-	(2.16 ± 0.56)
UO_3F^-	(1.57 ± 0.34)
$UO_2F_2^-$	(1.56 ± 0.35)

The recessed sample material geometry due to a cone shaped surface of the sample did not show significantly increased ionization efficiency. Furthermore, higher variability in UF_5^- ionization efficiency results was observed. No statistical advantage was apparent to justify the effort required to prepare the conical sample surface.

The theory of competing processes to form $UO_xF_y^-$ molecules is supported by the data. The ionization efficiency confidence intervals overlap within $1\,\sigma$ for all of the three molecules. The above findings emphasize the need for a environmental sample preparation where the initial matrix material powderr should be thoroughly

homogenized with PbF_2 powder to ensure high UF_5^- production and less other $UO_xF_y^-$ molecules. Another approach to achieve this could be the liquid admixture of the sample matrix to PbF_2 or the preparation of an already fluorine-rich sample matrix that is mixed with PbF_2.

6.5. $^{238}UF_5^-$ Ionization yield for new sample preparation procedures

In this experiment four new sample preparation procedures and materials were investigated for their UF_5^- ionization efficiency. For each of the four methods a batch of samples matrices were prepared and mixed with PbF_2 1:9 by weight ratio. Two batches were prepared according the preparation procedures described in chapter 4. Samples were individually dried from a solution of Vienna-KkU on Fe in contrast to the co-precipitated Vienna-KkU-D30 in previous experiments. The mixture of the first batch was prepared including a calcination step and the material was called "Vienna-KkU_+calc" accordingly (compare section 4.2). The second material mixture was dried without calcination of the matrix an was therefore denoted "Vienna-KkU_dry" (compare section 4.1).
In addition, a third and fourth batch was prepared, using a different chemical procedure based on changing to the co-precipitation of Vienna-KkU as UF_4 within the respective matrix of NdF_3 or PrF_3 in hydrofluoric acid. The preparation was designed and executed by Tomáš Prášek from CTU Prague according to Prášek et al. 2020 [43]. Subsequently the matrices were dried at up to 400°C under Ar-H_2 atmosphere and afterwards mixed 1:9 with PbF_2 and pressed into NEC Cu cathodes. The two mixtures were called "Vienna-KkU_NdF" and "Vienna-KkU_PrF".

The measurement procedure to investigate $^{238}U^{19}F_5^-$ extraction was adapted from previous experiments in this thesis. The optimally lowered ion source control current (of $I_C = 27.5\,\mu$A, compare section 6.3) was applied. Additionally, the atomic mass area in which the evaluation program searched for the maximum UF_5^- current was restricted to 332.9-333.2 u to further avoid Cu_5F^- contribution.

6.5.1. Results on UF_5^- ionization for new sample preparation procedures

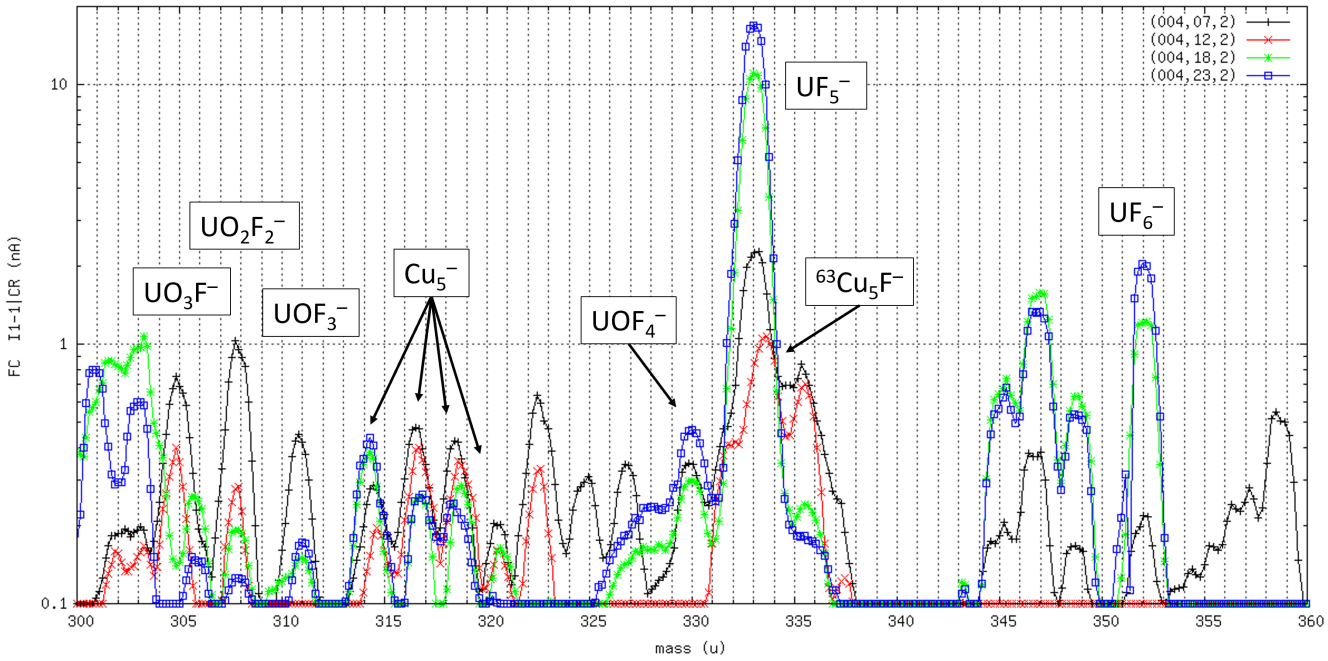

Figure 6.11.: Logarithmic ion current vs. mass for material mixtures produced from four new sample preparation procedures. The material Vienna-KkU_dry is shown by a red line. The mixtures Vienna-KkU_anneal is indicated by a black line. Vienna-KkU_NdF is shown in green and Vienna-KkU_PrF in blue. The mass scan was taken after about 45 min of sputter duration. Sample details are shown in table A.7

The calcinated mixture Vienna-KkU_calc indicated by the black line in Fig. 6.11 shows a clear $^{238}UF_5^-$ signal while it was also possible to identify other extracted $UO_xF_y^-$ molecules. The UF_5^- peak of mixture Vienna-KkU_dry (red line) was shifted to a higher atomic mass. This indicates that mainly $^{63}Cu_5F^-$ ions were extracted instead of UF_5^-. For example the molecule UOF_4^- was not extracted at all for this material that was only dried and mixed with PbF_2. Both co-precipitated materials Vienna-KkU_NdF (green line) and Vienna-KkU_PrF (blue line) produced strong UF_5^- ion currents with up to 7 times the intensity of the oxide based mixtures. Moreover, a clear $^{238}UF_6^-$ peak without significant background of $^{63}Cu_5F_2^-$ was extracted. In the following the UF_5^- ion current characteristics and

ionization efficiency over the whole sputter duration is presented for every mixture.

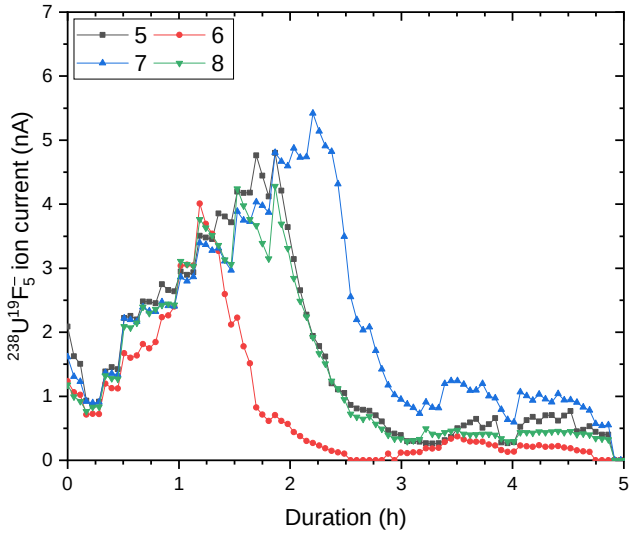

(a) UF_5^- ion current per mass scan for samples of the mixture Vienna-KkU_calc.

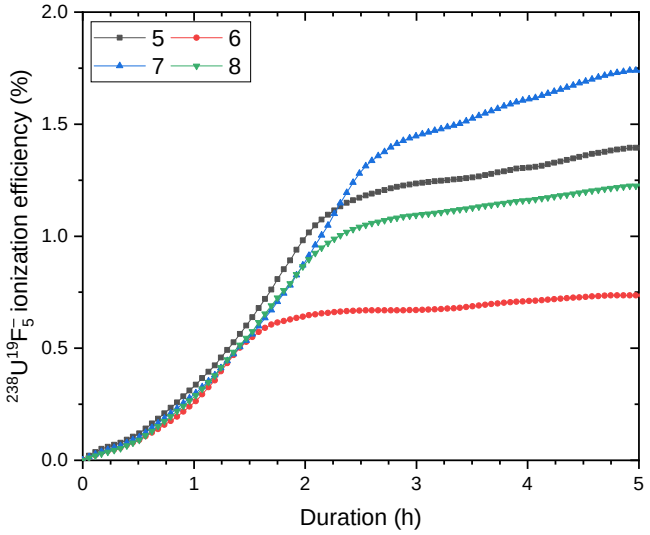

(b) UF_5^- ionization efficiency for samples of the mixture Vienna-KkU_calc.

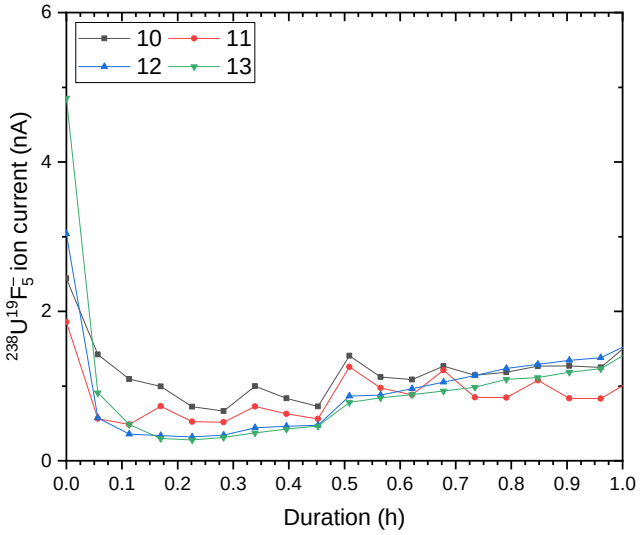

(c) UF_5^- ion current per mass scan for samples fo the mixture Vienna-KkU_dry.

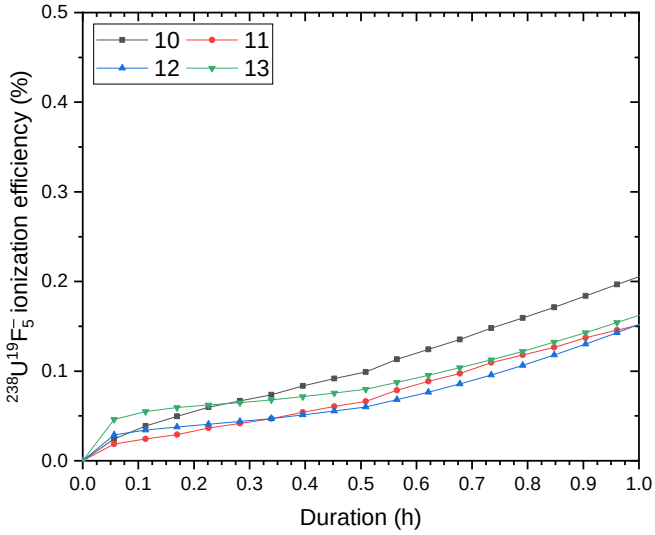

(d) UF_5^- ionization efficiency for samples fo the mixture Vienna-KkU_dry.

Figure 6.12.: Results on UF_5^- extraction from samples of the mixture Vienna-KkU_calc with calcinated U containing iron oxide matrix and for the mixture Vienna-KkU_dry including a dried ion matrix. Details on the measured samples are given in the appendix A.7.

Investigation of the UF_5^- ion current output from samples of the mixture Vienna-

KkU_calc showed a different extraction pattern over time compared to previous experiments. Initially, the ion current in Fig. 6.12a started from levels of around 2 nA and rose to its maximum after about two hours of sputter duration. The UF_5^- ion current decreased sharply for all samples after this maximum.
The UF_5^- ionization efficiency results in Fig. 6.12b showed a substantial variability between the samples. The mean cumulative ionization efficiency of the mixture Vienna-KkU_calc accounted for (1.30±0.45)%. The ionization efficiency of Vienna-KkU_calc showed about 65% of the powder mixed results of Vienna-KkU-D30 with PbF_2 of (1.99±0.24) from previous measurements in this thesis. However, the evaluation of the ionization efficiency for Vienna-KkU_calc includes possible transfer losses through the preparation process and is therefore a first conservative result for the UF_5^- ionization efficiency from this material. The variability of ionization efficiency results of samples containing Vienna-KkU_calc is most probably a result of different transfer efficiencies. Electrostatic charging of the quartz crucibles and the usage of quartz rods for homogenization of the mixtures left significant amounts of sample material inside the crucibles. Only two of the samples were prepared solely using anti-electrostatic spatulas.

As shown in the mass scan in Fig. 6.11 the mixture Vienna-KkU_dry almost exclusively extracted an ion current that peaked near $^{238}UF_5^-$. This peak was attributed to $^{63}Cu_5F^-$. This was unique to Vienna-KkU_dry relative to all other mixtures during this experiment. However, from the start of the measurement up to 45 min sputter duration the peak center of the mainly extracted ion current showed contribution of $^{238}UF_5^-$. Therefore, only the first hour of extracted ion current between 332.9-333.2 u was taken into account for the evaluation of the UF_5^- ionization efficiency of Vienna-KkU_dry. The UF_5^- ion current started around 2-3 nA and decreased after the first few minutes to 1 nA and remained at this level for the first hour of sputter duration (compare fig. 6.12c). The evaluation of the UF_5^- ionization efficiency for Vienna-KkU_dry resulted in (0.176±0.023)%. Comparison of the ionization efficiency of other extracted ions i.e. $UO_2F_2^-$ shows 0.67 ± 0.20% for Vienna-KkU_dry and 0.66 ± 0.27 for Vienna-KkU_calc. This indidates that possible remaining humidity could favour production of $UO_xF_y^-$ molecules. Thus, two most probable reasons for the distinctively lower UF_5^- ionization efficiency are remaining humidity due to low temperature drying of the U containing matrix or

U sample losses using the vacuum transfer mechanism (compare chapter 4). To assess the formation of UF_5^- samples of Vienna-KkU_dry cathode materials that do not show interfering ions would be needed.

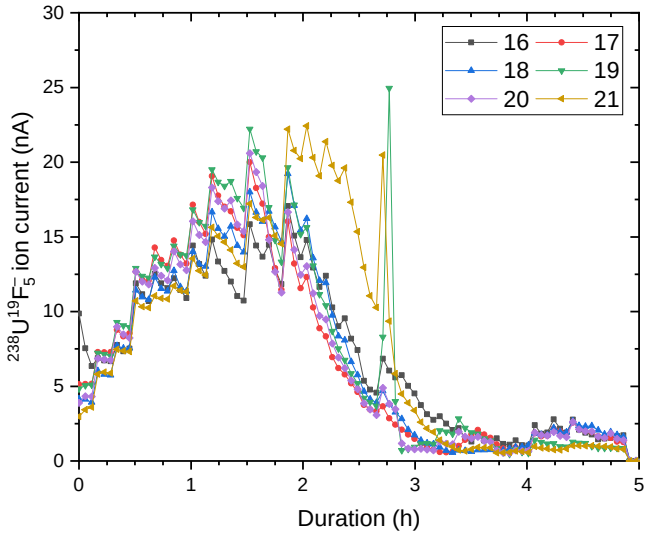

(a) UF_5^- ion current per mass scan for samples of mixture Vienna-KkU_NdF.

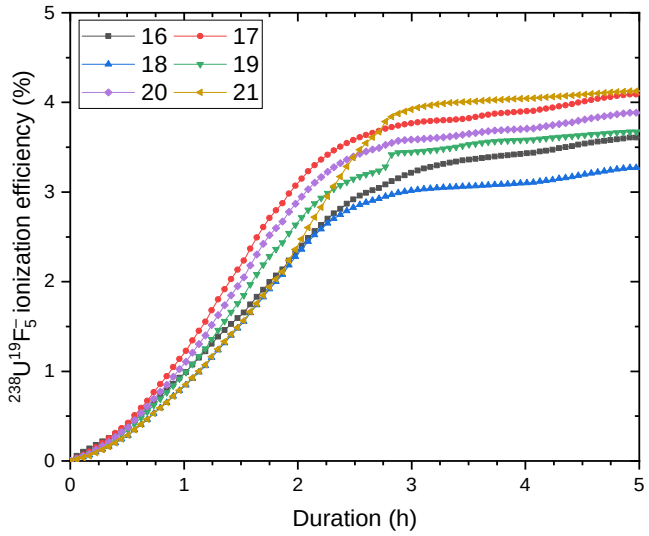

(b) Cumulative UF_5^- ionization efficiency for samples of Vienna-KkU_NdF.

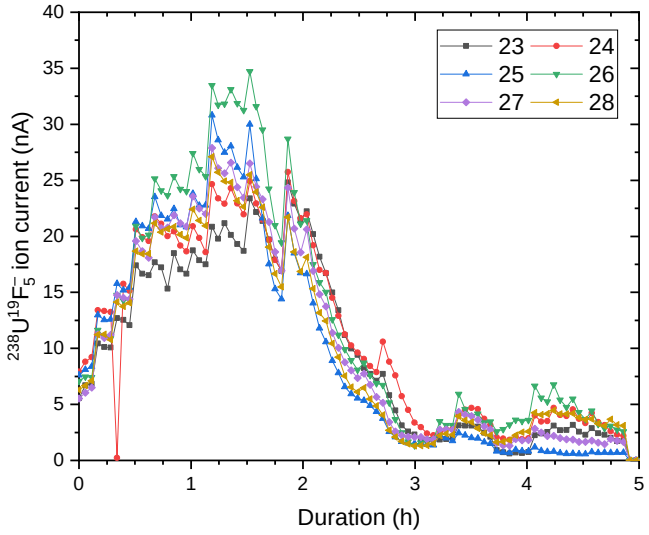

(c) UF_5^- ion current per mass scan for samples of Vienna-KkU_PrF.

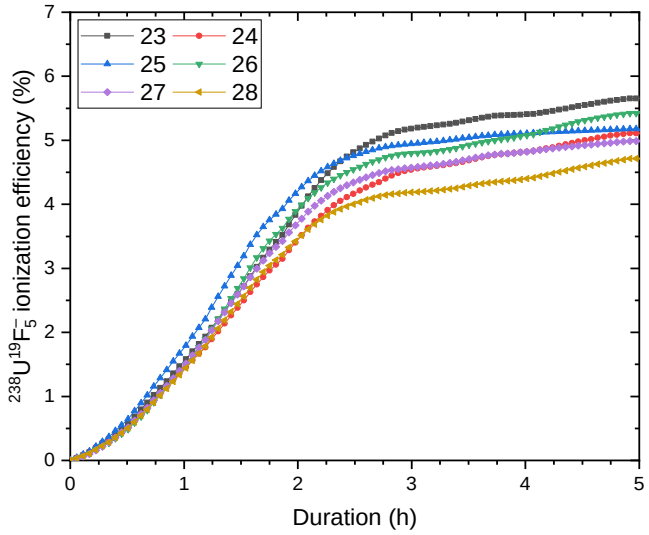

(d) Cumulative UF_5^- ionization efficiency for samples of Vienna-KkU_PrF

Figure 6.13.: Results on UF_5^- extraction for samples prepared from Vienna-KkU_NdF or Vienna-KkU_PrF. Details on the individual samples is given in the appendix A.7).

The UF_5^- ion current extracted from the samples containing Vienna-KkU_NdF started from levels of around 5 nA and stabilized at the maximum output around 15-20 nA (compare fig. 6.13a). The extracted ion current remained at this level between 1 h to 2 h after the start of the measurement. This led to a nearly constant ionization efficiency increase for the first 2.5 h of sputter duration in Fig. 6.13b. About 90% of total extracted UF_5^- ions were measured within the first 2.5 h. The sample batch prepared Vienna-KkU_NdF showed a mean cumulative UF_5^- ionization efficiency of $(3.40 \pm 0.28)\%$.
The investigation of Vienna-KkU_NdF showed a factor of up to 2 higher mean cumulative ionization efficiency compared with Vienna-KkU-D30 mixed with PbF_2 from previous measurements. Samples of Vienna-KkU_PrF extracted up to 2.5 times higher UF_5^- ionization efficiency. Drying of the co-precipitated sample materials Vienna-KkU_NdF and Vienna-KkU_PrF under Ar-H_2 atmosphere with temperatures of 300°C or 400°C compared to 50°C did not result in a further increase of UF_5^- ionization efficiency.

Table 6.8.: Summary of mean cumulative UF_5^- ionization efficiency results with 1σ uncertainty of four sample preparation methods.

Material	Ionization efficiency η (%)
Vienna-KkU_dry	(0.176 ± 0.023)
Vienna-KkU_calc	(1.30 ± 0.45)
Vienna-KkU_NdF	(3.40 ± 0.28)
Vienna-KkU_PrF	(4.67 ± 0.28)

Initially extracted UF_5^- ion currents from samples of Vienna-KkU_PrF of 5-10 nA were measured and peaked at 25-35 nA after 1.5 h of sputter duration. This is given in Fig. 6.13c. The extraction of UF_5^- ion current over time was similar to Vienna-KkU_NdF, but showed slightly higher ion currents. The batch of samples including Vienna-KkU_PrF showed a mean cumulative ionization efficiency of $(4.67 \pm 0.28)\%$ (compare fig. 6.13d). A summary of mean cumulative UF_5^- ionization efficiency results of all investigated materials during this experiment is given in table 6.8.
Both Vienna-KkU_NdF and Vienna-KkU_PrF showed, that the production of O containing $UO_xF_y^-$ molecules was clearly reduced through the preparation of U as UF_4. They therefore seem to allow the extraction of U ionized as i.e. $UO_2F_2^-$ or

UOF_3^- from mixtures that included an uranium oxide based matrix.
The findings for PrF_3 co-precipitated UF_4 present the optimal combination of matrix composition and the possibility to steadily extract large amounts of U as UF_5^- even with reduced Cs supply. However, for the preparation of this matrix material by means of HF, extended personal protective equipment is required in addition to the appliances for HF use.

7. Uranium fluorides for AMS

An AMS measurement was started to investigate the possible use of UF_5^- as low energy molecule for U extraction by AMS. The isotope ratios $^{236}U/^{238}U$, $^{233}U/^{238}$, $^{233}U/^{236}U$ and $239^{3+}/^{238}U^{3+}$ of the materials which were presented in previous chapters i.e. Vienna-KkU-D30, Vienna-KkU_NdF and Vienna_PrF mixed with 1:9 PbF_2 were studied. Furthermore, an air filter sample and its process blank were studied using UF^-. The $^{236}U/^{238}U$ ratios of the sample and process blank were then compared to the results obtained by previous AMS measurements using UO^-. The formation of uranium hydrides by AMS using UF_5^- was assessed with the $239^{3+}/^{238}U^{3+}$ ratio from the Pu-free [64] Vienna-KkU-D30 mixed with 1:9 PbF_2.

7.1. AMS setup for $^{236}U^{3+}$ and $^{233}U^{3+}$ detection from UF_5^-

For present AMS measurements of U using UO^- at VERA, $^{238}UO^-$ is extracted from Vienna-KkU-D30 and used to deliver a pilot beam ion current for the ion optical adjustment up to the tandem accelerator. The optimal charge state for transmission through the accelerator is U^{3+} with electron stripping by He gas and an accelerator terminal voltage of 1.65 MV with the most recent setup [64]. The $^{238}U^{3+}$ pilot ion current is measured in the Faraday cup FC L4-1 (compare fig 7.1). To achieve optimal ion optical adjustment of the VERA instrument for trace isotope measurements, $^{238}U^{3+}$ is extracted from either a cathode containing residual environmental graphite material (as $^{238}UC^-$) or pure iron oxide (as $^{238}UO^-$). Several $\approx 10^3$ counts per second of $^{238}U^{3+}$ are sufficient. Vienna-KkU-D30 is also used as an isotope standard material, for the measurement of $^{236}U/^{238}U$ ratios [63].

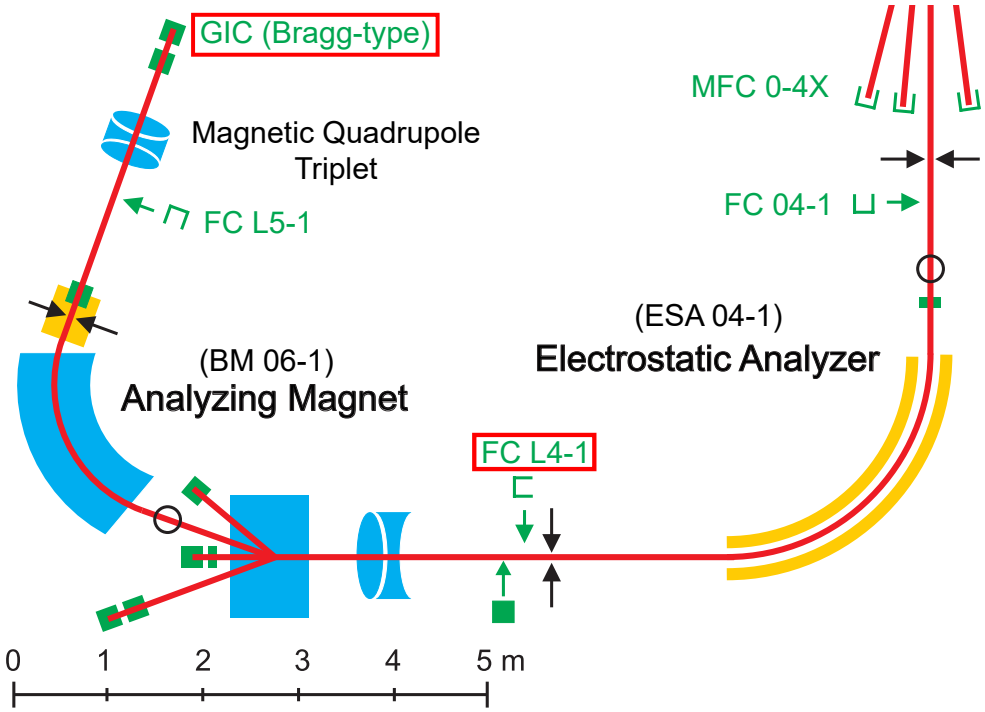

Figure 7.1.: Terminal section setup of the VERA instrument used for the detection of actinides with most important parts labeled. The ion current of abundant isotopes as $^{238}U^{3+}$ is measured in FC L4-1 and trace isotope ions like $^{236}U^{3+}$ and $^{233}U^{3+}$ are detected in the Bragg-type GIC.

The main difference between measurement procedures incorporating uranium fluoride instead of oxide molecules was the ion optical adjustment for the UF_5^- pilot beam on the low energy side. To inject $^{236}UO^-$ ions in the accelerator, VERA uses the Multi Beam Switcher (MBS) at BM01-1 (compare Fig. A.1), where ions can be decelerated by different electric potentials in recurring cycles. Individual ion optical settings were used to inject the other investigated ions i.e. $^{238}UHF_5^-$ (or $^{239}PuF_5^-$), $^{233}UF_5^-$, $^{232}ThF_5^-$. The injected low energy ions and their corresponding high energy fragment masses are shown in table 7.1. High energy settings for components past the accelerator were not substantially changed in comparison to AMS using UO^-. The ion current of $^{238}U^{3+}$ at the high energy section was measured at the Faraday cup FC L4-1 (Fig. 7.1) using. Trace isotope detection was conducted

at the beamline after the Faraday Cup and after another magnetic spectrometer BM06-1.

Table 7.1.: Atomic masses of the investigated low and high energy ions of the current (^{238}U) and trace isotopes detected during the AMS measurement presented in this work. Shown masses per ion indicate the values for ion optical adjustment of the VERA instrument. Ions of atomic mass 239.05 u in charge state $q = 3+$ were considered either as $^{238}UH^{3+}$ or $^{239}Pu^{3+}$).

Detection	Low energy ion	mass (u)	high energy ion	mass (u)
FC L4-1	$^{238}UF_5^-$	333.04	$^{238}U^{3+}$	238.05
GIC	$^{236}UF_5^-$	331.04	$^{236}U^{3+}$	236.05
	$^{238}UHF_5^-$ ($^{239}PuF_5^-$)	334.04	$^{238}UH^{3+}$ ($^{239}Pu^{3+}$)	239.05
	$^{233}UF_5^-$	328.04	$^{233}U^{3+}$	233.05
	$^{232}ThF_5^-$	327.03	$^{232}Th^{3+}$	232.04

Individual charged ions from trace isotopes were detected in the gas ionization chamber (GIC). There they deposited their energy and were distinguished for their proton number Z by the pulse height and width of the ionized particle drifting between the electrodes. When detected count rates of trace isotopes in the GIC i.e. $^{232}Th^{3+}$ rose above 10^5 counts per second, the corresponding high energy ion current was measured instead. Ions of mass 239.05 u in the charge state 3+ (i.e $^{238}UH^{3+}$) were measured for every cathode consisting of Vienna-KkU to monitor molecular isobaric interference due to the formation of hydrides [73].

The measurement duration was divided into sequences for each individual isotope. The sequences were set for ^{238}U to several seconds, and increased for rare isotopes ^{239}UH (^{239}Pu) to 60 s, ^{236}U to 360 s and for ^{233}U to 2100 s. Between every trace isotope an additional ^{238}U current measurement was performed to interpolate the $^{238}U^{3+}$ currents. A whole cycle of all trace isotopes and current measurements was called a "run". In total a single run would take between 3200 s to 3600 s.

$$\eta_{det} = \sum_i \frac{\tau_j \cdot I_j^q}{m_{\text{sample}} \cdot n_{iso} \cdot q \cdot e} \tag{7.1}$$

The quantity to assess the efficiency of a single isotope to that is present in a sample to be detected in the FC L4-1 was denoted as the total detection efficiency. It also included the ionization efficiency, the particle transport at the low energy section of VERA, the injection to the accelerator and the selection for the most probable charge state after the accelerator. The interpolated $^{238}U^{3+}$ current was integrated for every run duration to obtain the total detection efficiency relative to the U amount per sample. The total detection efficiency is given in equation 7.1. Therein τ_j is the duration of the j-th run, I_j^{3+} is the measured and interpolated isotope ($^{238}U^{3+}$) current in the j-th run, q the ion charge state at FC L4-1, m_{sample} the sample mass, n_{iso} the number of isotopes per mass and e the elemental charge. The isotopic ratios were determined by the measured ion currents of $^{238}U^{3+}$ in comparison to the single detected ions for $^{233}U^{3+}$ and $^{236}U^{3+}$. The evaluation per cathode was performed with a spreadsheet file adapted from a template of Prof. Peter Steier. The average isotope ratios per investigated sample material or mixture were calculated by the author. Details on the evaluation are given in the appendix A.7.

According to Winkler et al. 2015 [73], the observation of possibly occurring $^{238}UH^{3+}$ can be used to assess the formation of uranium hydrides in general. As ^{235}U is up to 10^{10} times more abundant than ^{236}U, even minor production of $^{235}UH^{3+}$ would be a consequential background to the detection of $^{236}U^{3+}$. In order to determine the formation of uranium hydrides by using UF_5^- extraction, ions that fulfill the condition of atomic mass 239 u and charge state 3+, were detected. Vienna-KkU [63] is regarded Pu-free [64] and detected "mass 239^{3+}" ions were counted as $^{238}UH^{3+}$. For the investigation of unknown sample material, detected counts could also include $^{239}Pu^{3+}$, which had also to be considered for added matrix materials comparably to PbF_2 in this work.

7.2. Materials analyzed by AMS using UF_5^- extraction

Typically, three categories of materials are necessary to carry out actinide AMS measurements at VERA in addition to the investigated samples and blank materials: tuning materials for a current pilot beam, an isotopic standard and a material for trace isotope components tuning.
Firstly, ion current tuning material is needed to adjust the beam optics of the whole VERA instrument. Ion currents for reliable pilot beam tuning should be at least in the order of pA at the Faraday cup FC L4-1. The mixture of Vienna-KkU-D30 combined with PbF_2 in the optimal weight ratio of 1:9 served this purpose. Cathodes from this mixture are indicated cur01 to cur03 in table 7.2.
Secondly, an isotopic standard material was needed. Vienna-KkU-D30, the $^{236}U/^{238}U$ standard, for routine actinide measurements at VERA for AMS using UO^-, was mixed with PbF_2. Then it was checked if the $^{236}U/^{238}U$ ratio of this mixture using UF_5^- extraction would be in line with results by AMS using UO^- extraction. Cathodes cur01 to cur03 were therefore also used for the evaluation as isotopic standard.
Thirdly, a material to adjust beam optics for detection of single trace isotope ions e.g. $^{236}U^{3+}$ and $^{233}U^{3+}$ for the Bragg-type GIC was needed. An approximate rate of (0.5 - 5)$\times 10^4$ counts per second (cps) is sufficient for the optimization of ion optics of the VERA instrument up to the point of the GIC. A mixture of Fe powder (material details (f)) powder combined with PbF_2 (material details (c)) was found as adequate count rate tuning material. The optimal mixing ratio of annealed Fe Powder to PbF_2 was 1:9. The used isotope for count rate tuning was $^{235}U^{3+}$. Repeated count rate measurements detected (0.5 - 7)$\times 10^4$ cps of $^{235}U^{3+}$ from this mixture. The cathodes used for count rate tuning are denoted cnt01 to cnt03 in table 7.2

Three different mixtures were prepared as proxies for the investigation of their total detection efficiency and isotopic ratios. The first was the material Vienna-KkU-D30 mixed 1:9 with PbF_2 which was already investigated for its ionization yield in the previous chapters. This time with AMS, it was possible to examine each mixture for their total $^{238}U^{3+}$ detection efficiency without background from Cu_5F clusters. The mixture is indicated by "I" and individual cathodes filled with this mixture are denoted pwd01 to pwd06 in table 7.2.
The second mixture consisted of co-precipitated Vienna-Kku_NdF indicated as "II" with the individual cathodes denoted TP01 to TP03. The third mixture was Vienna-KkU_PrF indicated as "III" in all figures and tables. Both co-precipitated matrices were also mixed 1:9 PbF_2 weight ratio. Individual cathodes are called TP04 to TP06. These mixtures were identical to the investigated samples in the previous chapter 6.5.

In addition, a Whatman 501 type air filter sample called "3C_U" and a corresponding process blank "BLK_2C" were first chemically purified and subsequently prepared by drying without calcination with an Fe matrix of about 190 μg (from pre-nuclear Fe solved in 6M HCL) and mixed 1:9 with PbF_2 (compare chapter 4). The sample 3C_U is an air filter sample that represents the quarterly mean of aerosol constituents from July to September 1966 at the air sampling station Hohe Warte in Vienna, Austria [69]. Both sample and process blank were investigated before on their $^{236}U/^{238}U$ ratio at VERA extracted as UO^- giving the $^{236}U/^{238}U$ results of $(1.48 \pm 0.14) \times 10^{-6}$ (3C_U) and $(8.3 \pm 4.6) \times 10^{-8}$ (BLK_2C). A roughly 9:1 higher amount of sample material was used for AMS analysis using UF_5^- extraction in comparison to the previous measurement with extraction as UO^- molecule. In contrast to the material investigated in section 6.5 an easier way to transfer the sample into the cathode was chosen. Instead of the "sample vacuum cleaner" (compare chapter 4) 3C_U and BLK_2C were directly transferred to their Cu cathodes using weighing paper. The comparison of the $^{236}U/^{238}U$ ratios via UO^- and UF_5^- extraction was intended as a test for AMS using UF_5^- extraction.

Table 7.2.: Detailed information for the investigated samples by AMS. Every matrix was mixed 1:9 with PbF_2. The mixture abbreviation is given in brackets. Cathodes for count rate tuning cnt01-cnt03 were loaded with an iron oxide (material specs (f)) matrix. Samples "pwd0X" consisted of Vienna-KkU-D30 (I), TP01-TP03 of Vienna-KkU_NdF (II) and TP04-TP06 of Vienna-KkU_PrF (III). The weight ratios of PbF_2 to matrix materials, the total mass of each sample m_c and the total uranium mass per cathode $m_{U_{cat}}$ are given for those samples with known content. At positions 15 and 16 the individually dried samples with about 190 μg Fe (from pre-nuclear Fe solved in 6M HCL) matrix mass are shown.

wheel pos.	label	mixture	$m_{PbF_2} : m_{matrix}$	m_c (mg)	$m_{U_{cat}}$ (μg)
5	cnt01	-	8.96	(7.04 ± 0.01)	unknown
6	cnt02	-	8.96	(8.35 ± 0.01)	unknown
7	cnt03	-	8.96	(6.82 ± 0.01)	unknown
5	cur01	I	8.99	(4.56 ± 0.01)	(12.7 ± 0.3)
6	cur02	I	8.99	(7.65 ± 0.01)	(21.3 ± 0.5)
7	cur03	I	8.99	(7.57 ± 0.01)	(21.1 ± 0.5)
8	pwd01	I	9.00	(2.04 ± 0.01)	(5.7 ± 0.2)
9	pwd02	I	9.00	(2.07 ± 0.01)	(5.8 ± 0.2)
10	pwd03	I	9.00	(2.01 ± 0.01)	(5.6 ± 0.2)
11	pwd04	I	9.00	(1.90 ± 0.01)	(5.3 ± 0.2)
12	pwd05	I	9.00	(1.95 ± 0.01)	(5.4 ± 0.2)
13	pwd06	I	9.00	(2.26 ± 0.01)	(6.3 ± 0.2)
15	BLK_2C	-	$1.92 : (0.19 + X)$	not weighed	unknown
16	3C_U	-	$1.93 : (0.19 + X)$	not weighed	unknown
18	TP01	II	8.88	(1.98 ± 0.01)	(7.5 ± 0.2)
19	TP02	II	8.88	(2.11 ± 0.01)	(7.9 ± 0.2)
20	TP03	II	8.88	(2.16 ± 0.01)	(8.1 ± 0.2)
21	TP04	III	9.04	(1.79 ± 0.01)	(6.6 ± 0.2)
22	TP05	III	9.04	(1.86 ± 0.01)	(6.9 ± 0.2)
23	TP06	III	9.04	(2.02 ± 0.01)	(7.5 ± 0.2)

7.3. Results for AMS using UF_5^- extraction

7.3.1. AMS detection efficiency of $^{238}U^{3+}$ from $^{238}UF_5^-$

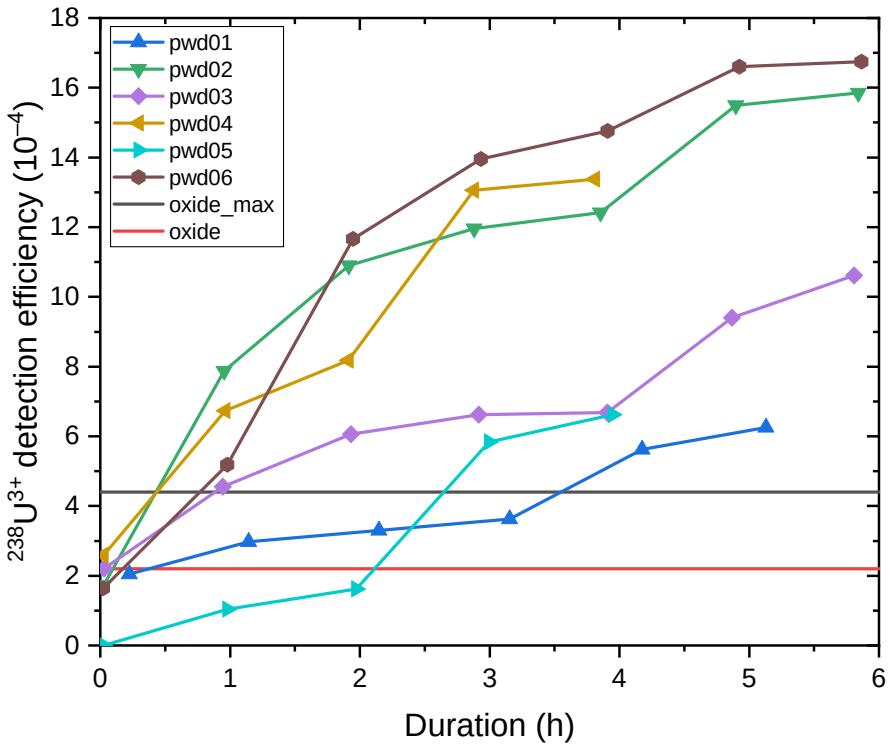

Figure 7.2.: Detection efficiency of $^{238}U^{3+}$ for samples of Vienna-KkU-D30 mixed 1:9 with PbF_2 material (pwd0X). The average (oxide) and maximum (oxide_max) detection efficiency achieved with advanced dried sample treatment for environmental material [13] via UO^- extraction are indicated by red and black straight lines for comparison.

The detection efficiency of the investigated mixtures over measurement duration are shown in Fig. 7.2 and 7.3. Data points are only shown for complete runs per each cathode. Six turns were completed for this work, but not every sample was measured for all the turns. This explains differences in the measurement duration per cathode. The detection efficiency for cathodes pwd01 to pwd06 ranged $(6.3-16.7)\times10^{-4}$. The average detection efficiency resulted in $(11.6\pm4.6)\times10^{-4}$. The average (solid red line) of 2.2×10^{-4} and the highest (black) ever achieved detection efficiency ($\approx 4.4\times10^{-4}$) for UO^- extraction are also shown for comparison in Fig. 7.2. The detection efficiency of samples containing Vienna-KkU-D30

mixed 1:9 with PbF_2 of $(11.6 \pm 4.6) \times 10^{-4}$ is about five times higher than the average for the best measurement using UO^- extraction [13; 64]. Also cathodes that were not measured during all runs of the measurement were included for the evaluation, which lowered this average.

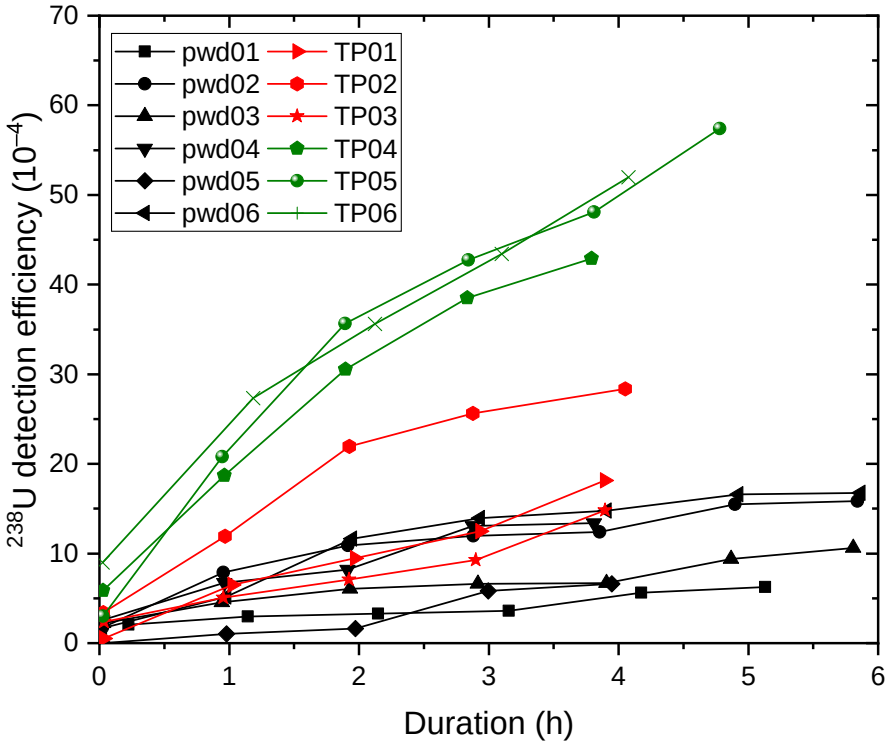

Figure 7.3.: Detection efficiency for all samples with known total ^{238}U content, given in table 7.2. Samples containing Vienna-KkU-D30 mixed 1:9 with PbF_2 are shown in black. The samples of Vienna-Kku_NdF are given in red and Vienna-Kku_PrF in green. Both were additionally mixed 1:9 with PbF_2.

The analysis of the detection efficiency over time for samples containing Vienna-Kku_NdF (TP01 to TP03) or Vienna-Kku_PrF (TP04 to TP06), led to the results in Fig. 7.3. Samples TP01 to TP03 are colored in red and showed an average detection efficiency of $(20.4 \pm 7.1) \times 10^{-4}$. The samples and TP04 to TP06 in green delivered an average value of $(47.6 \pm 7.6) \times 10^{-4}$. Results for Vienna-KkU-D30 mixed 1:9 with PbF_2 in pwd01 to pwd06 are demonstrated in black

for comparison. Samples containing co-precipitated Vienna-KkU_NdF or Vienna-KkU_PrF, showed even higher detection efficiency results of $(20.4 \pm 7.1) \times 10^{-4}$ and $(47.6 \pm 7.6) \times 10^{-4}$ respectively. These findings show, that matrix materials with U already prepared as UF_4, increase the total ^{238}U detection efficiency by a factor of 2 to 4 compared to the most efficient uranium oxide based matrices, to levels unattained at VERA until now. Especially co-precipitated Vienna-KkU_PrF mixed with PbF_2 by 1:9 achieved about four-fold increase to the powder mixtures of Vienna-KkU-D30 combined with PbF_2.

7.3.2. Trace isotope results using UF_5^- extraction

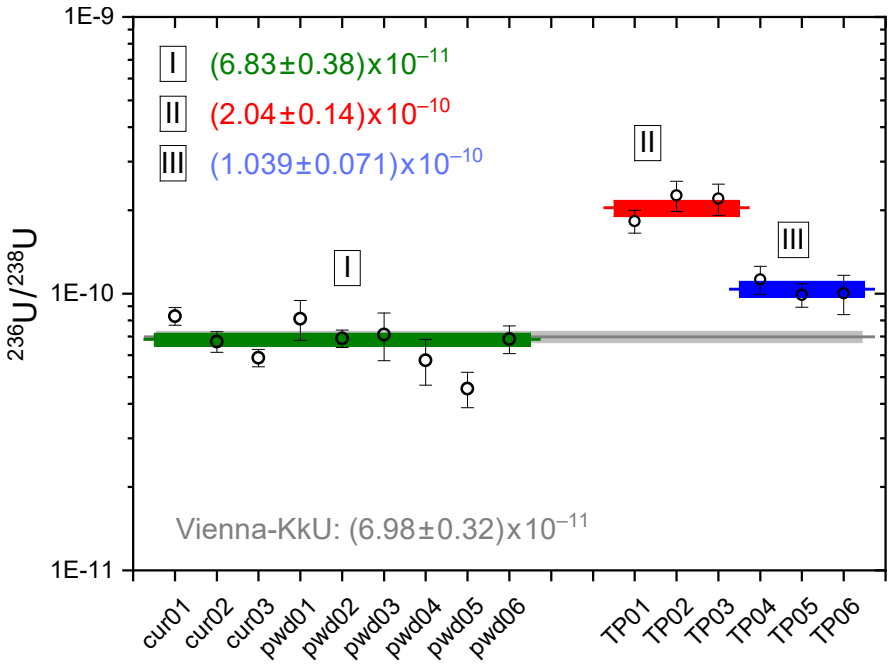

Figure 7.4.: $^{236}U/^{238}U$ ratio results with corresponding $\pm 1\,\sigma$ uncertainty for the individual cathodes and their comparable mixture weighted averages I, II and III (lines = weighted average, box = $\pm 1\,\sigma$ uncertainty). The Vienna-KkU consensus ratio derived via UO^- extraction is given in grey. See Tab. 7.2 (samples) and Tab. 7.3 (results) for further information and a summary.

The trace isotope results of the three mixtures of Vienna-KkU-D30 (I), Vienna-Kku_NdF (II) and Vienna-Kku_PrF (III) each with 1:9 PbF_2 are given in this section in the figures for $^{236}U/^{238}U$: 7.4, $^{233}U/^{238}U$: 7.6 and $^{233}U/^{236}U$: 7.7. Fig. 7.4 shows the $^{236}U/^{238}U$ ratio for every single cathode with their corresponding $\pm 1\,\sigma$ uncertainties. For every of the three tested materials (I, II, III) a weighted average was calculated and is given in the upper left corner. The used weight was $1/(\text{rel. uncert.})^2$ with the relative uncertainty of the individual isotopic ratios (see A.7). Trace isotope ratios for the sample 3C_U and its process blank BLK_2C are separately shown in Fig. 7.5. The derived averages are given by rich colored lines and the related uncertainties are indicated by light colored boxes. Averaging the trace isotope results for material I (Vienna-KkU-D30) leads to $^{236}U/^{238}U = (6.83 \pm 0.38) \times 10^{-11}$. Material II (Vienna-KkU_NdF) yielded a value of $(2.04 \pm 0.14) \times 10^{-10}$ and Mixture III (Vienna-KkU_PrF) showed $(1.039 \pm 0.071) \times 10^{-10}$.

These results indicate that mixture I represents a ready-to-use standard for AMS applications by UF_5^- extraction. It confirmed the Vienna-KkU consensus value derived from AMS measurements using UO^- within its $1\,\sigma$ uncertainty [63]. However, the mixtures II and III showed increased $^{236}U/^{238}U$ ratios, and thus did not agree with the $^{236}U/^{238}U$ Vienna-KkU consensus ratio within 1σ. In addition, the mixtures II and III need to be investigated for the origin of their increased $^{236}U/^{238}U$ ratios due to their high overall detection efficiency and possible use for AMS in the future. As all the mixture compositions stem from the same uranyl nitrate precursor that was used to produce the Vienna-KkU standard, additional ^{236}U from the used matrix precursor chemicals, e.g. Nd_2O_3 and $PrCl_3$ [43] are most probable. The used reagents were formerly situated in a laboratory with a history of nuclear chemistry and possibly including traces of reprocessed nuclear fuel material.

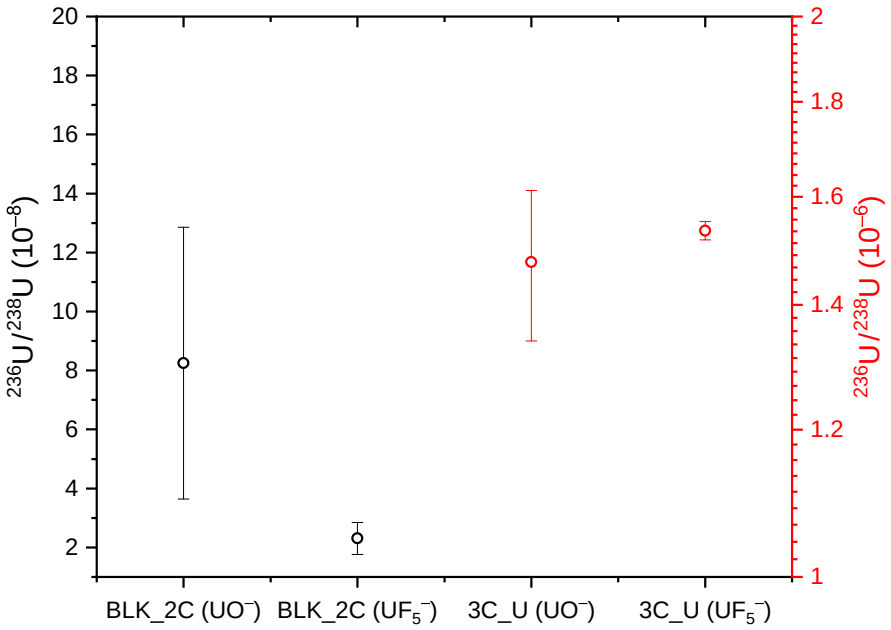

Figure 7.5.: The sample material 3C_U and its process blank BLK_2C were investigated for their respective $^{236}U/^{238}U$ isotopic ratios. (UO^-) denotes the respective results for uranium oxide extraction and (UF_5^-) denotes fluoride extraction using AMS at VERA.

$^{236}U/^{238}U$ results for the two cathodes BLK_2C as process blank and 3C_U as an environmental sample are given in Fig. 7.5 for UO^- extraction on the left side and UF_5^- on the right side. Individual black and red axis labels were used, because the isotopic ratios differed roughly two orders of magnitude. The ^{236}U count rates of the AMS measurements using UF_5^- and UO^- were compared while accounting for the 9 times higher sample mass using UF_5^- extraction. This showed, that only an insignificantly higher count rate was detected by using the sample preparation by drying of the Fe matrix and UF_5^- extraction for AMS. The $^{236}U/^{238}U$ trace isotope results of sample 3C_U were determined to $(1.535 \pm 0.018) \times 10^{-6}$. This is in good agreement with previous results at VERA (UO^- result: $^{236}U/^{238}U = (1.48 \pm 0.14) \times 10^{-6}$). This shows, that using the preparation method in 4 reproducible results are possible. In particular, this is true for chemically purified and digested air filter and Seawater samples as long as a U containing matrix mass of about 200 μg can be achieved.
Results for the process blank BLK_2C showed an even lower $^{236}U/^{238}U$ ratio of

$(2.31 \pm 0.55) \times 10^{-8}$ compared to $(8.3 \pm 4.6) \times 10^{-8}$ using UO^- extraction. This lower isotope ratio result could have several reasons: While using 9 times higher matrix material mass during UF_5^- extraction yielded lower statistical uncertainty as the result from AMS by UO^- extraction could have been a statistically less probable result. Both results still agree within $2\,\sigma$ uncertainty. Another explanation could be possible ^{238}U contamination on the used PTFE watch glass of BLK_2C material during this thesis. Even smallest amounts of Vienna-KkU-D30 would lead to lower $^{236}U/^{238}U$ ratios as process blanks only contain tiniest amounts of U.

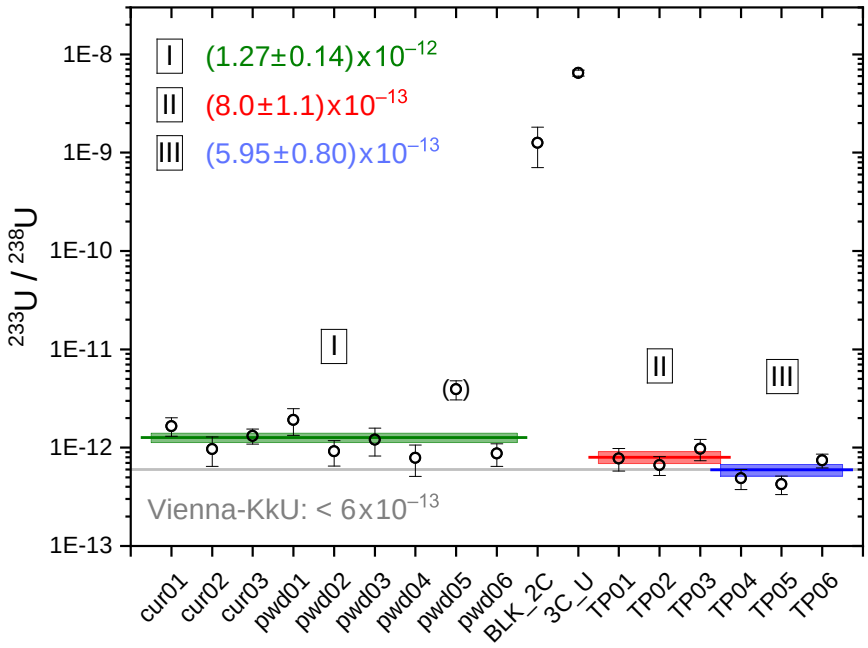

Figure 7.6.: $^{233}U/^{236}U$ ratios with corresponding $\pm 1\,\sigma$ uncertainty for individual cathodes including BLK_2C and 3C_U and mixture weighted averages I, II and III (lines = weighted average, box = $\pm 1\,\sigma$ uncertainty). The cathode denoted pwd05 was excluded from the average due to irregularities in the ^{233}U detection cycle. The upper limit of the Vienna-KkU ratio derived via UO^- extraction is given in grey. See Tab. 7.2 (samples) and Tab. 7.3 (results) for a summary.

Fig. 7.6 displays the obtained $^{233}U/^{238}U$ ratios per cathode for all samples analyzed within this thesis together with the corresponding $\pm 1\,\sigma$ uncertainties.

No $^{233}U/^{238}U$ values from previous measurements are available for BLK_2C and 3C_U. The $^{233}U/^{238}U$ ratio results for the process blank BLK_2C were found to be $(1.26 \pm 0.56) \times 10^{-9}$ and $(6.46 \pm 0.47) \times 10^{-9}$ for sample 3C_U. Averaged and weighted ratio results with uncertainty regions are given for the three mixtures I, II and III (compare table 7.3).
The cathode pwd05 was excluded from the evaluation of the mean $^{233}U/^{238}U$ ratio of mixture I (Vienna-KkU-D30) because of an unknown and seemingly unrelated higher count rate in one detection cycle of ^{233}U. Excluding the results from this one detection cycle of ^{233}U for the evaluation of the cathode average, the $^{233}U/^{238}U$ ratio ranged between 1.1×10^{-12} and 1.5×10^{-12} for the cathode pwd05. The $^{233}U/^{238}U$ mixture ratio results are $(1.27 \pm 0.14) \times 10^{-12}$ for I (Vienna-KkU-D30), $(8.0 \pm 1.1) \times 10^{-13}$ for II (Vienna-KkU_NdF) and $(5.95 \pm 0.80) \times 10^{-13}$ for III (Vienna-KkU_PrF).
The upper limit of $^{233}U/^{238}U$ using UO^- extraction that was presented in Hain et al. 2020 [24] could only be attained by mixture III. A comparison of the $^{232}Th/^{238}U$ results with $^{233}U/^{238}U$ ratios showed no clear correlation (Pearson's $r < 0.1$). The results for the averaged mixtures I, II and III for $^{233}U/^{238}U$ represent machine blanks levels for the method of using UF_5^- extraction for AMS at VERA. In general, trace amounts of ^{233}U could have originated from the used PbF_2. In the case of ^{233}U purely from PbF_2 the resulting $^{233}U/^{238}U$ ratio would have been lower for II and slightly higher for III compared to mixture I, due to the PbF_2 mixture ratios (compare table 7.2). Most probably cross-contamination of ^{233}U spread from the investigated process blank BLK_2C and sample 3C_U to all other cathodes. They showed isotopic ratios of $^{233}U/^{238}U$ of more than three to four orders of magnitude higher than the mixtures I, II and III.

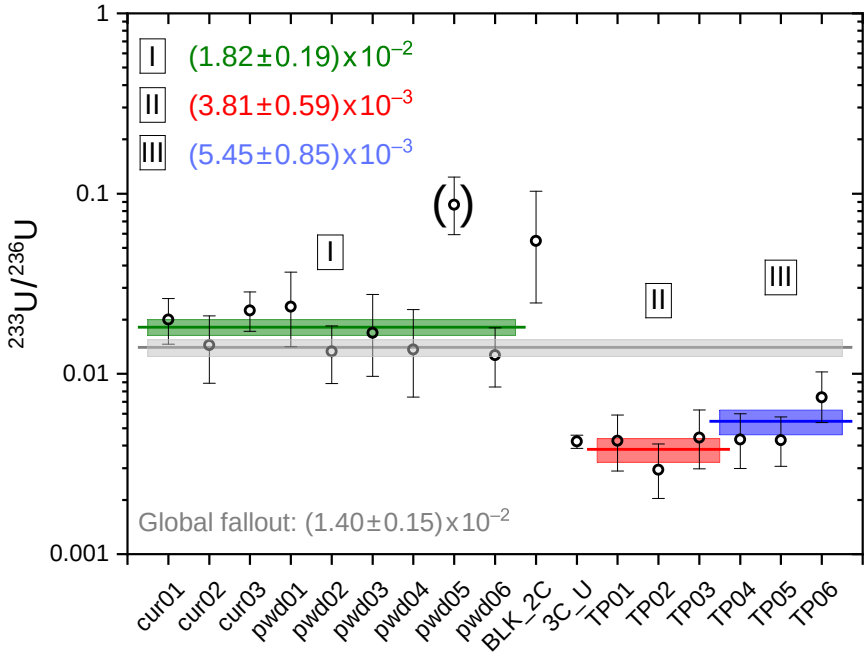

Figure 7.7.: ^{233}U/^{236}U isotope ratios with corresponding $\pm 1\,\sigma$ uncertainties for individual cathodes including BLK_2C and 3C_U and mixture weighted averages I, II and III (lines = weighted average, box = $\pm 1\,\sigma$ uncertainty). Exclusion of cathode pwd05 was also performed for ^{233}U/^{236}U average, as ^{233}U detection was affected. The ^{233}U/^{236}U global fallout ratio derived via UO^- extraction by Hain et al. 2020 [24] is given in grey. Mixture and sample results are summarized in Tab. 7.2 and Tab. 7.3.

The combination of the data from Fig. 7.4 and Fig. 7.6 yielded the ^{233}U/^{236}U results given in Fig. 7.7. The data points with uncertainty bars represent the ratio of ^{233}U/^{236}U for every cathode with its $\pm 1\,\sigma$ uncertainty. Furthermore the averaged ratio and uncertainty for each mixture I, II and III is shown by a colored box and rectangle. The grey line shows the ^{233}U/^{236}U ratio attributed to global fallout U for comparison. The corresponding ratio of $(1.40 \pm 0.15) \times 10^{-2}$ was taken from Hain et al. 2020 [24]. Regarding the three investigated mixtures it was found that their ^{233}U/^{236}U isotopic ratios are $(1.82 \pm 0.19) \times 10^{-2}$ for I, $(3.81 \pm 0.59) \times 10^{-3}$ for II and $(5.45 \pm 0.85) \times 10^{-3}$ for III. The ^{233}U/^{236}U results for each mixture relative to the global fallout level indicate a surplus of ^{236}U for the mixtures II and III that most likely stem from civil nuclear industry (compare Fig. 7.4 and discussion).

Mixture I on the other hand shows an average value that nearly overlapped with the global fallout ratio in its $\pm 1\,\sigma$ uncertainty. This indicates the contribution of chemicals incorporating uranium isotopes in about the ratio of global fallout. The most probable source is PbF_2 which makes up about 90% of the individual samples and already showed a possible influence for the $^{233}U/^{238}U$ ratio of mixture I. In addition, the environmental sample 3C_U is clearly to be attributed with an increased abundance of ^{236}U with $^{233}U/^{236}U = (4.21 \pm 0.36) \times 10^{-3}$ which is also well below the global fallout signature of $(1.40 \pm 0.15) \times 10^{-2}$.

7.3.3. Results on uranium hydride formation

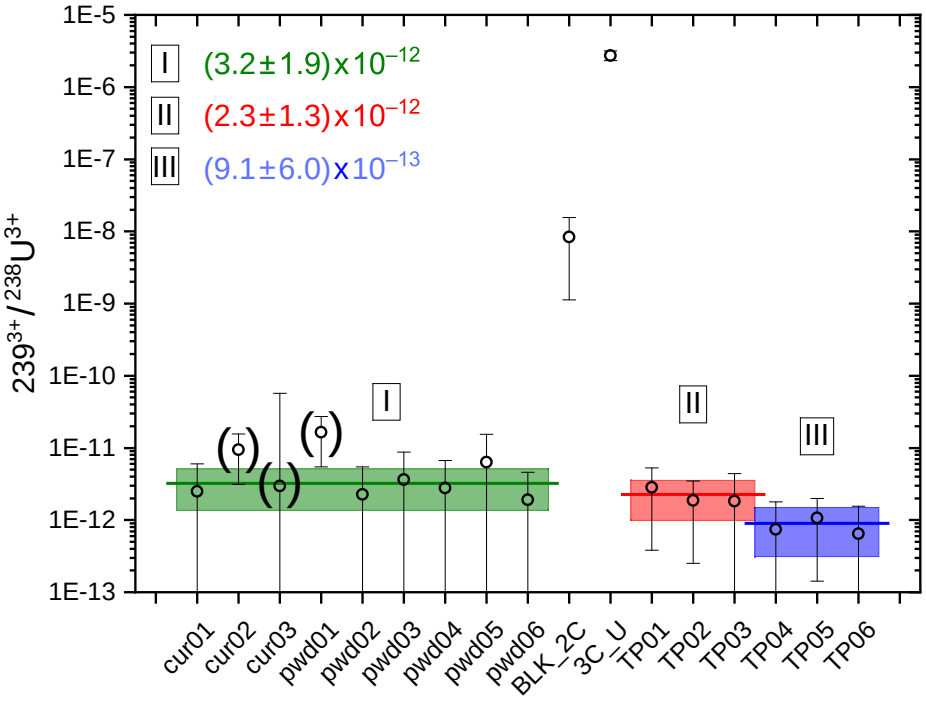

Figure 7.8.: Mass $239^{3+}/^{238}U^{3+}$ data with $\pm 1\,\sigma$ uncertainty for individual cathodes including BLK_2C and 3C_U and mixture weighted averages I, II and III (lines = weighted average, box = $\pm 1\,\sigma$ uncertainty). The term "mass 239^{3+}" corresponds to the sum of detected ions with atomic mass 239 u and charge state $q = 3$. Cathodes denoted cur02, cur03 and pwd01 were excluded due to possible unintended ion beam steering and probable ^{239}Pu cross contamination from 3C_U. A summary on the data and cathode details are shown in Tab. 7.3 and Tab. 7.2.

The mass $239^{3+}/^{238}U^{3+}$ results on uranium hydrides are shown in Fig. 7.8. The ratio of detected "239^{3+}" ions with atomic mass 239 u and charge state $q = 3+$ vs $^{238}U^{3+}$ ions was measured at a stripper gas pressure that corresponds to 1 Pa He at the accelerator terminal. The He stripper gas pressure was not measured inside the stripper tube of the accelerator, but determined by a proxy measurement with an ionization gauge at the stripper gas canal [64]. Cathodes that contained the mixtures I, II and III were averaged and presented with their $\pm 1\,\sigma$ uncer-

tainties indicated by colored boxes in Fig. 7.8. The process blank BLK_2C and sample 3C_U exhibited values of mass $239^{3+}/^{238}U^{3+} = (8.4 \pm 7.3) \times 10^{-9}$ and $(2.74 \pm 0.43) \times 10^{-9}$, respectively. The mixtures resulted in $239^{3+}/^{238}U^{3+}$ ratios of $(3.2 \pm 1.9) \times 10^{-12}$ for I (Vienna-KkU-D30), $(2.3 \pm 1.3) \times 10^{-12}$ for II (Vienna-KkU_NdF) and $(9.1 \pm 6.0) \times 10^{-13}$ for III (Vienna-KkU_PrF). This data is based on about 1 to 2 counts at mass 239 u during the whole measurement which lasted between 300 s and 420 s, was distributed over five to seven hours for each cathode. The cathodes denoted cur02, cur03 and pwd01 were excluded from the evaluation for the following reasons: 1422 of a total 1425 detected 239^{3+} events for cathode cur03 were recorded in the single last measurement sequence of this cathode Therefore, this is to be attributed to detection of the neighboring $^{238}U^{3+}$ ion beam inside the GIC. The cathodes cur02 and pwd01 only showed 239^{3+} events when measured before and after sample 3C_U. The peak UF_5^- ion current from cathode 3C_U was measured between the former two cathodes. Only in this third turn ion events were detected. Not a single one before or afterwards, what suggests 239^{3+} cross-contamination from ^{239}Pu in 3C_U.

The $239^{3+}/^{238}U^{3+}$ results of uranium hydride formation presented in this work showed significantly higher ratios than found during a UH^{3+} analysis of Vienna-KkU by Steier et al. 2019 [64]. There, levels for $239^{3+}/^{238}U^{3+}$ of below 10^{-14} were reported for Vienna-KkU at a stripper gas pressure of ≈ 1 Pa using UO^- extraction. To put the hydride results of this thesis into perspective, two conditions have to be kept in mind. First, that only up to 10^{12} ions of ^{238}U were counted during the dedicated cycles for $239^{3+}/^{238}U^{3+}$ detection in this AMS measurement. Second, the sample 3C_U showed a $^{239}Pu/^{238}U$ ratio 6 orders of magnitude higher than I, II and III (compare Fig. 7.8). An earlier test run with only samples of Vienna-KkU-D30 mixed 1:9 with PbF_2 at around 0.5 Pa He stripper gas pressure equivalent showed no detected 239^{3+} ions. Thus, overall hydride suppression using UF_5^- for AMS in comparison to UO^- extraction is still suspected and should be further investigated.

The isotopic ratios of $^{236}U/^{238}U$, $^{233}U/^{238}U$ and $^{233}U/^{236}U$ are summed in table 7.3.

Table 7.3.: Results summary for mixture averaged and 1/(rel.uncert.)^2-weighted trace isotope ratios found during this thesis. Most importantly $^{236}U/^{238}U$, $^{233}U/^{238}U$, $^{233}U/^{236}U$ and $239/^{238}U$ ratios are given for the investigated mixtures and an environmental air filter sample 3C_U and its process blank BLK_2C. Results using UF_5^- and UO^- extraction for AMS at VERA were only available for 3C_U and BLK_2C. The Vienna-KkU consensus ratio of $^{236}U/^{238}U = (6.98 \pm 0.32) \times 10^{-11}$[63], the global fallout signature of $^{233}U/^{236}U = (1.40 \pm 0.15) \times 10^{-2}$ and an upper limit for $^{233}U/^{238}U < 6 \times 10^{-13}$ using UO^- extraction [24] are cited for comparison. Detailed in formation on the data evaluation is given in the appendix A.7.

mixture / sample	$^{236}U/^{238}U$	$^{233}U/^{238}U$	$^{233}U/^{236}U$	$239^{3+}/^{238}U^{3+}$
I	$(6.83 \pm 0.38) \times 10^{-11}$	$(1.27 \pm 0.14) \times 10^{-12}$	$(1.82 \pm 0.19) \times 10^{-2}$	$(3.2 \pm 1.9) \times 10^{-12}$
II	$(2.04 \pm 0.14) \times 10^{-10}$	$(8.0 \pm 1.1) \times 10^{-13}$	$(3.81 \pm 0.59) \times 10^{-3}$	$(2.3 \pm 1.3) \times 10^{-12}$
III	$(1.039 \pm 0.071) \times 10^{-10}$	$(5.95 \pm 0.80) \times 10^{-13}$	$(5.45 \pm 0.85) \times 10^{-3}$	$(9.1 \pm 6.0) \times 10^{-13}$
3C_U (UO^-)	$(1.48 \pm 0.14) \times 10^{-6}$	-	-	-
3C_U (UF_5^-)	$(1.535 \pm 0.018) \times 10^{-6}$	$(6.46 \pm 0.47) \times 10^{-9}$	$(4.21 \pm 0.36) \times 10^{-3}$	$(2.74 \pm 0.43) \times 10^{-6}$
BLK_2C (UO^-)	$(8.3 \pm 4.6) \times 10^{-8}$	-	-	-
BLK_2C (UF_5^-)	$(2.31 \pm 0.55) \times 10^{-8}$	$(1.26 \pm 0.56) \times 10^{-9}$	$(5.5 \pm 2.7) \times 10^{-2}$	$(8.4 \pm 7.3) \times 10^{-9}$

8. Conclusion and Outlook

In this Master's thesis the ionization efficiency of UO^- and UF_5^- extracted from environmental samples was investigated using a caesium sputter ion source. The Vienna-KkU [63] uranium standard diluted 1:30 in Fe_2O_3 (Vienna-KkU-D30) was used as a proxy for environmental samples that are produced according to the current standard procedure [48; 51]. Fe_2O_3 was the matrix in which uranium occurred as uranium oxides.

First, UO^- was measured from Vienna-KkU-D30 with added Fe or Nb powder. Second, UF_5^- was extracted from Vienna-KkU-D30 mixed with PbF_2. Using the optimal Vienna-KkU-D30 to PbF_2 ratio a new dried sample preparation procedure was tested. Thereafter, a method to directly prepare Vienna-KkU as UF_4 co-precipitated with NdF_3 or PrF_3 mixed with PbF_2 was investigated for the UF_5^- ionization efficiency. Thirdly, an AMS measurement was conducted to test the method of UF_5^- extraction for AMS at VERA. This included the verification of the $^{236}U/^{238}U$ ratio of the Vienna-KkU based mixtures and an environmental air filter sample relative to their ratios previously known from UO^- extraction. Furthermore, $^{233}U/^{238}U$ and $^{233}U/^{236}U$ ratios as well as possible ^{235}UH formation was investigated. The following conclusion is divided in three parts for the measurements of the individual molecules.

Improvements of the UO^- ionization efficiency using Fe or Nb

Increased ionization efficiency was found by adding Fe or Nb powder to Vienna-KkU-D30. The highest values were obtained with $(0.519 \pm 0.073)\%$ for 1:3 weight ratio dilution in Fe and $(0.80 \pm 0.14)\%$ for 1:1 in Nb, respectively. In comparison, the ionization efficiency of U in pure Fe_2O_3 as matrix is about 0.3% for the present AMS measurements [17].
Measurements with about 0.5 mg, 1.5 mg and 4.5 mg, but the same relative U concentration, confirmed the influence of total sample mass as indicated in [13]. The 0.5 mg samples were not only consumed the fastest but also showed the highest overall ionization efficiency after 2 h of sputtering. The 1.5 mg samples could roughly attain the same values after 4 hours.
Longer Cs exposition without sputtering was investigated for its impact on ionization efficiency, but did not show significantly increased results. UO^- measurements yielded the best results by adding 1:1 Nb powder with a factor of 2.5 times higher ionization efficiency compared to the standard procedure. The sample preparation was not changed except for adding the powder.

Ionization efficiency measurements to investigate UF_5^- formation

Several $UO_xF_y^-$ molecules were found to readily produce negative ion currents while UF_5^- showed the highest among them. A weight ratio of about 1:9 turned out to yield about $(2.49 \pm 0.12)\%$ UF_5^- ionization efficiency. $^{63}Cu_5F^-$ influence on the $^{238}UF_5^-$ current accounted for approximately 10% of the overall UF_5^- output. UF_5^- ionization efficiency showed an optimal sample size of 1.5 mg to 2 mg. Over 90% of detected UF_5^- ions were extracted in less than 2 hours. In contrast to UO^-, the UF_5^- ion current output starts fast from a maximum and then decreases almost independently of ion source conditions. UF_5^- extraction combines high ionization efficiency with a significant speed-up in measurement duration per sample. Forming a cone-shaped crater at the surface of the sample could not significantly increase ionization efficiency. Lowering the ion source control current to 1/3 indicated, that minimal amounts of Cs are sufficient to extract high UF_5^- currents. While powder mixed preparation instantly allowed for increased UF_5^- extraction,

the standard precipitation via at least 1.4 mg to 4.3 mg of Fe_2O_3 limits the use of high ratio (1:9) PbF_2 admixture. The resulting total sample mass (approx. 10 mg to 30 mg) could not be loaded into a single standard NEC cathode.
A new sample preparation step based on [13] was developed and tested. It replaced the U precipitation with a step where the sample (Vienna-KkU in HNO_3) was dried with 150 to 200μ g Fe as carrier with a total resulting mass of about 2 mg. This alone yielded very low ionization efficiency results, probably due to residual moisture. A short calcination step for 2 h at 600°C after initial drying proved to be essential for increased UF_5^- ionization. The resulting ionization efficiency using this method in combination with 1:9 PbF_2 admixture yielded $(1.30 \pm 0.45)\%$ including possible transfer losses to the cathode. This result presents a conservative estimate for application to environmental samples, still showing more than 4-fold increase compared to UO^- extraction [13]. Nevertheless, handling sub-milligram samples is difficult and other $UO_xF_y^-$ molecules are still produced, reducing the yield
Alternative to the standard preparation method, the $UO_xF_y^-$ formation should be limited by directly preparing U as UF_4. Thus, UF_4 was co-precipitated with either NdF_3 or PrF_3 and tested for the UF_5^- ionization efficiency. These samples were produced with a solution made from Vienna-KkU by colleagues from CTU Prague [43]. To provide enough fluorine the co-precipitated materials were mixed with 1:9 PbF_2. Results for these showed substantially increased UF_5^- ionization efficiencies $(3.40 \pm 0.30)\%$ for NdF_3 carrier and $(4.67 \pm 0.30)\%$ for PrF_3. Different drying temperatures after precipitation of up to 400°C under Ar-H_2 atmosphere did not yield a statistically relevant change in ionization efficiency. The direct co-precipitation could maximize the UF_5^- extraction, whereas virtually no other $UO_xF_y^-$ molecules were formed. For the preparation of UF_4 by means of HF, extended personal protective equipment is required in addition to the appliances for HF use.

UF_5^- extraction for AMS applications

In order to utilize UF_5^- for AMS measurements of ^{233}U and ^{236}U suitable materials for ion current and count rate tuning had to be found. The measurement setup from UO^- was scaled for UF_5^- on the low-energy side up to the accelerator. For the UF_5^- pilot beam Vienna-KkU-D30 mixed 1:9 with PbF_2 was used. Count rate tuning of the high-energy components was conducted with an in-house iron powder mixed with 1:9 with PbF_2, from which a sufficient number of UF_5^- ions could be extracted. Three differently prepared materials and one environmental air filter sample with previously known $^{236}U/^{238}U$ isotope ratio from UO^- extraction were studied during the first AMS measurement using UF_5^- at VERA. The air filter sample was dried and mixed with PbF_2 by 1:9 weight ratio.
In that way, the $^{238}U^{3+}$ detection efficiency for Vienna-KkU-D30 mixed with PbF_2 by 1:9 weight ratio was found to be $(11.6 \pm 4.6) \times 10^{-4}$ in comparison to about 5-fold lower $\approx 2.2 \times 10^{-4}$ typical for UO^- extraction. The two materials of UF_4 co-precipitated with NdF_3 or PrF_3 showed even higher $^{238}U^{3+}$ detection efficiencies of $(20.4 \pm 7.1) \times 10^{-4}$ and $(47.6 \pm 7.6) \times 10^{-4}$ respectively.
The isotope ratio $^{236}U/^{238}U$ of the powder mixed and co-precipitated materials were measured, whether they could reproduce the Vienna-KkU consensus value. The Vienna-KkU-D30 mixed 1:9 with PbF_2 powder showed $^{236}U/^{238}U = (6.83 \pm 0.38) \times 10^{-11}$ which agreed within 1σ with the Vienna-KkU consensus value of $(6.98 \pm 0.32) \times 10^{-11}$. Unfortunately, both UF_4 with NdF_3 or PrF_3 and mixed 1:9 with PbF_2 did not agree within 1σ. UF_5^- extraction of the air filter sample confirmed the previously known $^{236}U/^{238}U$ isotope ratio by UO^- extraction measured at VERA within $1\,\sigma$.
The three Vienna-KkU based materials showed values of $^{233}U/^{238}U$ below $(1.27 \pm 0.14) \times 10^{-12}$, which defined the machine blank level for this measurement. This allows for the analysis of environmental $^{233}U/^{238}U$ concentrations [24]. Hence, the suitability of UF_5^- extraction as a low-energy U molecule for AMS applications is strongly suggested. While the $^{233}U/^{236}U$ signature of Vienna-KkU-D30 mixed 1:9 with PbF_2 agrees within $2\,\sigma$ with the global fallout value of $(1.40 \pm 0.15) \times 10^{-2}$ [24], the co-precipitated materials showed significantly lower values that indicate influence of civil nuclear industry. Nd_2O_3 and $PrCl_3$ were the only two recently

introduced materials to the VERA laboratory. Thus, they remain the most probable source for ^{236}U contamination.
The interference of $^{235}UH^{3+}$ on ^{236}U was estimated by the "mass 239"/^{238}U ratio as proxy [73]. Upper limits below $(3.2 \pm 1.9) \times 10^{-12}$ for the 1:9 PbF_2 mixed materials were obtained. These results are higher than previously measured at VERA. This could be possibly attributed to the presence of real ^{239}Pu in the air filter sample, that showed up to 6 orders of magnitude higher "mass 239"/^{238}U ratio. Cross-contamination therefore could not be ruled out. UF_5^- would indicate less UH formation due to being more strongly bound than UH^-. It is not clear whether UF_5^- compared to UO^- leads to decreased formation of uranium hydrides.

Outlook

For UO^- a further increase of ionization efficiency is not clearly evident. In order to determine the exact $^{238}UF_5^-$ ionization efficiency without $^{63}Cu_5F^-$ cluster background, materials with the right isotopic mass i.e. graphite, Ag or Au should be investigated as cathodes. This would also allow to precisely determine the U transmission through the accelerator without Cu cluster background. To assess possible interference of ^{232}ThH on ^{233}U the abundance of Th from pure PbF_2 needs to be tested. Subsequent work also further investigate the formation of uranium hydrides using UF_5^- extraction. If a He stripper gas pressure less than the presently used 1 Pa would deliver sufficient UH suppression, higher stripping yields of up to 25% would be possible. The Vienna-KkU standard in lower dilution than 1:30 in Fe_2O_3 mixed with PbF_2 could be immediately used to provide the required $^{238}U^{3+}$ current. Increased stripping yields would in turn allow for less Cs supply and lower output current regulation to possibly achieve more steady UF_5^- currents. Moreover, the preparation method by drying and calcination of the sample matrix should be tested with samples of other origins than Seawater and air filter samples.

9. Acknowledgements

When I first thought about studying, there was this feeling of freedom and the curiosity to look what lies behind all the things we see, feel, smell and those that sometimes hurt us. I have to admit that physics did not always satisfy my desire to research what lies hidden in the dark. I grew more to a person who recognizes this precious science as a way to think and to cope with unknown situations, a solution for ones small problems with all the knowledge that we accumulated in time. If there is one truth I found, then it's that your biggest enemy as well as your most fanatic coach can be yourself. Concerning Physics, I have to emphasize that I especially liked those professors, exercise coordinators and lab course supervisors that could explain the most peculiar effects and relations in simple words. I miss those Feynmen and Feynwomen. I also want to thank the people who had the gift to set a deadline that forced me to bring the best possible version and the most effort to the surface of myself.

For every obstacle in between, family and good friends are THE solution. Vienna used to become the place where I could find friends for the evening, the semester or even in rare cases a kind of friendship that will last until the day we die in the event of jumping into a fresh-cut ice hole in the middle of the Danube, getting caught while invading the Disneyland in a far away country, or when we enjoy the one and only Italian restaurant-of-our-choice. Here, I found a companion for my mammoth, for whom there was always a way forward and never back. A true Spanish James Bond. In Vienna, I was able to enjoy the only real Premium-WG with the world's best roommate. Baumi approves! Moreover, Vienna emerged to be the place where I found love and freedom during a snowy night-hike through the Viennese mountains and watching the happy rats partying with leftovers on Karlsplatz while we had the best Canisibus menu in town. It was and still is the home base we enjoy to come back after every adventure across Europe with the

best Talentina of all.

I want to express my sincere gratitude to all the people, that make VERA such a unique place. In particular,

... Gabi, Ewald, Luki and Wolfgang that I could keep my ten fingers and for your technical support during my thesis as well as to grasp the importance of proper greeting.

... Helga, Sigrid and Eva, for all your efforts to navigate us all through matter more densely packed than neutron stars.

... 谢谢你啊Alfred, for your cross-topic advice ranging from ultra-high vacuum pressure gauges to practical Chinese and good English.

... Johannes, for your in-depth physics conversations, your "How-to" class on eggnog punch and guidance through the world of physics conferences.

... Martin, for explaining the philosophy of the "limit of control" values, your travel stories, photos and enthusiasm for the world's most powerful handheld laser.

... Karin, for your patience and reminders in the lab, the mental strength to comment my thesis and your valuable advice on scientific writing and writing in general.

... Peter, for your coding support, late-night discussions on a plethora of topics and for lending the Lupo.

... Robin, for being a challenging and not less supportive boss and the epiphany of the long minus.

... Alex, Oscar, Johanna and Andi for providing the impetus to do the Master's thesis at VERA, the challenge to train for a post-COVID-19 marathon, lessons in work ethics and a strong opinion on what is right and wrong as well as the best conversations about coffee and how not to clean a fume hood.

A. Appendix

A.1. Information on used materials and equipment

(a) VERA inventory: #4 Alfa Aesar, Johnson Matthey GmbH, Iron powder, -200 mesh, 99+%, metal basis, LOT K12H06

(b) VERA inventory: #195 Alfa Aesar, Johnson Matthey GmbH, niobium powder, -325 mesh, Puratronic, 99.99%, (m. b. excl. Ta), Ta $< 500\,\mathrm{ppm}$, LOT H05J19

(c) VERA inventory: #243 Sigma Aldrich, Lead(II) fluoride, powder, ∼5 micron, 99+%, LOT 09417TH

(d) VERA inventory: #346 VWR International, PROLABO AVS TITRINORM, AAS Standard, Iron $1000\,\mathrm{mg/l}$ ($\pm\,0.2\%$) in nitric acid $0.5\,\mathrm{mol/l}$, $500\,\mathrm{ml}$, Product No.: 86677.260, batch: S73712

(e) Vienna-KkU solution in 4M HNO_3, conc. $^{238}U = 0.12\,\mathrm{mg/g}$

(f) VERA inventory: #4 Merck EMSURE Iron powder, for analysis reduced, particle size $10\,\mu\mathrm{m}$ purity, ≥99.5%, Product No.: 103819

(g) $30\,\mathrm{mL}$ FEP centrifuge tubes with rounded bottom, form factor: Oak Ridge high speed centrifuge tubes, link: *Thermofisher website*

(h) Logarithmic amplifier "EU" for Faraday Cup FC I1-1, 1NA-1MA/9-3VQC-ASSY (OP), National Electrostatics Corporation (NEC), Serial No.: 19336.

(i) Scale used for sample preparation: SARTORIUS Type: 1712, ID: 3403045, link: *Online manual*

A.2. Detailed VERA scheme

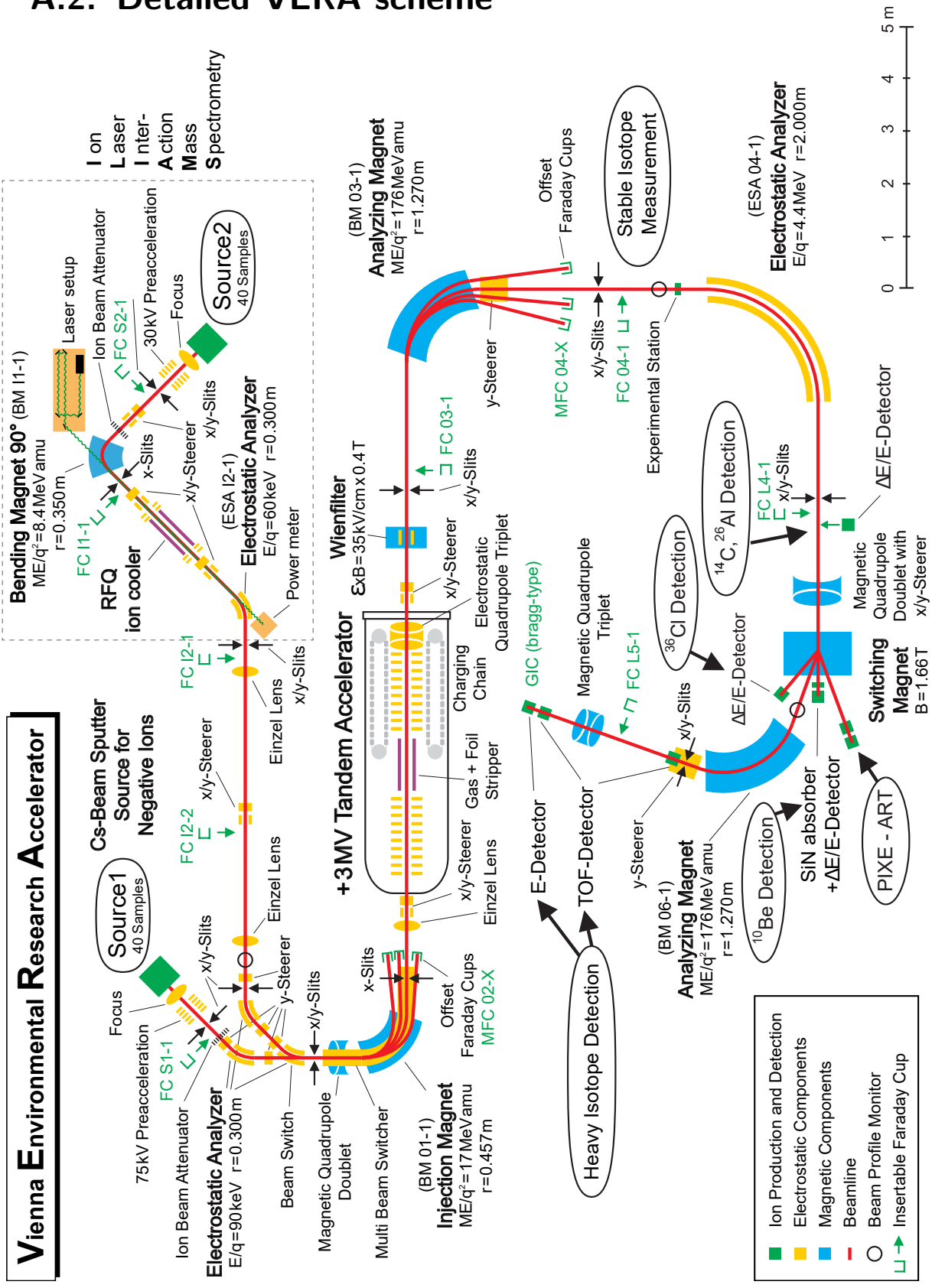

Figure A.3.: A scheme of VERA where all major parts of VERA are labeled. The scheme was adapted from VERA documents. Courtesy of VERA Laboratory.

A.3. Cross-section data on ^{233}U production

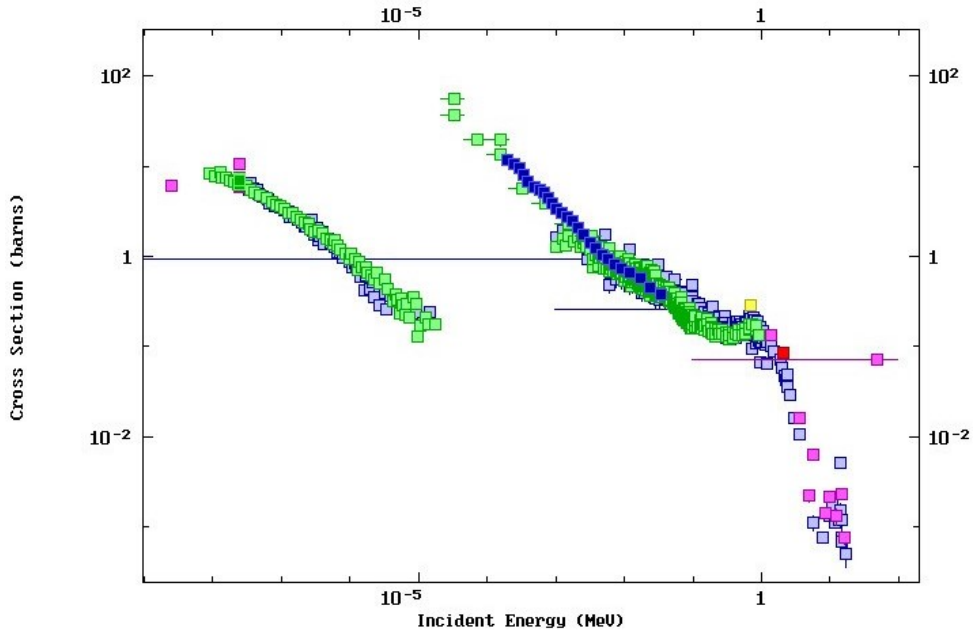

(a) $\sigma[^{232}\mathrm{Th}(\mathrm{n},\gamma)^{233}\mathrm{Th}]$.

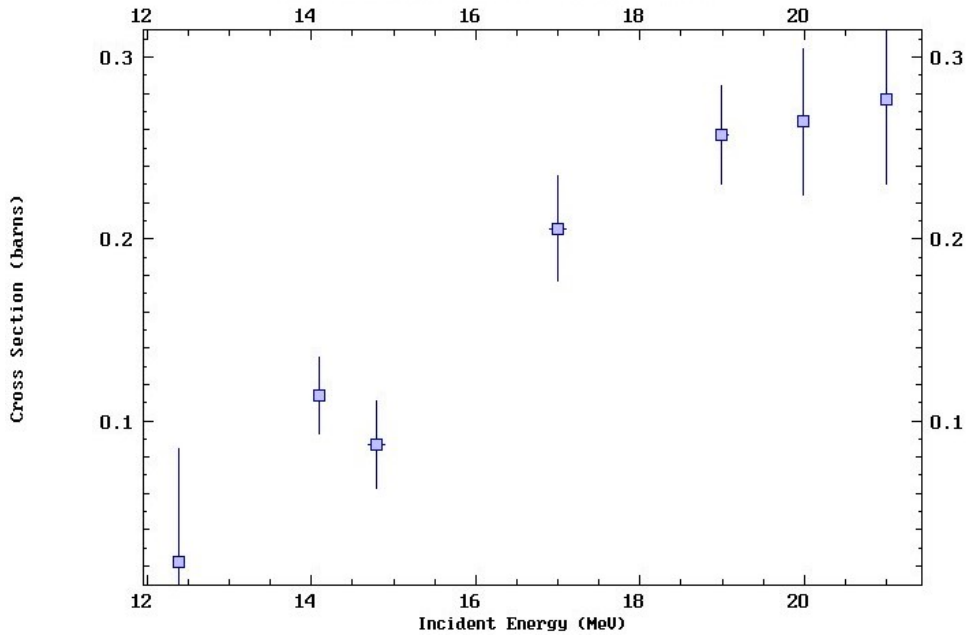

(b) $\sigma[^{235}\mathrm{U}(\mathrm{n}_f,3\mathrm{n})^{233}\mathrm{U}]$.

Figure A.4.: Cross-section data for two selected reaction for the production of ^{233}U retrieved from EXFOR database [74].

A.4. Batch measurement automation code

```
#!/bin/bash

. $SCRIPTDIR/scriptheader

CATHODES="0 1 2 3 4 5 6 7 8 9 10 11 12 13 14 15 16 17 18 19 20 21
↪  22 23 24 25 26 27 28 29 30 31 32 33 34 35 36 37 38 39"

TURN=1
while true ; do
    for CAT in $CATHODES ; do
        CATID=$(($CAT+100)) ;
        CATID=${CATID#1} ;
        TURNID=$(($TURN+1000)) ;
        TURNID=${TURNID#1} ;
        mkdir -p cat$CATID ;
        SCANS=$(getinf "control.log:TARGETS :$CAT,SCANS")
        if test $SCANS == 0 ; then
            continue ;
          fi ;
        script chcat -S2 $CAT
        SCAN=0
        while test $SCAN -lt $SCANS ; do
            fsetpar "HVS S2-1|VC" -4
            script -i scan -Q -p 380 -I 4 -r 100 -i -s 0.1 -S 0.1
            ↪  hvss2 fci1 cat${CATID}/
            ↪  MassScan_turn${TURNID}_cat${CATID}_scan${SCAN}.plotdef
            SCAN=$(($SCAN+1))
          done
        script savesetup cat${CATID}/setup_turn${TURNID}
      done
    TURN=$(( $TURN + 1 ))
  done
```

This program searches for every cathode in CATHODES if there is a dedicated number of scans in the control.log file. This specifies how many mass scans should be taken. Each individual mass scan was carried out with the following options in line script -i scan. The number of sampling points -p XXX, the initial wait time -I in seconds, the range to both sides of a sampling interval $r = (a - b)/(2 \cdot 0.025)$ in machine specific incremental steps, the sampling points per second and delay interval after every point -s and -S in seconds could be set. At last, the scanned parameter hvss2 (for the U_{HVS} acceleration voltage) and the read parameter fci1 of the Faraday cup FC I1-1 were chosen. After the scan, the script saves the source conditions and the ion source changes to the next cathode on the sample wheel and goes on to the next cathode.

A.5. Peak maximum search program

```
#!/bin/bash

MASS=333
HVS_PATTERN="^-3.38654\|^-3.37335\|^-3.36016"

export CATS="5 6 7 8 10 11 12 13 16 17 18 19 20 21 23 24 25 26 27
↪  28 30 31 32 33 35 36 37 38"

SCANS="0 1 2"

TURNS="1 2 3 4 5 6 7 8 9 10 12 13 14 15 16 17 18 19 20 21 22 23 24
↪  25 26 27 28 29 30"

rm -vf cat??/cat??_mass${MASS}_cur_vs_time.txt ;

echo >&2 "Extracted cathodes: $CATS"

for CAT in $CATS ; do
```

```
    echo >&2 "cathode $CAT..."
    CATID=$(($CAT+100)) ;
    CATID=${CATID#1} ;
        {
        echo $CAT
        for TURN in $TURNS ; do
          TURNID=$(($TURN+1000)) ;
          TURNID=${TURNID#1} ;
            for SCAN in $SCANS ; do
                grep "$HVS_PATTERN" cat${CATID}/
                ↪  MassScan_turn${TURNID}_cat${CATID}_scan${SCAN}.plotdef
                ↪  \
                  | cut -d" " -f 2 \
                  | awk 'BEGIN{a=0}{if (-$1>0+a) a=-$1} END{print
                   ↪  a}'
              done ;
          done ;
        } > cat${CATID}/cat${CATID}_mass${MASS}_cur_vs_time.txt
  done

echo >&2 "Completed"

paste $(
    for CAT in $CATS ; do
        CATID=$(($CAT+100)) ;
        CATID=${CATID#1} ;
        echo cat${CATID}/cat${CATID}_mass${MASS}_cur_vs_time.txt ;
      done
    ) > mass${MASS}_cur_vs_time.txt
```

This Bash script was modified together with Prof. Peter Steier from an earlier template. It searches for the maximum ion peak current inside a set of sampling steps called `HVS_PATTERN`. For every cathode an individual "cur_vs_time.txt" file

was created. The data results of every cathode was written into a combined "massXXX_cur_vs_time.txt" file for further analysis.

A.6. Gnuplot code to fit UF_5^- and interfering ions

```
# amplitudes of the single peaks are indicated in nA
# x are the positions in units of atomic mass

a0 = 20
al = 8
acu = 8
x0 = 333.04
xl = 330.04
xr = 333.65
xr2 = 335.64
xr3 = 337.64
sig0 = 0.5
sigl = 0.55
sigr = 0.7

normal(x, mu, sigma) =
 ↪  (1/(sigma*sqrt(2*pi)))*exp(-(x-mu)**2/(2*sigma**2))
fit [329:337] a0*normal(x,x0,sig0) + al*normal(x,xl,sigl) +
 ↪  acu*0.158*normal(x,xr,sigr) + acu*0.353*normal(x,xr2,sigr) +
 ↪  acu*0.315*normal(x,xr3,sigr) "< getinf -l
 ↪  MassScan_turn1_cat12_scan2.plotdef:DATA" using
 ↪  (mass0*(-hvs0+E0)/(-%1+E0)):((-%2)/1e-9) via
 ↪  a0,al,acu,sig0,sigl,sigr

plot a0*normal(x,x0,sig0) title "UF_5- @ 333.04" with lines 3
plot al*normal(x,xl,sigl) title "UOF_4- @ 330.04" with lines 4
plot acu*0.158*normal(x,xr,sigr) title "63Cu_5F- @ 333.65" with
 ↪  lines 5
```

```
plot acu*0.353*normal(x,xr2,sigr) title "(63Cu_4)(65Cu)- @ 335.64"
 ↪  with lines 6
plot acu*0.315*normal(x,xr3,sigr) title "(63Cu_3)(65Cu_2)- @
 ↪  337.64" with lines 8
plot a0*normal(x,x0,sig0) + al*normal(x,xl,sigl) +
 ↪  acu*0.158*normal(x,xr,sigr) + acu*0.353*normal(x,xr2,sigr) +
 ↪  acu*0.315*normal(x,xr3,sigr) title "Peak sum fitted" with
 ↪  linespoints 10
```

A.7. AMS data evaluation

The following mathematical expressions shall outline the calculations needed to find the presented isotope ratios in this work. Square brackets are used for better visibility and do not refer to any unit considerations. For the ratio $^{236}U/^{238}U$ it will be demonstrated. Key quantities for the measurement of isotopic ratios are the number of detected isotopes per run ($N_{[^{236}U]}$), the time per run (t_{run}), its charge +3e ($Q = q \cdot e$), as well as the high energy current of the reference isotope ($I_{[^{238}U]}$). Only the uncertainty of the Poisson counting statistics ($\sqrt{N_{[^{236}U]}}$) of each individual trace isotope (^{236}U) is used for the calculation of the overall uncertainty for the investigated material inside each cathode. Firstly, the ^{236}U count rate

$$R_{[^{236}U],\,i} = \frac{N_{[^{236}U],\,i}}{t_{run,\,i}} \tag{A.1}$$

for each cathode in run "i"was determined. Subsequently, the isotopic ratio $^{236}U/^{238}U$ for the standard materials (containing Vienna-KkU) and for each individual sample, was calculated.

$$[^{236}U/^{238}U]_{run,\,i} = \frac{R_{[^{236}U],\,i} \cdot Q}{I_{[^{238}U],\,i}} \tag{A.2}$$

The next important goal is to compute a weighted average ratio for the standard material correction factor K. The used weight w_i is the inverted and squared

uncertainty u_{i} from the Poisson distributed counting statistics.

$$w_{\mathrm{i}} = \frac{1}{(u_{\mathrm{i}})^2} \text{ , with } u_{\mathrm{i}} = \frac{\sqrt{\mathrm{N}_{[^{236}\mathrm{U}],\,\mathrm{i}}} \cdot Q}{(\mathrm{I}_{[^{238}\mathrm{U}],\,\mathrm{i}} \cdot t_{\mathrm{i}})} \tag{A.3}$$

After calculating the individual weights per run, the turnwise weighed average of every cathode containing a certain standard material is performed. A number of j (3 to 6) cathodes that involve standard material are used for a typical actinide measurement. For these, the following equation gives the turnwise average of a single material species "X" or "std" (standard material).

$$[^{236}\mathrm{U}/^{238}\mathrm{U}]_{\mathrm{turn,\,X}} = \frac{\sum_{i=1}^{j} w_{\mathrm{i}} \cdot [^{236}\mathrm{U}/^{238}\mathrm{U}]_{\mathrm{run,\,i}}}{\sum_{i=1}^{j} w_{\mathrm{i}}} \tag{A.4}$$

If this is now compared to the known consensus ratio for the used standard material, the correction factor K amounts to

$$K = \frac{[^{236}\mathrm{U}/^{238}\mathrm{U}]_{\mathrm{consensus,\,std}}}{[^{236}\mathrm{U}/^{238}\mathrm{U}]_{\mathrm{turn,\,std}}}. \tag{A.5}$$

Then K enables the correction of the single run ratios of material X with unknown isotopic composition simply by multiplying

$$[^{236}\mathrm{U}/^{238}\mathrm{U}]_{\mathrm{corr,\,X}} = K \cdot [^{236}\mathrm{U}/^{238}\mathrm{U}]_{\mathrm{run,\,i}} \tag{A.6}$$

for turn-specific changes in measurement efficiency. These turnwise corrected isotopic ratios are then again weight averaged like the standard material before. Equation A.4 is substituted by weights using the scaled uncertainty $u_{\mathrm{corr,\,i}} = K \cdot u_{\mathrm{i}}$ according equation A.3 to each specific material X. This represents the isotopic ratio of the material in a single cathode over the course of t turns composing the whole measurement.

$$[^{236}\mathrm{U}/^{238}\mathrm{U}]_{\mathrm{cat,\,X}} = \frac{\sum_{i=1}^{t} w_{\mathrm{turn,\,i}} \cdot [^{236}\mathrm{U}/^{238}\mathrm{U}]_{\mathrm{corr,\,X}}}{\sum_{i=1}^{t} w_{\mathrm{turn,\,i}}} \tag{A.7}$$

In terms of uncertainty assessment it has to be added, that the uncertainty for material X per cathode, hence the uncertainty $u_{\mathrm{cat,\,X}}$ of $[^{236}\mathrm{U}/^{238}\mathrm{U}]_{\mathrm{cat,\,X}}$ hast two contributing factors. One is the internal uncertainty $u_{\mathrm{in\_cat,\,X}}$ and the external

uncertainty $u_{\text{ex\_cat, X}}$. Whichever is greater, is taken as $u_{\text{cat, X}}$. Their individual formulae is shown in equation A.8 and A.9.

$$u_{\text{in\_cat, X}} = \sqrt{\frac{\sum_{i=1}^{t} \left(w_{\text{turn, i}} \cdot \left[^{236}\text{U}/^{238}\text{U}\right]_{\text{corr, X}}\right)^2}{\sum_{i=1}^{t} w_{\text{turn, i}}^2}} \tag{A.8}$$

$$u_{\text{ex\_cat, X}} = \sqrt{\frac{\sum_{c=1}^{t} \frac{\left[^{236}\text{U}/^{238}\text{U}\right]_{\text{corr, X}} - \left[^{236}\text{U}/^{238}\text{U}\right]_{\text{cat, X}}}{u_{\text{corr, i}}}}{(t-1)\sum_{c=1}^{t} w_{\text{turn, i}}^2}} \tag{A.9}$$

For the case that an investigated material is situated in multiple target cathodes $c \,\epsilon\, m$, an extra averaging step is performed with the following notation to arrive at a material averaged isotope ratio $\left[^{236}\text{U}/^{238}\text{U}\right]_{\text{overall, X}}$ over all cathodes incorporating the material of interest X. Weights $w_{\text{cat, X}}$ are analogously calculated according equation A.3.

$$\left[^{236}\text{U}/^{238}\text{U}\right]_{\text{overall, X}} = \frac{\sum_{c=1}^{m} w_{\text{cat, X}} \cdot \left[^{236}\text{U}/^{238}\text{U}\right]_{\text{cat, X}}}{\sum_{c=1}^{m} w_{\text{cat, X}}} \tag{A.10}$$

A.8. Detailed cathode data summary

Table A.1.: Cathode details for the investigation on UO^- ionization efficiency with Fe or Nb admixture. The mixing ratio of Vienna-KkU-D30 to Fe or Nb, the total mass m_c and the total uranium mass per cathode $m_{U_{cat}}$ are given.

wheel pos.	sample label	ratio	m_c (mg)	$m_{U_{cat}}$ (μg)
5	Vienna-KkU-D30+Fe_1-1_1	1.56	(1.17 ± 0.01)	(12.7 ± 0.3)
6	Vienna-KkU-D30+Fe_1-1_3	1.22	(2.17 ± 0.01)	(27.1 ± 0.6)
7	Vienna-KkU-D30+Fe_1-3_1	3.50	(1.72 ± 0.01)	(10.6 ± 0.3)
8	Vienna-KkU-D30+Fe_1-3_3	2.95	(2.20 ± 0.01)	(15.5 ± 0.4)
9	Vienna-KkU-D30+Fe_1-8_1	7.03	(2.37 ± 0.01)	(8.2 ± 0.2)
10	Vienna-KkU-D30+Fe_1-8_3	8.23	(1.77 ± 0.01)	(5.3 ± 0.2)
12	Vienna-KkU-D30+Nb_1-1_1	1.22	(0.22 ± 0.01)	(2.8 ± 0.1)
13	Vienna-KkU-D30+Nb_1-1_3	0.96	(2.07 ± 0.01)	(29.4 ± 0.7)
14	Vienna-KkU-D30+Nb_1-3_1	2.92	(2.47 ± 0.01)	(17.5 ± 0.4)
15	Vienna-KkU-D30+Nb_1-3_3	3.01	(1.98 ± 0.01)	(13.7 ± 0.3)
16	Vienna-KkU-D30+Nb_1-8_1	7.99	(2.92 ± 0.01)	(9.0 ± 0.2)
17	Vienna-KkU-D30+Nb_1-8_3	8.61	(1.84 ± 0.01)	(5.3 ± 0.2)
25	Vienna-KkU-D30+Fe_1-1_2	1.56	(1.23 ± 0.01)	(13.4 ± 0.3)
26	Vienna-KkU-D30+Fe_1-1_4	1.22	(2.09 ± 0.01)	(26.1 ± 0.6)
27	Vienna-KkU-D30+Fe_1-3_2	3.50	(2.04 ± 0.01)	(12.6 ± 0.3)
28	Vienna-KkU-D30+Fe_1-3_4	2.95	(2.57 ± 0.01)	(18.1 ± 0.4)
29	Vienna-KkU-D30+Fe_1-8_2	7.03	(1.69 ± 0.01)	(5.9 ± 0.2)
30	Vienna-KkU-D30+Fe_1-8_4	8.23	(2.00 ± 0.01)	(6.0 ± 0.2)
32	Vienna-KkU-D30+Nb_1-1_2	1.22	(1.23 ± 0.01)	(25.5 ± 0.6)
33	Vienna-KkU-D30+Nb_1-1_4	0.96	(2.11 ± 0.01)	(30.0 ± 0.7)
34	Vienna-KkU-D30+Nb_1-3_2	2.92	(3.03 ± 0.01)	(21.5 ± 0.5)
35	Vienna-KkU-D30+Nb_1-3_4	3.01	(1.60 ± 0.01)	(11.1 ± 0.3)
36	Vienna-KkU-D30+Nb_1-8_2	7.99	(2.89 ± 0.01)	(8.9 ± 0.2)
37	Vienna-KkU-D30+Nb_1-8_4	8.61	(2.43 ± 0.01)	(7.0 ± 0.2)

Table A.2.: Detailed cathode information for the investigation on the total sample mass influence on UO^- extraction. The total mass of each sample m_c and the total uranium mass per cathode $m_{U_{cat}}$ are given. The index "b" was only used for the author's needs.

wheel pos.	sample label	ratio	m_c (mg)	$m_{U_{cat}}$ (μg)
5	Vienna-KkU-D30+Fe_1-3_S1b	2.99	(0.62 ± 0.01)	(4.3 ± 0.1)
6	Vienna-KkU-D30+Fe_1-3_S2b	2.99	(0.64 ± 0.01)	(4.5 ± 0.1)
7	Vienna-KkU-D30+Fe_1-3_M1b	2.99	(1.73 ± 0.01)	(12.0 ± 0.3)
8	Vienna-KkU-D30+Fe_1-3_M2b	2.99	(1.62 ± 0.01)	(11.3 ± 0.3)
9	Vienna-KkU-D30+Fe_1-3_L1b	2.99	(3.80 ± 0.01)	(26.4 ± 0.6)
10	Vienna-KkU-D30+Fe_1-3_L2b	2.99	(3.64 ± 0.01)	(25.3 ± 0.6)
25	Vienna-KkU-D30+Fe_1-1_S3b	2.99	(0.76 ± 0.01)	(5.3 ± 0.2)
26	Vienna-KkU-D30+Fe_1-1_S4b	2.99	(0.74 ± 0.01)	(5.2 ± 0.2)
27	Vienna-KkU-D30+Fe_1-3_M3b	2.99	(1.53 ± 0.01)	(10.6 ± 0.3)
28	Vienna-KkU-D30+Fe_1-3_M4b	2.99	(1.42 ± 0.01)	(9.9 ± 0.2)
29	Vienna-KkU-D30+Fe_1-8_L3b	2.99	(4.04 ± 0.01)	(28.1 ± 0.6)
30	Vienna-KkU-D30+Fe_1-8_L4b	2.99	(4.47 ± 0.01)	(31.1 ± 0.7)

Table A.3.: Detailed cathode information for the investigation on optimal mixtures of Vienna-KkU-D30 and PbF_2. The total mass of each sample m_c, the respective mixing ratio and the total uranium mass per cathode $m_{U_{cat}}$ are given.

wheel pos.	sample label	ratio	m_c (mg)	$m_{U_{cat}}$ (μg)
5	Vienna-KkU-D30+PbF_2_1-1_1	1.01	(0.53 ± 0.01)	(7.4 ± 0.2)
7	Vienna-KkU-D30+PbF_2_1-1_2	1.01	(1.16 ± 0.01)	(16.2 ± 0.4)
8	Vienna-KkU-D30+PbF_2_1-3_1	2.96	(0.56 ± 0.01)	(4.0 ± 0.1)
9	Vienna-KkU-D30+PbF_2_1-3_2	2.96	(0.31 ± 0.01)	(2.2 ± 0.1)
11	Vienna-KkU-D30+PbF_2_1-9_1	8.53	(1.87 ± 0.01)	(5.5 ± 0.2)
12	Vienna-KkU-D30+PbF_2_1-9_2	8.53	(1.97 ± 0.01)	(5.8 ± 0.2)

Table A.4.: Detailed cathode information for the investigation on the total sample mass influence on UF_5^- extraction. Total mass of each sample m_c, mixing ratio and the total uranium mass per cathode $m_{U_{cat}}$ are given.

wheel pos.	sample label	ratio	m_c (mg)	$m_{U_{cat}}$ (μg)
5	Vienna-KkU-D30+PbF_2_1-9_S1	8.93	(0.56 ± 0.01)	(1.6 ± 0.1)
6	Vienna-KkU-D30+PbF_2_1-9_S2	8.93	(0.81 ± 0.01)	(2.3 ± 0.1)
7	Vienna-KkU-D30+PbF_2_1-9_M1	8.93	(1.86 ± 0.01)	(5.2 ± 0.2)
8	Vienna-KkU-D30+PbF_2_1-9_M2	8.93	(1.83 ± 0.01)	(5.12 ± 0.2)
9	Vienna-KkU-D30+PbF_2_1-9_L1	8.93	(5.41 ± 0.01)	(15.2 ± 0.4)
10	Vienna-KkU-D30+PbF_2_1-9_L2	8.93	(5.52 ± 0.01)	(15.5 ± 0.4)
12	PbF_2_1	pure PbF_2 (c)	(2.43 ± 0.01)	none added
13	PbF_2_2	pure PbF_2 (c)	(3.00 ± 0.01)	none added
25	Vienna-KkU-D30+PbF_2_1-9_S3	8.93	(0.70 ± 0.01)	(2.0 ± 0.1)
26	Vienna-KkU-D30+PbF_2_1-9_S4	8.93	(0.62 ± 0.01)	(1.7 ± 0.1)
27	Vienna-KkU-D30+PbF_2_1-9_M3	8.93	(2.02 ± 0.01)	(5.7 ± 0.2)
28	Vienna-KkU-D30+PbF_2_1-9_M4	8.93	(1.80 ± 0.01)	(5.0 ± 0.2)
29	Vienna-KkU-D30+PbF_2_1-9_L3	8.93	(5.77 ± 0.01)	(16.2 ± 0.4)
30	Vienna-KkU-D30+PbF_2_1-9_L4	8.93	(6.04 ± 0.01)	(16.9 ± 0.4)
32	PbF_2_3	pure PbF_2 (c)	(2.81 ± 0.01)	none added
33	PbF_2_4	pure PbF_2 (c)	(2.16 ± 0.01)	none added

Table A.5.: Detailed cathode information for the investigation of different ion source control currents on UF_5^- extraction over time. Total mass of each sample m_c, mixing ratio and the total uranium mass per cathode $m_{U_{cat}}$ are given.

wheel pos.	sample label	ratio	m_c (mg)	$m_{U_{cat}}$ (μg)
4	Vienna-KkU-D30+PbF_2_IE_01	9.13	(1.31 ± 0.01)	(3.6 ± 0.1)
5	Vienna-KkU-D30+PbF_2_IE_02	9.13	(1.17 ± 0.01)	(3.2 ± 0.1)
6	Vienna-KkU-D30+PbF_2_IE_03	9.13	(1.00 ± 0.01)	(2.7 ± 0.1)
24	Vienna-KkU-D30+PbF_2_IE_04	9.13	(2.25 ± 0.01)	(6.2 ± 0.2)
25	Vienna-KkU-D30+PbF_2_IE_05	9.13	(1.37 ± 0.01)	(3.8 ± 0.1)
26	Vienna-KkU-D30+PbF_2_IE_06	9.13	(1.73 ± 0.01)	(4.8 ± 0.1)

Table A.6.: Detailed cathode information for the investigation on recessed sample geometry. Total mass of each sample m_c, mixing ratio and the total uranium mass per cathode $m_{\mathrm{U_{cat}}}$ are given.

wheel pos.	sample label	ratio	m_c (mg)	$m_{\mathrm{U_{cat}}}$ (μg)
6	Vienna-KkU-D30+PbF_2_1-9_1	8.98	(0.84 ± 0.01)	(2.3 ± 0.1)
7	Vienna-KkU-D30+PbF_2_1-9_2	8.98	(0.76 ± 0.01)	(2.1 ± 0.1)
8	Vienna-KkU-D30+PbF_2_1-9_3	8.98	(0.58 ± 0.01)	(1.6 ± 0.1)
9	Vienna-KkU-D30+PbF_2_1-9_4	8.98	(0.79 ± 0.01)	(2.2 ± 0.1)
10	Vienna-KkU-D30+PbF_2_1-9_5	8.98	(0.59 ± 0.01)	(1.6 ± 0.1)
11	Vienna-KkU-D30+PbF_2_1-9_6	8.98	(0.60 ± 0.01)	(1.7 ± 0.1)

Table A.7.: Detailed information of the investigated samples for the measurement exploring new sample preparation procedures for UF_5^- extraction.

wheel pos.	sample label	ratio	m_c (mg)	$m_{\mathrm{U_{cat}}}$ (μg)
5	Vienna-KkU_dry_anneal+PbF_2_1-9_1 (A_6)	9.72	(1.23 ± 0.01)	(3.9 ± 0.1)
6	Vienna-KkU_dry_anneal+PbF_2_1-9_2 (B_6)	9.22	(0.47 ± 0.01)	(1.5 ± 0.1)
7	Vienna-KkU_dry_anneal+PbF_2_1-9_3 (C_6)	9.16	(1.68 ± 0.01)	(5.8 ± 0.2)
8	Vienna-KkU_dry_anneal+PbF_2_1-9_4 (D_6)	8.51	(0.90 ± 0.01)	(3.4 ± 0.1)
10	Vienna-KkU_dry+PbF_2_1-9_1 (A_7)	12.06	$(2,08 \pm 0.01)$	(5.2 ± 0.2)
11	Vienna-KkU_dry+PbF_2_1-9_2 (B_7)	11.44	$(1,76 \pm 0.01)$	(4.6 ± 0.1)
12	Vienna-KkU_dry+PbF_2_1-9_3 (C_8)	11.52	(2.42 ± 0.01)	(6.7 ± 0.2)
13	Vienna-KkU_dry+PbF_2_1-9_4 (D_8)	11.55	(2.64 ± 0.01)	(7.2 ± 0.2)
16	Vienna-KkU_NdF+PbF_2_1-9_1	8.88	(2.30 ± 0.01)	(8.7 ± 0.2)
17	Vienna-KkU_NdF+PbF_2_1-9_2	8.88	(1.98 ± 0.01)	(7.5 ± 0.2)
18	Vienna-KkU_NdF-Hp2+PbF_2_1-9_1	8.58	(2.29 ± 0.01)	(9.3 ± 0.2)
19	Vienna-KkU_NdF-Hp2+PbF_2_1-9_2	8.58	(2.28 ± 0.01)	(9.3 ± 0.2)
20	Vienna-KkU_NdF-H400+PbF_2_1-9_1	8.70	(1.95 ± 0.01)	(7.8 ± 0.2)
21	Vienna-KkU_NdF-H400+PbF_2_1-9_2	8.70	(2.18 ± 0.01)	(8.8 ± 0.2)
23	Vienna-KkU_PrF+PbF_2_1-9_1	9.04	(2.06 ± 0.01)	(7.6 ± 0.2)
24	Vienna-KkU_PrF+PbF_2_1-9_2	9.04	(2.59 ± 0.01)	(9.6 ± 0.2)
25	Vienna-KkU_PrF-Hp4+PbF_2_1-9_1	8.53	(2.07 ± 0.01)	(8.5 ± 0.2)
26	Vienna-KkU_PrF-Hp4+PbF_2_1-9_2	8.53	(2.50 ± 0.01)	(10.2 ± 0.3)
27	Vienna-KkU_PrF-H400+PbF_2_1-9_1	8.47	(2.25 ± 0.01)	(9.3 ± 0.2)
28	Vienna-KkU_PrF-H400+PbF_2_1-9_2	8.47	(2.32 ± 0.01)	(9.5 ± 0.2)

Bibliography

[1] Institut de la mer de Villefranche, GEOTRACES - cruise programme, 2020. URL http://www.geotraces.org/cruises/cruise-programme. accessed 13 February 2020.

[2] G. Alton. Semi-empirical mathematical relationships for electropositive adsorbate induced work function changes. *Surface Science*, 175(1):226 – 240, 1986. ISSN 0039-6028. doi: https://doi.org/10.1016/0039-6028(86)90094-4. URL http://www.sciencedirect.com/science/article/pii/0039602886900944.

[3] J. R. Arnold and W. F. Libby. Age Determinations by Radiocarbon Content: Checks with Samples of Known Age. *Science*, 110(2869):678–680, 1949. ISSN 00368075, 10959203. URL http://www.jstor.org/stable/1677049.

[4] J. E. Bartmess. Negative Ion Energetics Data / Electron Affinity Search. *National Institute of Standards and Technology, Gaithersburg MD, 20899*, 2020. doi: https://doi.org/10.18434/T4D303. URL https://webbook.nist.gov/chemistry/ea-ser/. (retrieved January 8, 2020).

[5] I. G. E. Brown and J. Ishikawa. *The Physics and Technology of Ion Sources*, pages 285–308. John Wiley & Sons, Second edition, 2004.

[6] W. Bu, J. Zheng, M. E. Ketterer, S. Hu, S. Uchida, and X. Wang. Development and application of mass spectrometric techniques for ultra-trace determination of ^{236}U in environmental samples - A review. *Analytica Chimica Acta*, 995:1 – 20, 2017. ISSN 0003-2670. doi: https://doi.org/10.1016/j.aca.2017.09.029. URL http://www.sciencedirect.com/science/article/pii/S0003267017310784.

[7] I. I. Buchinskaya and P. P. Fedorov. Lead difluoride and related systems. *Russian chemical reviews*, 73(4):371–400, 2004.

[8] N. Casacuberta, M. Christl, J. Lachner, M. R. van der Loeff, P. Masqué, and H.-A. Synal. A first transect of ^{236}U in the North Atlantic Ocean. *Geochimica et Cosmochimica Acta*, 133:34 – 46, 2014. ISSN 0016-7037. doi: https://doi.org/10.1016/j.gca.2014.02.012. URL `http://www.sciencedirect.com/science/article/pii/S0016703714001008`.

[9] D. Child, M. Hotchkis, K. Whittle, and B. Zorko. Ionisation efficiency improvements for AMS measurement of actinides. *Nuclear Instruments and Methods in Physics Research Section B: Beam Interactions with Materials and Atoms*, 268(7):820 – 823, 2010. ISSN 0168-583X. doi: https://doi.org/10.1016/j.nimb.2009.10.039. URL `http://www.sciencedirect.com/science/article/pii/S0168583X0901088X`. Proceedings of the Eleventh International Conference on Accelerator Mass Spectrometry.

[10] R. Cornett, Z. Kazi, X.-L. Zhao, M. Chartrand, R. Charles, and W. Kieser. Actinide measurements by AMS using fluoride matrices. *Nuclear Instruments and Methods in Physics Research Section B: Beam Interactions with Materials and Atoms*, 361:317 – 321, 2015. ISSN 0168-583X. doi: https://doi.org/10.1016/j.nimb.2015.02.039. URL `http://www.sciencedirect.com/science/article/pii/S0168583X15001561`. The Thirteenth Accelerator Mass Spectrometry Conference.

[11] S. Cotton. *Lanthanide and actinide chemistry*. John Wiley & Sons, 2013.

[12] N. Dutta, R. Tkach, D. Frohlich, C. Tang, H. Mahr, and P. Hartman. Resonance charge transfer from a photoexcited donor state. *Physical Review Letters*, 42(3):175, 1979.

[13] R. Eigl, P. Steier, S. Winkler, K. Sakata, and A. Sakaguchi. First study on ^{236}U in the Northeast Pacific Ocean using a new target preparation procedure for AMS measurements. *Journal of environmental radioactivity*, 162:244–250, 2016. URL `https://doi.org/10.1016/j.jenvrad.2016.05.025`.

[14] R. Eigl, P. Steier, K. Sakata, and A. Sakaguchi. Vertical distribution of ^{236}U in the North Pacific Ocean. *Journal of Environmental Radioactivity*, 169-170:70 – 78, 2017. ISSN 0265-931X. doi: https://doi.org/10.1016/j.jenvrad.2016.12.010. URL http://www.sciencedirect.com/science/article/pii/S0265931X16304489.

[15] M. Faraday. VII. Experimental researches in electricity.—twelfth series. *Philosophical Transactions of the Royal Society of London*, 128:90, 1838. URL https://doi.org/10.1098/rstl.1838.0008.

[16] J. Feige, A. Wallner, S. R. Winkler, S. Merchel, L. K. Fifield, G. Korschinek, G. Rugel, and D. Breitschwerdt. The Search for Supernova-Produced Radionuclides in Terrestrial deep-sea archives. *Publications of the Astronomical Society of Australia*, 29(2):109–114, 2012. doi: 10.1071/AS11070.

[17] L. Fifield, R. Cresswell, M. di Tada, T. Ophel, J. Day, A. Clacher, S. King, and N. Priest. Accelerator mass spectrometry of plutonium isotopes. *Nuclear Instruments and Methods in Physics Research Section B: Beam Interactions with Materials and Atoms*, 117(3):295 – 303, 1996. ISSN 0168-583X. doi: https://doi.org/10.1016/0168-583X(96)00287-X. URL http://www.sciencedirect.com/science/article/pii/0168583X9600287X.

[18] W. G. Graham. Proc. 2nd International Symposium on Production and Neutralization of Negative Hydrogen Ions and Beams. In *BNL Report*, volume 51304, page 126. BNL, Berkeley National Laboratory, 1980.

[19] Y. Guo and M. A. Whitehead. Electron affinities of alkaline-earth and actinide elements calculated with the local-spin-density-functional theory. *Phys. Rev. A*, 40:28–34, 07 1989. doi: 10.1103/PhysRevA.40.28. URL https://link.aps.org/doi/10.1103/PhysRevA.40.28.

[20] G. Gutsev and A. Boldyrev. DVM-Xα calculations on the ionization potentials of MX_{k+1} - complex anions and the electron affinities of MX_{k+1} superhalogens. *Chemical Physics*, 56(3):277 – 283, 1981. ISSN 0301-0104. doi: https://doi.org/10.1016/0301-0104(81)80150-4. URL http://www.sciencedirect.com/science/article/pii/0301010481801504.

[21] F. Gülce. Method for ultra-trace determination of Tc-99 from large Seawater samples. In *ENVIRA 2019*, 9 2019. URL http://www.envira2019.cz/. Conference date: 08-09-2019 Through 13-09-2019.

[22] K. Hain, T. Faestermann, L. Fimiani, R. Golser, J. M. Gómez-Guzmán, G. Korschinek, F. Kortmann, C. Lierse von Gostomski, P. Ludwig, P. Steier, H. Tazoe, and M. Yamada. Plutonium Isotopes ($^{239-241}$Pu) Dissolved in Pacific Ocean Waters Detected by Accelerator Mass Spectrometry: No Effects of the Fukushima Accident Observed. *Environmental Science & Technology*, 51(4):2031–2037, 2017. doi: 10.1021/acs.est.6b05605. URL https://doi.org/10.1021/acs.est.6b05605. PMID: 28110524.

[23] K. Hain, P. Steier, R. Eigl, M. Froehlich, R. Golser, J. Qiao, F. Quinto, and A. Sakaguchi. ^{233}U/^{236}U–A new tracer for environmental processes? In *4th International Conference on Environmental Radioactivity: Radionuclides as Tracers of Environmental Processes*, 2017.

[24] K. Hain, P. Steier, M. B. Froehlich, R. Golser, X. Hou, J. Lachner, T. Nomura, J. Qiao, F. Quinto, and A. Sakaguchi. ^{233}U/^{236}U allows to distinguish environmental emissions of civil nuclear industry from weapons fallout. Manuscript submitted for publication, 2020. URL https://www.nature.com/articles/s41467-020-15008-2.

[25] J. D. Hlavenka, H. Abrams, M. L. Roberts, and B. E. Longworth. Increased AMS Ion Source Efficiency and Ion Currents by Modifying SNICS Cathode Material and Geometry. *Physics Procedia*, 90:17 – 21, 2017. ISSN 1875-3892. doi: https://doi.org/10.1016/j.phpro.2017.09.011. URL http://www.sciencedirect.com/science/article/pii/S1875389217301700. Conference on the Application of Accelerators in Research and Industry, CAARI 2016, 30 October – 4 November 2016, Ft. Worth, TX, USA.

[26] J. Ishikawa. A heavy negative ion sputter source: Production mechanism of negative ions and their applications. *Nuclear Instruments and Methods in Physics Research Section B: Beam Interactions with Materials and Atoms*, 37:38–44, 1989.

[27] J. Ishikawa, H. Tsuji, and T. Maekawa. Electron detachment cross-sections in low energy heavy negative ion beam appratus. *Vacuum*, 39(11):1127 – 1130, 1989. ISSN 0042-207X. URL https://doi.org/10.1016/0042-207X(89)91105-6.

[28] Y. G. J. Ishikawa, H. Tsuji and S. Aze-gami. Particles and Fields Series 53: Production and Neutralization of Negative Ions and Beams, 6th Int. Symp. *AIP Con-ference Proceedings No.287*, page p.66, 1994.

[29] S. Kamleitner, J. Lachner, P. Steier, S. M. Weise, and S. Kraushaar. ^{129}I concentration in a high-mountain environment. *Nuclear Instruments and Methods in Physics Research Section B: Beam Interactions with Materials and Atoms*, 456:193 – 202, 2019. ISSN 0168-583X. doi: https://doi.org/10.1016/j.nimb.2019.05.003. URL http://www.sciencedirect.com/science/article/pii/S0168583X19303076.

[30] W. Kutschera, P. Collon, H. Friedmann, R. Golser, P. Hille, A. Priller, W. Rom, P. Steier, S. Tagesen, A. Wallner, E. Wild, and G. Winkler. Vera: A new AMS facility in Vienna. *Nuclear Instruments and Methods in Physics Research Section B: Beam Interactions with Materials and Atoms*, 123(1):47 – 50, 1997. ISSN 0168-583X. doi: https://doi.org/10.1016/S0168-583X(96)00782-3. Accelerator Mass Spectrometry.

[31] J. Lachner, M. Christl, C. Vockenhuber, and H.-A. Synal. Detection of UH^{3+} and ThH^{3+} molecules and ^{236}U background studies with low-energy AMS. *Nuclear Instruments and Methods in Physics Research Section B: Beam Interactions with Materials and Atoms*, 294:364–368, 2013.

[32] J. Lachner, C. Marek, M. Martschini, A. Priller, P. Steier, and R. Golser. ^{36}Cl in a new light: AMS measurements assisted by ion-laser interaction. *Nuclear Instruments and Methods in Physics Research Section B: Beam Interactions with Materials and Atoms*, 456:163 – 168, 2019. ISSN 0168-583X. doi: https://doi.org/10.1016/j.nimb.2019.05.061. URL http://www.sciencedirect.com/science/article/pii/S0168583X19303829.

[33] D. Langmuir. Uranium solution-mineral equilibria at low temperatures with applications to sedimentary ore deposits. *Geochimica et Cosmochimica Acta*, 42(6):547–569, 1978.

[34] W. B. Lewis. How much of the rocks and the oceans for power? Exploiting the uranium-thorium fission cycle. Technical report, Atomic Energy of Canada Limited, 1964.

[35] M. Martschini, P. Andersson, O. Forstner, R. Golser, D. Hanstorp, A. O. Lindahl, W. Kutschera, S. Pavetich, A. Priller, J. Rohlén, P. Steier, M. Suter, and A. Wallner. AMS of ^{36}Cl with the VERA 3-MV tandem accelerator. *Nuclear Instruments and Methods in Physics Research Section B: Beam Interactions with Materials and Atoms*, 294:115 – 120, 2013. ISSN 0168-583X. doi: https://doi.org/10.1016/j.nimb.2012.01.055. URL `http://www.sciencedirect.com/science/article/pii/S0168583X12001000`. Proceedings of the Twelfth International Conference on Accelerator Mass Spectrometry, Wellington, New Zealand, 20-25 March 2011.

[36] J. Meija, T. B. Coplen, M. Berglund, W. A. Brand, P. De Biévre, M. Gröning, N. E. Holden, J. Irrgeher, R. D. Loss, T. Walczyk, et al. Isotopic compositions of the elements 2013 (IUPAC technical report). *Pure and Applied Chemistry*, 88(3):293–306, 2016.

[37] R. Middleton. A versatile high intensity negative ion source. *Nuclear Instruments and Methods in Physics Research*, 214(2-3):139–150, 1983.

[38] R. Middleton. A negative ion cookbook, 1989. URL `https://www.pelletron.com/cookbook.pdf`.

[39] B. N. L. NNDC. Nudat (nuclear Structure and Decay Data), NuDat 2.7, 2019. URL `https://www.nndc.bnl.gov/nudat2/`. Retrieved 4 Nov. 2019.

[40] T. Nomura, A. Sakaguchi, P. Steier, R. Eigl, A. Yamakawa, T. Watanabe, K. Sasaki, T. Watanabe, R. Golser, Y. Takahashi, and H. Yamano. Reconstruction of the temporal distribution of ^{236}U/^{238}U in the Northwest Pacific Ocean using a coral core sample from the Kuroshio current area. *Marine*

Chemistry, 190:28 – 34, 2017. ISSN 0304-4203. doi: https://doi.org/10.1016/j.marchem.2016.12.008. URL http://www.sciencedirect.com/science/article/pii/S0304420316301323.

[41] E. Overbosch, B. Rasser, A. Tenner, and J. Los. The ionization of hyperthermal sodium atoms on W(110) as a function of temperature. *Surface Science*, 92(1):310 – 324, 1980. ISSN 0039-6028. doi: https://doi.org/10.1016/0039-6028(80)90259-9. URL http://www.sciencedirect.com/science/article/pii/0039602880902599.

[42] D. F. Peppard, G. W. Mason, P. R. Gray, and J. F. Mech. Occurrence of the $(4n + 1)$ Series in Nature. *Journal of the American Chemical Society*, 74 (23):6081–6084, 1952. doi: 10.1021/ja01143a074. URL https://doi.org/10.1021/ja01143a074.

[43] T. Prášek, M. Němec, P. Steier, M. Kern, M. Honda, K. Hain, and X. Zhang. New fluoride target matrix preparation procedure for determination of ^{236}U with accelerator mass spectrometry. *Nuclear Instruments and Methods in Physics Research Section B: Beam Interactions with Materials and Atoms*, 472:64–71, 2020.

[44] A. Priller, R. Golser, P. Hille, W. Kutschera, W. Rom, P. Steier, A. Wallner, and E. Wild. First performance tests of VERA. *Nuclear Instruments and Methods in Physics Research Section B: Beam Interactions with Materials and Atoms*, 123(1):193 – 198, 1997. ISSN 0168-583X. doi: https://doi.org/10.1016/S0168-583X(96)00780-X. URL http://www.sciencedirect.com/science/article/pii/S0168583X9600780X. Accelerator Mass Spectrometry.

[45] A. Priller, M. Auer, R. Golser, A. Herschmann, W. Kutschera, J. Lukas, P. Steier, and A. Wallner. Ion source refinement at VERA. *Nuclear Instruments and Methods in Physics Research Section B: Beam Interactions with Materials and Atoms*, 259(1):94 – 99, 2007. ISSN 0168-583X. URL https://doi.org/10.1016/j.nimb.2007.01.249. Accelerator Mass Spectrometry.

[46] A. Priller, K. Melber, O. Forstner, R. Golser, W. Kutschera, P. Steier, and A. Wallner. The new injection beamline at VERA. *Nuclear Instruments and Methods in Physics Research Section B: Beam Interactions with Materials and Atoms*, 268(7):824 – 826, 2010. ISSN 0168-583X. URL https://doi.org/10.1016/j.nimb.2009.10.040. Proceedings of the Eleventh International Conference on Accelerator Mass Spectrometry.

[47] K. H. Purser. Ultra-sensitive spectrometer for making mass and elemental analyses, 1977. US Patent 4,037,100.

[48] J. Qiao, X. Hou, P. Steier, S. Nielsen, and R. Golser. Method for ^{236}U Determination in Seawater Using Flow Injection Extraction Chromatography and Accelerator Mass Spectrometry. *Analytical Chemistry*, 87(14):7411–7417, 2015. doi: 10.1021/acs.analchem.5b01608. URL https://doi.org/10.1021/acs.analchem.5b01608. PMID: 26105019.

[49] J. Qiao, P. Steier, S. Nielsen, X. Hou, P. Roos, and R. Golser. Anthropogenic ^{236}U in Danish Seawater: Global Fallout versus Reprocessing Discharge. *Environmental Science & Technology*, 51(12):6867–6876, 2017. URL https://doi.org/10.1021/acs.est.7b00504. PMID: 28505439.

[50] F. Quinto, E. Hrnecek, M. Krachler, W. Shotyk, P. Steier, and S. R. Winkler. Measurements of ^{236}U in Ancient and Modern Peat Samples and Implications for Postdepositional Migration of Fallout Radionuclides. *Environmental Science & Technology*, 47(10):5243–5250, 2013. URL https://doi.org/10.1021/es400026m. PMID: 23614536.

[51] F. Quinto, R. Golser, M. Lagos, M. Plaschke, T. Schäfer, P. Steier, and H. Geckeis. Accelerator Mass Spectrometry of Actinides in Ground- and Seawater: An Innovative Method Allowing for the Simultaneous Analysis of U, Np, Pu, Am, and Cm Isotopes below ppq levels. *Analytical Chemistry*, 87(11):5766–5773, 2015. doi: 10.1021/acs.analchem.5b00980. URL https://doi.org/10.1021/acs.analchem.5b00980. PMID: 25938849.

[52] F. Quinto, C. Busser, T. Faestermann, K. Hain, D. Koll, G. Korschinek, S. Kraft, P. Ludwig, M. Plaschke, T. Schäfer, and H. Geckeis. Ultratrace De-

termination of ^{99}Tc in Small Natural Water Samples by Accelerator Mass Spectrometry with the Gas-Filled Analyzing Magnet System. *Analytical Chemistry*, 91(7):4585–4591, 2019. doi: 10.1021/acs.analchem.8b05765. URL https://doi.org/10.1021/acs.analchem.8b05765. PMID: 30843388.

[53] B. Rasser, J. V. Wunnik, and J. Los. Theoretical models of the negative ionization of hydrogen on clean tungsten, cesiated tungsten and cesium surfaces at low energies. *Surface Science*, 118(3):697 – 710, 1982. ISSN 0039-6028. URL https://doi.org/10.1016/0039-6028(82)90216-3.

[54] J. C. Rienstra-Kiracofe, G. S. Tschumper, H. F. Schaefer, S. Nandi, and G. B. Ellison. Atomic and Molecular Electron Affinities: Photoelectron Experiments and Theoretical Computations. *Chemical Reviews*, 102(1):231–282, 2002. URL https://doi.org/10.1021/cr990044u. PMID: 11782134.

[55] G. Rugel, S. Pavetich, S. Akhmadaliev, S. M. Enamorado Baez, A. Scharf, R. Ziegenrücker, and S. Merchel. The first four years of the AMS-facility DREAMS: Status and developments for more accurate radionuclide data. *Nuclear Instruments and Methods in Physics Research Section B: Beam Interactions with Materials and Atoms*, 370:94 – 100, 2016. ISSN 0168-583X. doi: https://doi.org/10.1016/j.nimb.2016.01.012. URL http://www.sciencedirect.com/science/article/pii/S0168583X16000604.

[56] A. Sakaguchi, K. Kawai, P. Steier, F. Quinto, K. Mino, J. Tomita, M. Hoshi, N. Whitehead, and M. Yamamoto. First results on ^{236}U levels in global fallout. *Science of The Total Environment*, 407(14):4238 – 4242, 2009. ISSN 0048-9697. doi: https://doi.org/10.1016/j.scitotenv.2009.01.058. URL http://www.sciencedirect.com/science/article/pii/S0048969709000886.

[57] A. Sakaguchi, A. Kadokura, P. Steier, Y. Takahashi, K. Shizuma, M. Hoshi, T. Nakakuki, and M. Yamamoto. Uranium-236 as a new oceanic tracer: A first depth profile in the Japan Sea and comparison with caesium-137. *Earth and Planetary Science Letters*, 333-334:165 – 170, 2012. ISSN 0012-821X. doi: https://doi.org/10.1016/j.epsl.2012.04.004. URL http://www.sciencedirect.com/science/article/pii/S0012821X12001719.

[58] K. Shibata, O. Iwamoto, T. Nakagawa, N. Iwamoto, A. Ichihara, S. Kunieda, S. Chiba, K. Furutaka, N. Otuka, T. Oshawa, T. Murata, H. Matsnobu, A. Zukeran, S. Kamada, and J. ichi Katakura. JENDL-4.0: A New Library for Nuclear Science and Engineering. *Journal of Nuclear Science and Technology*, 48(1):1–30, 2011. URL https://doi.org/10.1080/18811248.2011.9711675.

[59] J. A. Simpson. The cosmic ray nucleonic component: The invention and scientific uses of the neutron monitor. In *Cosmic Rays and Earth*, pages 11–32. Springer, 2000.

[60] H. L. Skriver and N. Rosengaard. Surface energy and work function of elemental metals. *Physical Review B*, 46(11):7157, 1992.

[61] J. Southon and G. Santos. Ion source development at KCCAMS, university of California, Irvine. *Radiocarbon*, 46:33, 01 2004. URL https://doi.org/10.2458/azu_js_rc.46.4241.

[62] P. Steier, R. Golser, W. Kutschera, A. Priller, C. Vockenhuber, and S. Winkler. Vera, an AMS facility for "all" isotopes. *Nuclear Instruments and Methods in Physics Research Section B: Beam Interactions with Materials and Atoms*, 223-224:67 – 71, 2004. ISSN 0168-583X. doi: https://doi.org/10.1016/j.nimb.2004.04.017. URL http://www.sciencedirect.com/science/article/pii/S0168583X04005336. Proceedings of the Ninth International Conference on Accelerator Mass Spectrometry.

[63] P. Steier, M. Bichler, L. K. Fifield, R. Golser, W. Kutschera, A. Priller, F. Quinto, S. Richter, M. Srncik, and P. Terrasi. Natural and anthropogenic ^{236}U in environmental samples. *Nuclear Instruments and Methods in Physics Research Section B: Beam Interactions with Materials and Atoms*, 266(10):2246–2250, 2008. URL https://doi.org/10.1016/j.nimb.2008.03.002.

[64] P. Steier, K. Hain, U. Klötzli, J. Lachner, A. Priller, S. Winkler, and R. Golser. The actinide beamline at VERA. *Nuclear Instruments and Methods in Physics Research Section B: Beam Interactions with Materials and Atoms*, 458:82 – 89, 2019. ISSN 0168-583X. doi: https://doi.org/10.

1016/j.nimb.2019.07.031. URL http://www.sciencedirect.com/science/article/pii/S0168583X19305233.

[65] C. Sublette. The nuclear weapon archive - Operation Teapot, 1997. URL http://nuclearweaponarchive.org/Usa/Tests/Teapot.html. accessed 10 February 2020.

[66] C. Sublette. The nuclear weapon archive - Operation Hardtack I, 2001. URL http://nuclearweaponarchive.org/Usa/Tests/Hardtack1.html. accessed 20 March 2020.

[67] H.-A. Synal. Developments in accelerator mass spectrometry. *International Journal of Mass Spectrometry*, 349-350:192–202, 2013. ISSN 1387-3806. doi: https://doi.org/10.1016/j.ijms.2013.05.008. URL http://www.sciencedirect.com/science/article/pii/S1387380613001772. 100 years of Mass Spectrometry.

[68] H. Tsuji, J. Ishikawa, T. Maekawa, and T. Takagi. Electron detachment cross-sections for heavy negative-ion beam. *Nuclear Instruments and Methods in Physics Research Section B: Beam Interactions with Materials and Atoms*, 37-38:231 – 234, 1989. ISSN 0168-583X. doi: https://doi.org/10.1016/0168-583X(89)90175-4. URL http://www.sciencedirect.com/science/article/pii/0168583X89901754.

[69] H. H. Uguz. Bestimmung von ^{236}U und Pu-Isotopen in Luftfiltern und Lungenaschen aus den frühen 1960er Jahren, 2019. Master's thesis, University of Vienna.

[70] J. Van Wunnik, J. Geerlings, E. Granneman, and J. Los. The scattering of hydrogen from a cesiated tungsten surface. *Surface Science*, 131(1):17 – 33, 1983. ISSN 0039-6028. URL https://doi.org/10.1016/0039-6028(83)90117-6.

[71] J. S. Vogel. Anion formation by neutral resonant ionization. *Nuclear Instruments and Methods in Physics Research Section B: Beam Interactions with Materials and Atoms*, 361:156 – 162, 2015. ISSN 0168-583X. doi: https:

//doi.org/10.1016/j.nimb.2015.02.062. URL http://www.sciencedirect.com/science/article/pii/S0168583X15001871. The Thirteenth Accelerator Mass Spectrometry Conference.

[72] B. E. Watt. Energy Spectrum of Neutrons from Thermal Fission of ^{235}U. *Phys. Rev.*, 87:1037–1041, 09 1952. doi: 10.1103/PhysRev.87.1037. URL https://link.aps.org/doi/10.1103/PhysRev.87.1037.

[73] S. R. Winkler, P. Steier, J. Buchriegler, J. Lachner, J. Pitters, A. Priller, and R. Golser. He stripping for AMS of ^{236}U and other actinides using a 3-MV tandem accelerator. *Nuclear Instruments and Methods in Physics Research Section B: Beam Interactions with Materials and Atoms*, 361: 458 – 464, 2015. ISSN 0168-583X. doi: https://doi.org/10.1016/j.nimb.2015.04.029. URL http://www.sciencedirect.com/science/article/pii/S0168583X15003754. The Thirteenth Accelerator Mass Spectrometry Conference.

[74] V. V. Zerkin and B. Pritychenko. The experimental nuclear reaction data (EXFOR): Extended computer database and web retrieval system. *Nuclear Instruments and Methods in Physics Research Section A: Accelerators, Spectrometers, Detectors and Associated Equipment*, 888:31–43, 2018.

[75] X. Zhang. Experimental Ionisation Yields of Fluoride Anions in a Middleton Type Sputter Ion Source, 2018. Diploma thesis, University of Vienna.

[76] X.-L. Zhao and A. Litherland. The anions of the Li, Be and B fluorides: The super-halogens and AMS. *Nuclear Instruments and Methods in Physics Research Section B: Beam Interactions with Materials and Atoms*, 259(1):224 – 229, 2007. ISSN 0168-583X. URL https://doi.org/10.1016/j.nimb.2007.01.161. Accelerator Mass Spectrometry.

[77] X.-L. Zhao, A. Litherland, J. Eliades, W. Kieser, and Q. Liu. Studies of anions from sputtering I: Survey of MFn. *Nuclear Instruments and Methods in Physics Research Section B: Beam Interactions with Materials and Atoms*, 268(7-8):807–811, 2010. URL https://doi.org/10.1016/j.nimb.2009.10.036.